

The Design and Feasibility Analysis of Embedded Smart Technology in the Zero-Cast Wx Distal Radius Fracture Brace

Michael van Wyk

A thesis submitted to
Auckland University of Technology
in fulfilment of the requirements for the degree of
Master of Engineering (MEng)

2020

School of Engineering, Computer and Mathematical Sciences

Confidential

Abstract

The Zero-Cast Wx wrist brace is an adjustable orthotic device intended to stabilize distal radius (wrist) fractures (DRF). Designed and developed by the Auckland-based start-up company, Surgisplint Ltd, this patented stabilization system immobilizes the fracture while still retaining a significant degree of joint function – a feature not offered by traditional plaster and fibreglass casts. Additionally, the Zero-Cast Wx brace is a lightweight, foam-lined, plastic injection moulded orthosis that is waterproof and breathable, unlike conventional plaster and fibreglass casts.

The current Zero-Cast Wx fitting protocol requires clinician training to account for variations in hand and wrist morphology across patients. Furthermore, localized swelling may also affect the state of the fit after initial application. Clinicians require that patients be incentivized to comply with early stage hand rehabilitation which has been shown to mitigate healing complications and improve functional outcomes of the hand and wrist.

This project sought to determine if embedded smart technology in the Zero-Cast Wx brace could be used to assist the fitting procedure. Using structured engineering design methodology, the viability of using embedded smart technology to predict various hand rehabilitation exercises and functional hand tests was also investigated. Information provided by this smart technology could be used to incentivize patient adherence to hand physiotherapy and also inform the clinician on patient rehabilitation progress.

Physiological analysis of the hand and forearm enabled identification of suitable locations for a force sensing array to be placed within the confines of the pre-existing Zero-Cast Wx brace to use Force Myography (FMG). This non-invasive technique detects force patterns produced by changes in limb contour when various underlying muscles are contracted or relaxed. The force patterns correspond to a unique movement or position of the limb relative to a default state, which can be used to train a machine learning algorithm. This method could also be used to classify fitting force in the brace.

To demonstrate the feasibility of using embedded sensors in the brace, a machine learning algorithm was trained with FMG data from a single participant to wirelessly classify four hand exercises and a default relaxed position with an accuracy of 92% using a proof-of-concept embedded force sensing system in Zero-Cast Wx.

Having proven the viability of the smart system, a pilot study involving 21 participants investigating the use of multi-user FMG training data to classify fitting force, hand mobility exercises, and functional hand tests was undertaken. This study resulted in a

classification accuracy of 75% and above for fitting force and hand mobility exercises. Functional testing involving rotating a knob, squeezing a hand exercise ball, and lifting a water bottle resulted in poor classification accuracy.

This project has demonstrated the viability of using embedded smart technology in the Zero-Cast Wx brace system to better inform the clinician on brace fitting quality and on patient recovery progress, which may also incentivize patient adherence to hand rehabilitation programs. It was also identified that better classification of functional tests, and possibly other mobility exercises could be achieved through the addition of an inertial measurement unit to the smart brace system.

Table of Contents

Abstract.....	i
List of Figures.....	viii
List of Tables.....	xiii
List of Equations.....	xiv
Attestation of Authorship.....	xv
List of Abbreviations.....	xvi
Glossary.....	xvii
Acknowledgements.....	xviii
Intellectual Property Rights.....	xix
Confidential Material.....	xix
Chapter 1: Introduction.....	1
1.1 Background.....	1
1.2 Problem Definition.....	1
1.3 Research Question and Objectives.....	2
1.4 Research Scope.....	3
1.5 Closure.....	3
Chapter 2: Supporting Information and Literature Review.....	4
2.1 Introduction.....	4
2.2 An Overview of Forearm, Wrist, and Hand Anatomy.....	5
2.2.1 Bone Anatomy.....	5
2.2.2 Muscle and Tendon Anatomy.....	6
2.3 Distal Radius Fractures.....	10
2.3.1 Classification and Epidemiology.....	10
2.3.2 Risk Factors.....	13
2.3.3 Treatment and Bone Healing.....	14
2.3.4 Complications and Disadvantages Associated with Cast Immobilization.....	18
2.3.5 Rehabilitation and Prognosis.....	18
2.3.6 The Zero-Cast Wx Solution.....	20
2.3.7 Proposed Smart Enhancements to Zero-Cast Wx.....	22
2.4 Smart Wearable Technology.....	26
2.4.1 Sensors, digital communication, and signal processing.....	27
2.4.2 Machine Learning.....	31

2.4.3	The Internet of Things.....	35
2.4.4	Examples of Smart Wearable Medical Devices	35
2.4.5	Medical Device Regulation	38
2.4.6	Hand Motion and Gesture Recognition Technologies	39
2.5	Closure	46
Chapter 3: Design and Testing of a Proof-of-Concept Embedded Sensor System in the Zero-Cast Wx Brace		47
3.1	Introduction.....	47
3.2	Force Myography Applied in the Zero-Cast Wx Brace	47
3.2.1	Justification	47
3.2.2	Resistive Polymer Thick Film Sensors.....	47
3.2.3	FSR 402 Design Selection.....	50
3.2.4	FSR 402 Circuit Design	53
3.2.5	FSR 402 Integration with Zero-Cast Wx	55
3.2.6	Volar Plate Modification, Circuitry and Software used for Data Acquisition	61
3.2.7	Test Results	66
3.3	Closure	68
Chapter 4: Design of a Wireless Proof-of-Concept Force Myography System in the Zero-Cast Wx Brace		69
4.1	Introduction.....	69
4.2	Electronic Component Selection and Protoboard Layout Design.....	69
4.2.1	Wireless Microcontroller Design Selection.....	69
4.2.2	FSR Sampling Schematic and Protoboard Layout Design	73
4.2.3	Battery and Switch Selection	75
4.3	Electronic Enclosure Design.....	78
4.3.1	Part Assembly and Enclosure Features.....	78
4.3.2	Design Details and Final Assembly Photographs	80
4.4	Closure	82
Chapter 5: Applied Machine Learning using Force Myography with the Zero-Cast Wx Brace.....		83
5.1	Introduction.....	83
5.2	Feature Engineering.....	83

5.2.1	Feature Extraction.....	83
5.2.2	Feature Scaling.....	83
5.2.3	Feature Selection.....	84
5.3	Algorithm Training and Evaluation.....	85
5.3.1	Cross-Validation.....	85
5.3.2	Classification Accuracy	87
5.3.3	Dataset Size.....	88
5.4	Using Waikato Environment for Knowledge Analysis.....	89
5.4.1	Background and Justification for Use	89
5.4.2	Interface and Primary Applications Used.....	89
5.5	Machine Learning Algorithms for Classification Problems	94
5.5.1	Logistic Regression.....	94
5.5.2	Naïve Bayes	94
5.5.3	Decision Tree.....	94
5.5.4	K-Nearest Neighbours	94
5.5.5	Support Vector Machines.....	94
5.5.6	Random Forest	94
5.6	Machine Learning using WEKA and User-Specific FMG Training Data...	95
5.6.1	Acquisition of Training Data	95
5.6.2	Feature Extraction.....	96
5.6.3	Algorithm Training and Evaluation with WEKA	97
5.6.4	Demonstration of a Real-Time Multi-Class Classifier	98
5.7	Closure	99
Chapter 6: Pilot Study Investigating Multi-User Force Myography Training Data for Algorithms that Classify Fitting Force and Hand Motion Artefacts . 100		
6.1	Introduction.....	100
6.2	Study Design and Methodology.....	100
6.2.1	Justification for a Pilot Study	100
6.2.2	Outcome 1: Classifying Fitting Force in the Two Stage Fit of Zero-Cast Wx	101
6.2.3	Outcome 2: Classifying Passive Finger and Thumb Motion	101

6.2.4	Outcome 3: Classifying Tendon Gliding Exercises	101
6.2.5	Outcome 4: Classifying Functional Hand Tests	102
6.2.6	Summary of Classification Algorithms Produced from Pilot Study.....	104
6.2.7	Pilot Study Ethics Approval.....	105
6.2.8	Hardware Preparation and Data Acquisition Tools	105
6.2.9	Testing and Data Gathering Protocol.....	108
6.3	Closure	115
Chapter 7: Machine Learning Analysis and Pilot Study Results		116
7.1	Introduction.....	116
7.2	Feature Engineering using Excel and Waikato Environment for Knowledge Analysis.....	116
7.2.1	Feature Extraction.....	116
7.2.2	Feature scaling/normalization	117
7.2.3	Feature Selection Using Waikato Environment for Knowledge Analysis	118
7.2.4	Algorithm Training and Evaluation Using WEKA	118
7.3	Machine Learning Results	122
7.3.1	Application 1: Ratchet Arm Fit	122
7.3.2	Application 2: Dorsal Tilt Fit	123
7.3.3	Application 3: Passive Motion Detection.....	125
7.3.4	Application 4: Tendon Gliding Exercises	126
7.3.5	Application 5: Functional Hand Tests	127
7.3.6	FSR Contribution to Algorithm Training	128
7.4	Summary of Results	129
7.5	Closure	130
Chapter 8: Conclusions, Recommendations, and Future Work		131
8.1	Introduction.....	131
8.2	Conclusions	131
8.2.1	The Design and Development of a Proof-of-Concept Embedded Technology System in Zero-Cast Wx was Successfully Achieved.....	131

8.2.2	Applied Machine Learning with Force Myography Data from a Single User is Feasible using the Zero-Cast Wx Brace.....	131
8.2.3	Applied Machine Learning with Multi-User Force Myography Data is Feasible using the Zero-Cast Wx Brace	131
8.2.4	The Identification of Improved Force Sensing Resistor Positions was Achieved.....	132
8.3	Recommendations.....	132
8.3.1	Integrate Inertial Measurement Unit with Current Embedded Technology	132
8.3.2	Increase Number of Participants in Future Studies	133
8.3.3	Consult Data Scientists for Algorithm Tuning to Boost Classification Performance	133
8.3.4	Perform Finite Element Analysis to Simulate and Quantify Force Distribution on Healthy and Injured Wrist	133
8.3.5	Perform Physical Tests on Simulated Swollen Tissue.....	134
8.3.6	Design Volar and Dorsal Plates with Integrated Electronic Hardware ..	134
8.3.7	Include Additional Classes in Cross-User Algorithms and Automate Machine Learning for User-Specific Algorithms.....	134
8.3.8	Integrate App with Wireless Prototype Design.....	135
8.3.9	Perform Clinical Trials on DRF Patients with Manufacturable Prototype	135
	List of References	136
	Appendix A-1: Arduino C code	141
	Appendix A-2: LabVIEW Code for Sampling Analogue Data from Arduino Device....	142
	Appendix B: Detailed Descriptions of Classification Algorithms Used.....	143
	Appendix C: LabVIEW Code Implementing J-48 Decision Tree Algorithm	149
	Appendix D: Ethics Approval.....	150
	Appendix E: Participant Information Sheet.....	152
	Appendix F: Study Poster.....	158
	Appendix G: Participant Consent Form.....	160

List of Figures

Figure 1.1: An image of Zero-Cast Wx fitted to the left wrist of a patient	1
Figure 2.1: Bones of the right hand and forearm in the supinated position	5
Figure 2.2: Superficial view (left) and deep view (right) of the right posterior forearm ..	6
Figure 2.3: Intermediate (left) and deep (right) view of the right anterior forearm	7
Figure 2.4: Muscles that supinate and pronate the right forearm	8
Figure 2.5: A cross-sectional view of the right forearm showing muscles of the anterior and posterior compartments and resulting movements	9
Figure 2.6: Cross-sectional view of the right wrist showing carpal tunnel and converging tendons	9
Figure 2.7: An illustration of a Colle's fracture and Smith's fracture	10
Figure 2.8: An illustration showing various ways the distal radius can be fractured and displaced.....	10
Figure 2.9: Reported incidence of distal radius fractures in men per 100 000 py over the last six decades	11
Figure 2.10: Reported incidence of distal radius fractures in women per 100 000 over the last six decades	12
Figure 2.11: Comparison of DRF incidence between men and women by age in Stockholm, Sweden, 2004–2010	13
Figure 2.12: A standard treatment protocol for distal radius fractures.....	14
Figure 2.13: Images of fibreglass cast (left) and plaster cast (right).....	15
Figure 2.14: An illustration of the three-point fixation technique applied to a fracture..	16
Figure 2.15: Three point fixation applied to a Colle's fracture (left) and Smith's fracture (right)	16
Figure 2.16: The four stages of bone fracture repair	17
Figure 2.17: Tendon gliding exercises recommended for DRF patients	19
Figure 2.18: An illustration of Zero-Cast Wx components	20
Figure 2.19: Three-Point Fixation applied in the Zero-Cast Wx	21
Figure 2.20: Image showing the dorsal plate fitted to the volar plate via ratchet arms.	22
Figure 2.21: Image showing a correctly applied ratchet arm fit as per current fitting guidelines	23
Figure 2.22: Image of volar plate locking screw	23
Figure 2.23: An image illustrating the dorsal tilt fit.....	24
Figure 2.24: Examples of smart wearable devices.....	26
Figure 2.25: Illustrations of common medical devices.....	27
Figure 2.26: A schematic diagram of a sensing system	28
Figure 2.27: Block diagrams of a) communication system and b) digital communication system.....	29

Figure 2.28: A sinusoidal signal represented in three forms	30
Figure 2.29: A block diagram showing a typical signal processing system	30
Figure 2.30: Block diagram of machine learning techniques	31
Figure 2.31: A graphical illustration of a binary classifier showing multiple linear decision boundaries	33
Figure 2.32: A graphical illustration of a non-linear decision boundary	34
Figure 2.33: A graphical illustration of a multiclass classifier using two linear decision boundaries	34
Figure 2.34: TracPatch, is a smart wearable medical device for tracking patient rehabilitation post-knee surgery	36
Figure 2.35: E-vive uses app-controlled muscle stimulation for patients who have undergone knee surgery	37
Figure 2.36: CarbonHand is a grip enhancing device for patients with orthopaedic or neurological problems	37
Figure 2.37: Zhang [56] used the MYO armband – an sEMG based device for real-time classification of five gestures with an accuracy of 98.7%	40
Figure 2.38: The WristFlex prototype used 15 FSRs in a custom Velcro wrist strap ...	41
Figure 2.39: Tomo shown worn on the forearm and wrist with generated impedance images.....	42
Figure 2.40: a) The SensIR wrist-worn device shown left b) One emitter on while all receivers capture the light level.....	42
Figure 2.41: Main hardware components shown in the Digits wrist brace	43
Figure 2.42: A forward kinematics model for a single finger with intersecting laser used in Digits brace	43
Figure 2.43: An example of Sonomyography and image processing to predict hand gestures	44
Figure 2.44: The forearm band set up with five embedded infra-red sensors	45
Figure 2.45: Gesture recognition using only a smart watch in the Serendipity system	46
Figure 3.1: a) FSR sensors and b) Flexiforce sensor.....	48
Figure 3.2: The FSR 400 Series by Interlink Electronics	49
Figure 3.3: Mechanical data of FSR model 402	52
Figure 3.4: FSR connected in voltage divider circuit	53
Figure 3.5: A series of curves for applied force vs output voltage using standard R_m values.....	54
Figure 3.6: Photograph comparing total surface area between dorsal plate (left) and volar plate (right).....	56
Figure 3.7: Photograph comparing surface curvature between dorsal plate (left) and volar plate (right).....	56

Figure 3.8: Tendon gliding exercises selected to test FMG in Zero-Cast Wx	57
Figure 3.9: Extensor muscles and tendons contracted and isolated in 'extended hand' gesture	58
Figure 3.10: FDP muscle and tendons contracted and isolated in 'hook-fist' gesture...	58
Figure 3.11:FDS muscle and tendons contracted and isolated in 'flat-fist' gesture	59
Figure 3.12: FPL muscle and tendon contracted and isolated in 'thumb opposition' gesture	59
Figure 3.13: Anatomy guided FSR array in the left volar plate of Zero-Cast Wx.....	60
Figure 3.14: Photograph comparing the modified volar plate with an unmodified volar plate (foam liners removed)	61
Figure 3.15: Arduino Pin Diagram	62
Figure 3.16: Full schematic circuit for FSR force sampling using Arduino Uno.....	63
Figure 3.17: High level data flow and process execution	64
Figure 3.18: Photograph of modified volar plate (4L) with fitted FSR 402 sensors	65
Figure 3.19:Full test setup with modified volar plate and wired circuitry	65
Figure 3.20: Participant fitted with modified test brace placing forearm at 90 degrees to desktop	66
Figure 3.21:Sequence of gestures performed during data sampling.....	67
Figure 3.22:Graph showing sampled FSR data for successive hand gestures.....	67
Figure 4.1: Full schematic circuit for wireless FSR force sampling using Beetle BLE..	73
Figure 4.2: Image of solderable protoboard used for through-hole pull-down resistors	74
Figure 4.3: Schematic of protoboard and pull-down resistor layout	74
Figure 4.4: An exploded view of main components and enclosure	78
Figure 4.5: Partially assembled electronic enclosure	79
Figure 4.6: Assembled enclosure with battery cover removed.....	79
Figure 4.7: Section views of assembled enclosure with main components.....	80
Figure 4.8: Image of cover with battery compartment (left) and base assembly (right).....	81
Figure 4.9: Images of fully assembled enclosure containing electronic components...	81
Figure 4.10: Images showing the final POC wireless embedded FSR design in Zero-Cast Wx	82
Figure 5.1: An algebraic representation of a supervised machine learning dataset	85
Figure 5.2: An illustration of the k-fold cross validation method with k equal to five.....	86
Figure 5.3: A) Examples of different levels of bias and variance in machine learning modesl B) The trade-off between bias and variance with changin model complexity	86
Figure 5.4: Confusion matrix for a binary classifier	87

Figure 5.5: A generic learning curve for a classification problem	88
Figure 5.6: Weka start-up window showing the various applications	89
Figure 5.7: Screenshot of the Preprocess Tab in the Weka Explorer Application.....	90
Figure 5.8: Screenshot of the <i>classifier tab</i> in the Weka <i>Explorer</i> application.....	91
Figure 5.9: Screenshot of the <i>Select Attributes</i> tab in the Weka Explorer application .	92
Figure 5.10: Screenshot of the <i>setup</i> tab in the Weka <i>Experiment</i> Environment.....	93
Figure 5.11: Plot of wirelessly sampled FSR voltage data during tendon gliding exercise sequence	95
Figure 5.12: Example of feature extraction for tendon gliding sequence	96
Figure 5.13: Screenshot of WEKA results for J48 algorithm	97
Figure 5.14: J48 decision tree algorithm used for five gesture classifier.....	98
Figure 5.15: Graphical interface designed for real-time gesture classifier	99
Figure 5.16: Image of the wireless classifier demonstration.....	99
Figure 6.1 : Image of 3D printed hand torque device used to simulate wrist rotation tasks.....	102
Figure 6.2: 3D-printed mass holder (left) and FSR tested with standardized mass (right)	105
Figure 6.3: FSR configuration for brace size 4 (left) and brace sizes 2 & 3 (right).....	106
Figure 6.4: Anatomy-based FSR tagging scheme.....	107
Figure 6.5: Image of volar plate strapped to the right forearm of a participant.....	109
Figure 6.6: Image of volar plate fitted to right forearm at two-finger width distance from wrist crease.....	109
Figure 6.7: Image of dorsal plate fitted volar plate via ratchet arms.....	110
Figure 6.8: Image of hand-bridge and c-arm fitted on participant.....	110
Figure 6.9: Image of participant's elbow perpendicular to desktop surface.....	111
Figure 6.10: Sequence of tendon gliding exercises performed	112
Figure 6.11: Image of participant performing ball finger-tip squeeze	113
Figure 6.12: Image of participant performing ball palm squeeze.....	113
Figure 6.13: Photograph of participant rotating torque instrument by supinating the forearm.....	114
Figure 6.14: Photograph of participant performing bottle lift.....	114
Figure 7.1: Participant M3R09 - Sampled FSR voltage data for a 'tight' fit in the ratchet arm fitting stage of Zero-Cast Wx	117
Figure 7.2: Participant M3R09 – Sampled FSR voltage data for Tendon Gliding Exercises	117
Figure 7.3: Flowchart showing experiment breakdown in WEKA.....	119
Figure 7.4: Results table from a single experiment in the WEKA Experiment Environment.....	120

Figure 7.5: FSR Force range across all three classes for sensor PR - Dorsal Tilt Fit Males	124
Figure 7.6: FSR graph of female participant showing similar force responses between extended hand and thumb flexion gestures	126
Figure 7.7: FSR Position Reference.....	129

List of Tables

Table 3-1: Mechanical specifications of FSR 400 series	50
Table 3-2: FSR selection criteria with design requirements/constraints.....	51
Table 3-3: Decision matrix for FSR Selection.....	51
Table 3-4: Approximate FSR 402 sensitivity and current drawn with various R_M values.....	54
Table 3-5: Arduino Uno Specifications	62
Table 4-1: Microcontroller selection criteria with design requirements/constraints	70
Table 4-2: Microcontroller options considered for the Zero-Cast Wx brace	71
Table 4-3: Decision matrix for microcontroller selection.....	72
Table 4-4: Battery selection criteria with design requirements/constraints.....	75
Table 4-5: Batteries options considered for integration with Zero-Cast Wx Smart brace	76
Table 4-6: Decision matrix for battery selection	76
Table 5-1: Sample of training dataset	96
Table 6-1: Classification Algorithms Generated from Pilot Study.....	104
Table 6-2: FSR position tags and descriptions.....	106
Table 6-3: Participant breakdown.....	108
Table 7-1: Confusion matrix for ratchet arm fit – males (92% / KNN)	122
Table 7-2: Confusion matrix for ratchet arm fit – females (96% / NBY).....	122
Table 7-3: Confusion matrix for ratchet arm fit – combined (95% / NBY).....	122
Table 7-4: Confusion matrix for dorsal tilt fit – males (53% / J48)	123
Table 7-5: Confusion matrix for dorsal tilt fit – females (89% / RF)	123
Table 7-6: Confusion matrix for dorsal tilt fit – combined (68% / SVM)	123
Table 7-7: Confusion matrix for passive motion detection – males (78% / LR).....	125
Table 7-8: Confusion matrix for passive motion detection – females (85% / RF).....	125
Table 7-9: Confusion matrix for passive motion detection – combined (84% / KNN). 125	
Table 7-10: Confusion matrix for tendon gliding exercises – males (80% / RF).....	126
Table 7-11: Confusion matrix for tendon gliding exercises – females (75% / RF).....	126
Table 7-12: Confusion matrix for tendon gliding exercises – combined (75% / RF)...	126
Table 7-13: Confusion matrix for functional tests – male (38% / J48)	127
Table 7-14: Confusion matrix for functional tests – female (53% / RF)	127
Table 7-15: Confusion matrix for functional tests – combined (42% / J48)	127
Table 7-16: FSR Selection Frequency by Application	128

List of Equations

Equation 3-1: Ohms Law applied in FSR Circuit	53
Equation 3-2: FSR voltage divider circuit	53
Equation 5-1: Min-Max data scaling	83
Equation 5-2: Classification Accuracy	87

Attestation of Authorship

I hereby declare that this submission is my own work and that, to the best of my knowledge and belief, it contains no material previously published or written by another person (except where explicitly defined in the acknowledgements), nor material which to a substantial extent has been submitted for the award of any other degree or diploma of a university or other institution of higher learning.

Signed:

Date: 18 June 2020

List of Abbreviations

ADC	Analogue to Digital Converter
BLE	Bluetooth Low Energy
CE	European Commission
DASH	Disabilities of Arm Shoulder and Hand
DRF	Distal Radius Fracture
EIT	Electrical Impedance Tomography
FDA	Federal Drug Administration
FMG	Force Myography
FSR	Force Sensing Resistor
IMU	Inertial Measurement Unit
IOT	Internet of Things
IR	Infrared
KNN	K-Nearest Neighbours
LR	Logistic Regression
ML	Machine Learning
NBY	Naïve Bayes
PDM	Pressure Distribution Mapping
POC	Proof-of-Concept
PRWE	Patient-Rated Wrist Evaluation
RF	Random Forest
ROM	Range of Motion
sEMG	Surface Electromyography
SVM	Support Vector Machine
WEKA	Waikato Environment for Knowledge Analysis

Glossary

Anatomical Position	refers to the human body in a standing upright position with arms relaxed at the sides and palms facing forward
Anterior	refers to the front side of the human body in the anatomical position
Articular	refers to a joint in the body
Distal	further away from the torso
Dorsal	refers to the posterior side of the wrist in the anatomical position
Posterior	refers to the back side of the human body in the anatomical position
Posterior	refers to the back side of the human body in the anatomical position
Prognosis	the progression of a medical condition
Pronation	arm and hand rotated toward the body i.e palms facing backward from a standard anatomical position
Proximal	nearer to the torso
Radius	a long bone in the forearm
Supination	arm and hand rotated away from the body i.e the default state of the arm and hand in the anatomical position
Volar	refers to the anterior side of the wrist in the anatomical position

Acknowledgements

I would like to sincerely thank my supervisors, Dr David White, and Dr Jeff Kilby, for their ongoing support and guidance during this project. I am especially grateful to David because if it had not been for him, I would not have had the opportunity to undertake an industry-based research project and engage with incredible professionals across multiple disciplines.

I would like to express my gratitude to the Surgisplint team, in particular, Dr Pranesh Kumar, the CTO, inventor and founder of Zero-Cast, and Steve Hamilton, CEO and co-founder of Zero-Cast. Their support, enthusiasm and expertise shown throughout this project has been nothing short of exceptional. I am very grateful and privileged to have contributed to the R&D of Zero-Cast and I share my excitement for the opportunities that lie ahead for this industry-transforming technology. I also extend my thanks to Mandy Gumbley, the consultant Physiotherapist to Surgisplint and Zero-Cast, for so generously giving her time and sharing her highly regarded clinical knowledge and experience in this research.

I would also like to acknowledge and thank AUT Ventures and Callaghan Innovation for their support in funding this project and giving students like myself the opportunity to work with New Zealand's top professionals, researchers, and academics.

Finally, I would like to thank my parents, Colin and Elza, for their unconditional love and support during my move to New Zealand and throughout my post-graduate journey. I am really blessed to have such incredible parents who have never stopped believing in my dreams and capabilities. Thank you.

Intellectual Property Rights

The IP relating to the use of FMG and machine learning in a wrist brace application is currently owned by AUT Ventures Ltd who are currently in commercialization discussions with Surgisplint Ltd.

Confidential Material

An embargo timeframe of 36 months has been approved for the information contained in this thesis. The confidential material relates to the use of FMG and machine learning in a wrist brace. Please see PGR16 on the following page.

Chapter 1: Introduction

1.1 Background

In 2019 the Auckland based medical technology start-up, Surgisplint Ltd, approached the Auckland University of Technology (AUT) BioDesign Lab to enhance the research and development efforts of their flagship product, Zero-Cast Wx.

Zero-Cast Wx is an adjustable wrist orthosis made from injection moulded plastic, designed to stabilize distal radius fractures (DRF) while still allowing significant hand function to be retained. The wrist brace has been designed with the intention of replacing the outdated and bulky plaster casts commonly used for immobilizing distal radius fractures. While the Zero-Cast Wx system is presently in the clinical phases of testing and development, the company have decided to further their innovation endeavours by exploring the possibility of acquiring fitting force and hand motion or position data using their system. Callaghan Innovation, New Zealand's innovation agency, has partnered with Surgisplint Ltd to fund this research through an R&D Fellowship Grant.

1.2 Problem Definition

The Zero-Cast Wx brace stabilizes a fracture by clamping the wrist with a two-part tightening mechanism and securing the hand in a fixed position via a hand bridge. Figure 1.1 shows the left wrist of a patient fitted with Zero-Cast Wx wrist brace.



Figure 1.1: An image of Zero-Cast Wx fitted to the left wrist of a patient [1]

A problem identified by the Surgisplint medical team is consistently obtaining a good fit that adequately stabilizes the fracture without causing the patient excessive discomfort. The current fitting guidelines are based only on a visual inspection technique used by a trained clinician and the subjective feedback of the patient. These qualitative measures vary amongst patients and clinicians which may result in patient discomfort and possibly multiple clinic visits where the clinician has to readjust the brace. Surgisplint would therefore like to investigate methods of quantifying fitting force which could provide the clinician with more confidence in the initial brace application, and also allow them to monitor any changes in swelling.

A secondary research opportunity with potentially far-reaching implications has also been identified. This opportunity involves the use of Zero-Cast Wx as an early stage rehabilitation tool for DRFs. There is evidence to suggest that early stage hand rehabilitation in DRF patients may reduce the risk of joint and tendon complications and possibly experience a quicker and more complete recovery [2, 3]. Clinical studies have shown that supervised rehabilitation and patient adherence to home-based therapy are crucial to improving functional outcomes following a DRF [4, 5]. Having the status of their recovery progress available would also likely incentivize a patient to adhere to a home-based rehabilitation program.

Furthermore, the case for virtual care, telemedicine and remote rehabilitation in modern healthcare systems seems to be stronger than ever before, given the current global COVID-19 pandemic. The advantages of implementing virtual care tools and systems extend well beyond the prevention of spreading disease. Significant time and cost savings have been reported by patients and physicians, while geographically remote populations have also been provided with accessible healthcare [6, 7].

Surgisplint have therefore expressed their interest in exploring non-invasive methods by which various hand motion or position data can be recorded for the purpose of monitoring and managing patient rehabilitation.

1.3 Research Question and Objectives

The primary research question of this project was:

Can embedded smart technology be used to classify fitting force and various hand motion artefacts in the Zero-Cast Wx brace system?

The research question would be answered by achieving the following objectives:

- a. The design and development of a proof-of-concept (POC) embedded technology system in Zero-Cast Wx for the purpose of obtaining fitting force and various hand motion or position data
- b. Assess the classification accuracy of a simple hand gesture recognition algorithm in a self-performed test using data exclusively from the same user
- c. Evaluate the viability of classifying fitting force, hand rehabilitation exercises and functional hand tests using data from multiple users in a small pilot study of 21 participants.
- d. Use the results from the pilot study to validate a sensor array that can be used in future design iterations

1.4 Research Scope

This project focused exclusively on proof-of-concept development to demonstrate the viability of embedded smart technology in the Zero-Cast Wx wrist brace for the purpose of classifying fitting force and hand motion artefacts. The remaining chapters of this thesis discuss how this was achieved. Chapter 2 explores the contemporary literature related to DRF and smart wearable technology, which serve to reinforce the necessity and significance of this research. Chapters 3 and 4 report on the POC brace development using a structured engineering design methodology. Chapter 5 discusses machine learning in more detail and describes its application using force myography (FMG) and training data from a single user to predict a series of hand mobility exercises. Chapter 6 reports the details of a pilot study undertaken to evaluate the feasibility of using multi-user FMG training data to classify fitting force, hand rehabilitation exercises and functional hand tests. In Chapter 7 the results of the pilot study are presented, discussed, and interpreted. Conclusions of the research, recommendations and future work are discussed in the 8th and final chapter of this project.

1.5 Closure

In this chapter the Zero-Cast Wx brace system for distal radius fractures was introduced. Justification was made to investigate the feasibility of developing a POC embedded technology system that could overcome potential issues associated with poor fitting and that can assist patient recovery through remote hand motion monitoring. The scope of the work was defined by outlining the remaining chapters of this thesis.

Chapter 2: Supporting Information and Literature Review

2.1 Introduction

In this chapter an extensive review of the contemporary literature pertaining to this project has been provided. Specifically, the latest research on distal radius fractures is explored which covers DRF epidemiology, typical treatment protocols and post-fracture rehabilitation. This is preceded by a short overview of forearm anatomy. The problematic effects of prolonged hand and wrist immobilisation due to traditional plaster and fibre casts are identified for which the Zero-Cast Wx brace has been developed. Additionally, research on early hand rehabilitation and patient non-compliance is used to justify the need for an embedded technology solution which could be integrated with Zero-Cast Wx.

Background information on sensors, digital communication, wearable medical devices, and machine learning is also provided, giving the reader a clear context for this project. Finally, the latest research on hand gesture recognition technology is investigated as it is essential for identifying the knowledge gap which this project intends to address.

2.2 An Overview of Forearm, Wrist, and Hand Anatomy

This section provides an overview of forearm, wrist, and hand anatomy, focusing only on bone, muscle, and tendon tissue.

2.2.1 Bone Anatomy

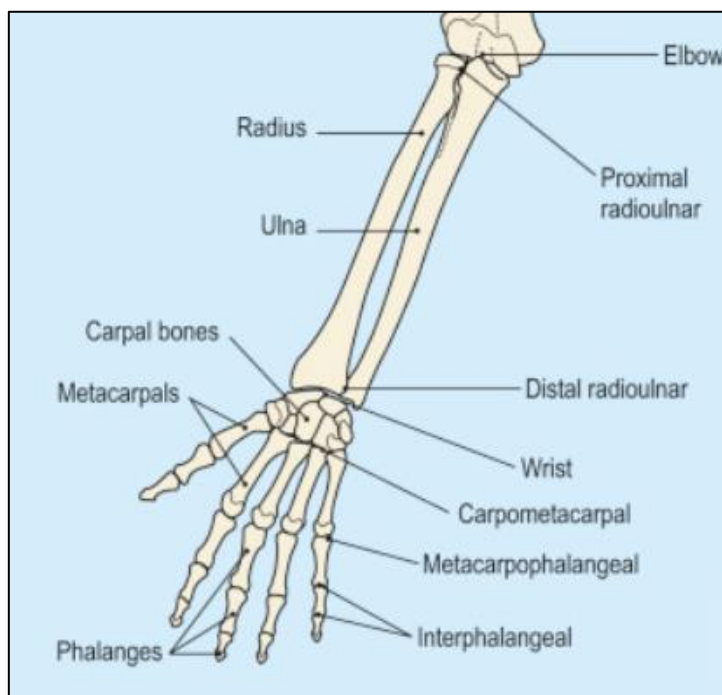


Figure 2.1: Bones of the right hand and forearm in the supinated position [8]

Figure 2.1 shows the long bones of the forearm which comprise the radius and the ulna. They provide structure to the forearm and together allow the wrist to rotate. In the anatomical position – palm of the hand facing forward, these two bones are said to be supinated and lie parallel to each other. The radius is situated laterally (further from arm midline) and ulna medially (closer to arm midline). The terms proximal and distal are frequently used in anatomy and quite simply describe whether a structure is nearer to the torso (proximal) or further from the torso (distal). The proximal ends of the radius and ulna therefore refer to the part of the bones at the elbow. The distal ends of the radius and ulna refer to parts nearest to the thumb and little finger, respectively. In the anatomical position, when the hand is pronated (palm facing backward), the distal radius crosses over the ulna to become the medial structure in the forearm while the proximal end remains lateral. The bones of the wrist and hand include the carpals, metacarpals, and phalanges. There are eight carpal bones of the wrist which are arranged roughly in two rows of four, a distal and proximal row. The small carpal bones allow for different types of wrist motion. Five metacarpal bones form the hand which join with the distal carpal bones and phalanges. The bones of the fingers and thumb

are called phalanges with each digit containing three, barring the thumb which only has two. There are a total of fourteen phalanges in each hand [8].

2.2.2 Muscle and Tendon Anatomy

Muscles that move the wrist and fingers are mostly located in the forearm. These muscles originate from the humerus, ulna and radius and extend into long tendons, inserting at the carpals, metacarpals, and phalanges. Extensor muscles are on the posterior side of the forearm which function to straighten the fingers and bend the wrist posteriorly. Figure 2.2 shows extensor muscles of the right posterior forearm.

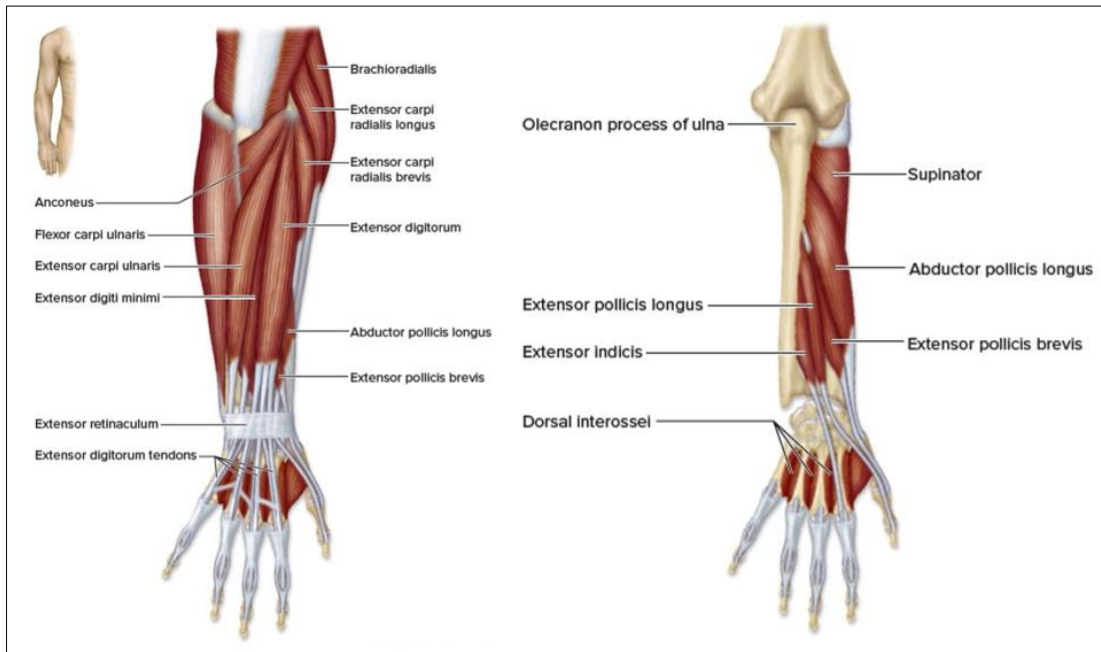


Figure 2.2: Superficial view (left) and deep view (right) of the right posterior forearm [9]

Flexor muscles are on the anterior side of the forearm which function by curling the fingers and bending the wrist anteriorly. Figure 2.3 shows intermediate and deep layers of the right anterior forearm where flexor muscles that curl the fingers are located.

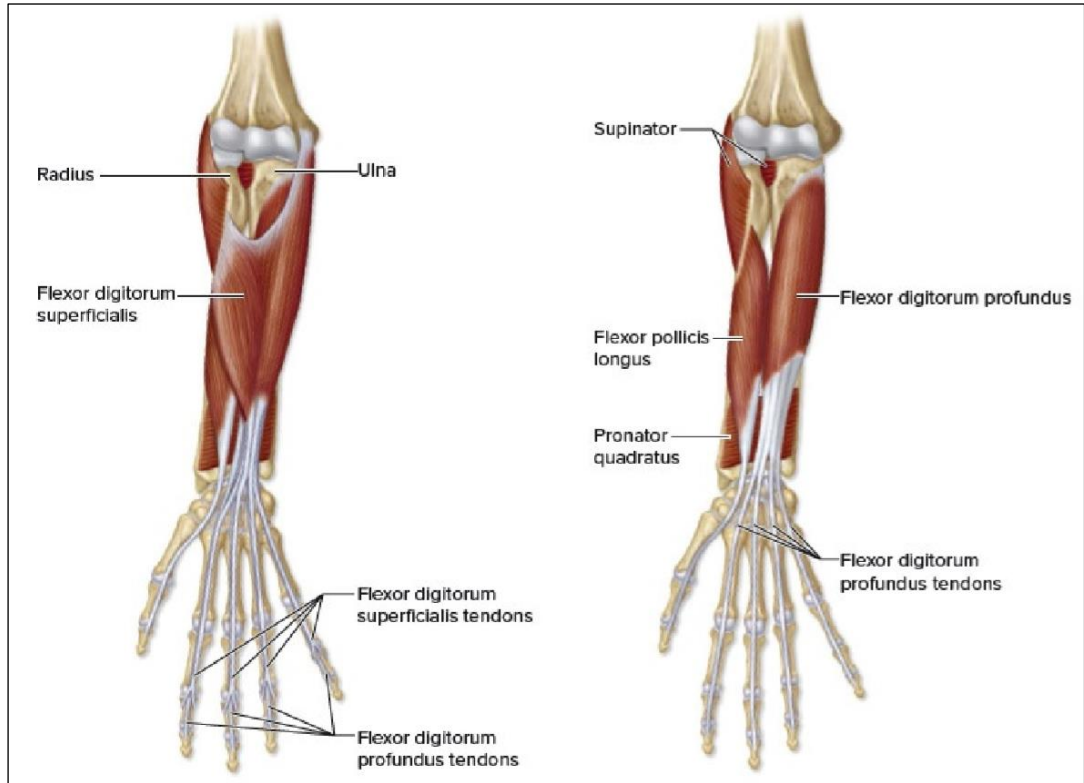


Figure 2.3: Intermediate (left) and deep (right) view of the right anterior forearm [9]

Supination (rotating palm anteriorly) is produced by the biceps brachii of the upper arm and the supinator muscle in the forearm. Similarly, the pronator teres muscle in the forearm produces pronation (rotating palm posteriorly) [9, 10]. Figure 2.4 shows the muscles that rotate the forearm.

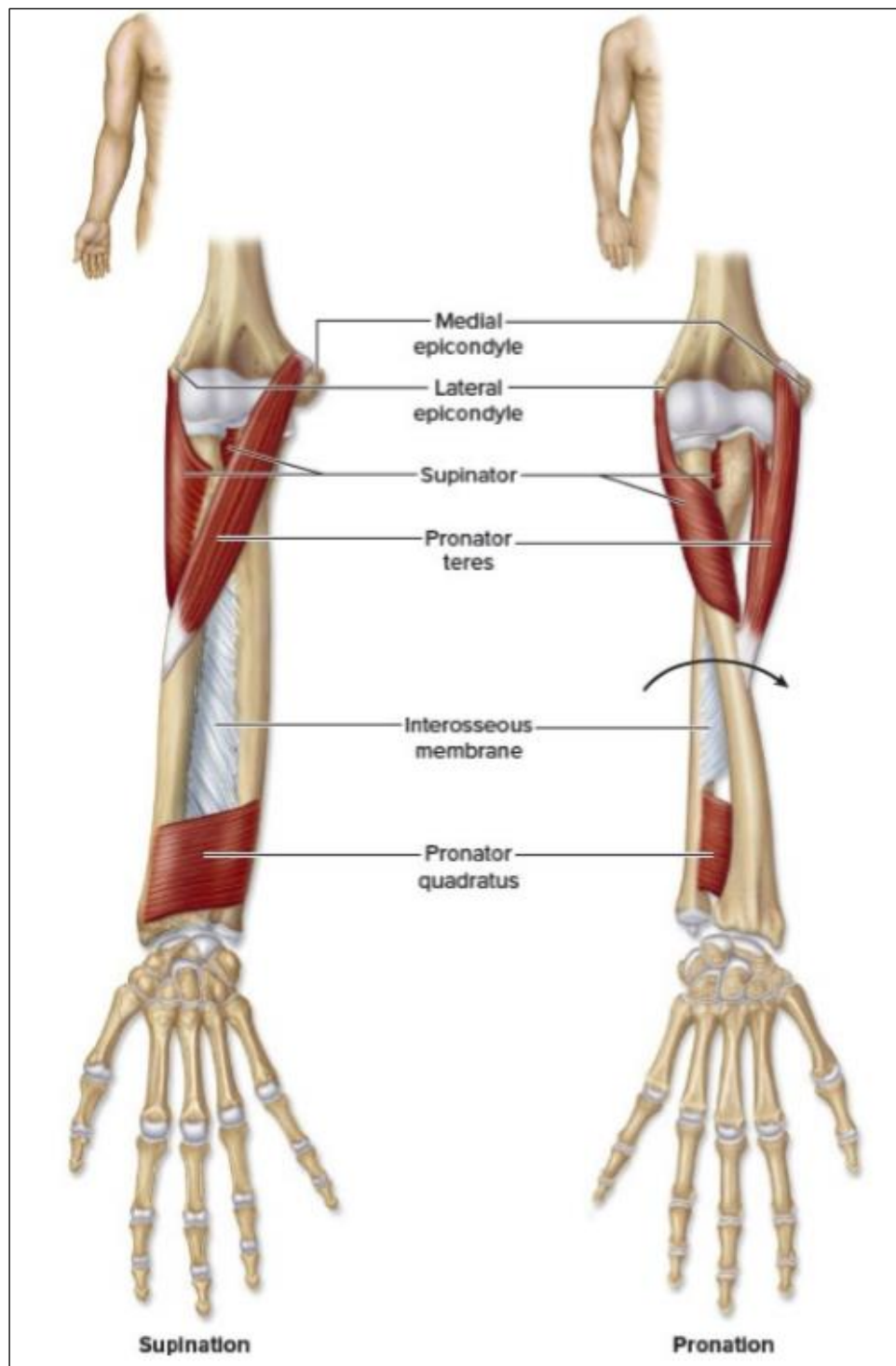


Figure 2.4: Muscles that supinate and pronate the right forearm [9]

The cross-sectional view of the right forearm shown by Figure 2.5 reveals the various layers of muscle. The cross-sectional view of the right wrist shown by Figure 2.6 reveals a narrow space called the carpal tunnel, where flexor tendons converge in a bundle.

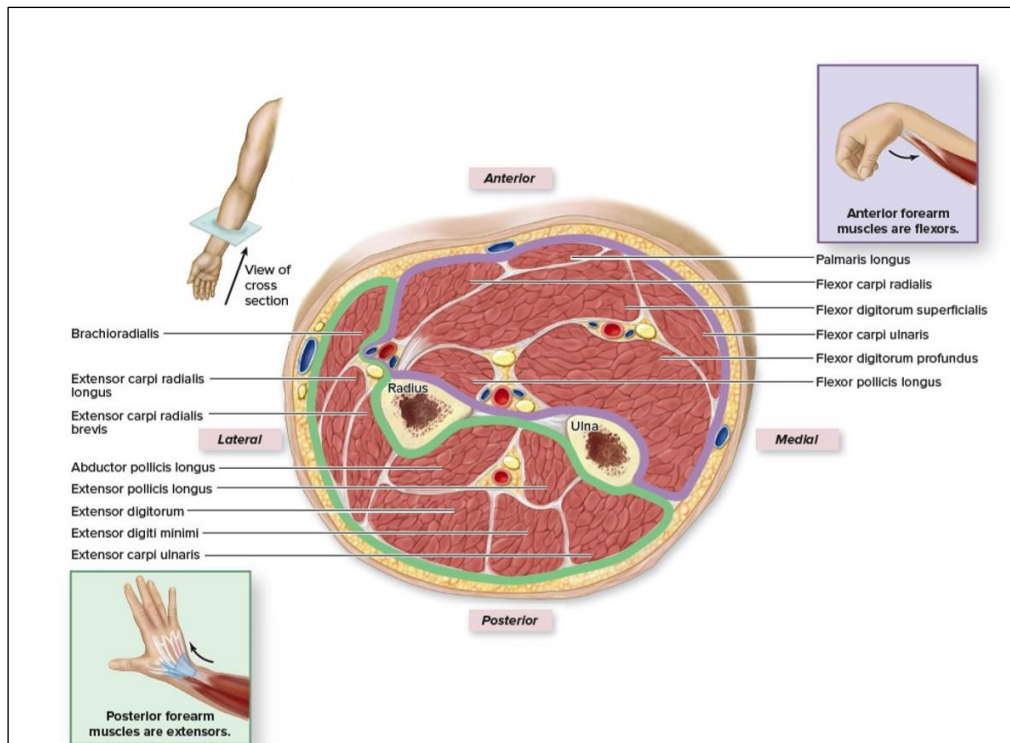


Figure 2.5: A cross-sectional view of the right forearm showing muscles of the anterior and posterior compartments and resulting movements [9]

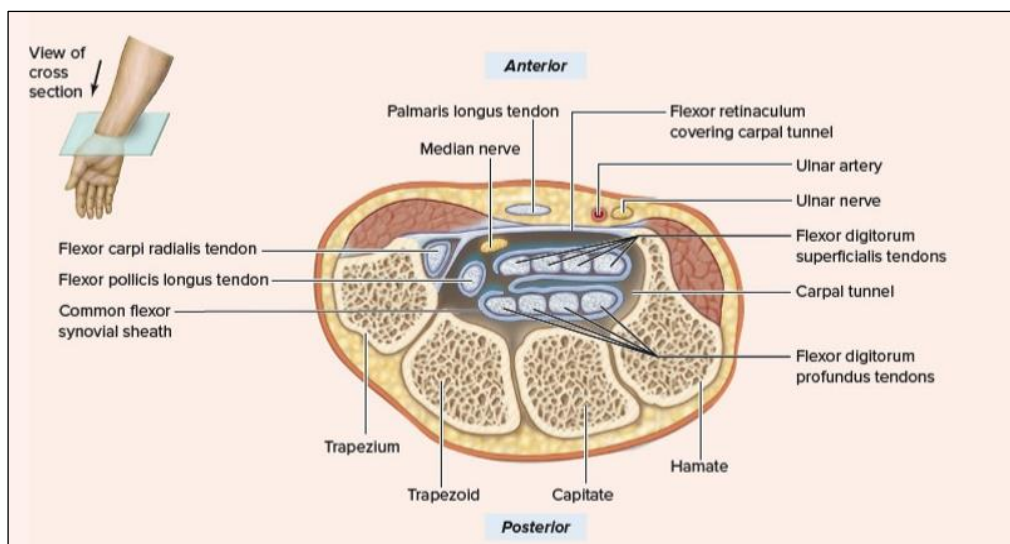


Figure 2.6: Cross-sectional view of the right wrist showing carpal tunnel and converging tendons [9]

2.3 Distal Radius Fractures

The following subsections discuss DRFs and its related topics. A detailed description of the Zero-Cast Wx brace is provided, along with proposed smart enhancements.

2.3.1 Classification and Epidemiology

A distal radius fracture (DRF) is a fracture of the radius bone of the forearm at the wrist joint. It is the most common bone fracture seen in adults and typically caused by a fall on an outstretched arm [11]. There are typical fracture patterns seen when it comes to classifying distal radial fractures. Eponyms are the oldest classification method and are still commonly used in clinical practice. One of the most common types of DRF is a Colle's fracture. Illustrated by Figure 2.7, a Colle's fracture is characterized by the upward tilting of the broken radius. Named after Abraham Colles in 1814, it describes an "extra-articular, dorsally displaced, metaphyseal fracture with radial shortening" [12]. Figure 2.8 shows various fracture patterns of DRFs and the terminology used to describe them. Although there are 15 validated DRF classification systems, no consensus has yet been reached in the medical community on which system is best to adopt in practice [12]. Despite this fact, classification systems may still assist the physician in choosing the appropriate treatment pathway.



Figure 2.7: An illustration of a Colle's fracture and Smith's fracture [13]

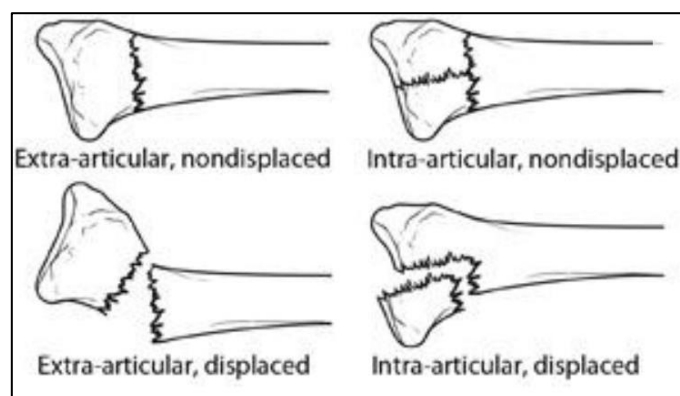


Figure 2.8: An illustration showing various ways the distal radius can be fractured and displaced [14]

Recent data from the United States revealed that the radius was the most common long bone to be fractured with DRF representing one sixth of all emergency room visits. Epidemiology research shows that the global incidence of DRFs vary considerably, with higher incidences occurring in developed nations like Scandinavia, New Zealand and the United States [16]. The graphs shown by Figure 2.9 and Figure 2.10 show an overall increase in DRF incidence for both men and women in the last six decades across numerous countries. Projections for the future suggest a similar trend - one study conducted on the Swedish population projects the incidence of DRFs to increase by 38% between 2017 and 2050 [15]. Another study projects a 23% increase in DRFs in the UK over the next 20 years [11]. These findings present a significant challenge to healthcare systems in terms of both financial and occupational implications.

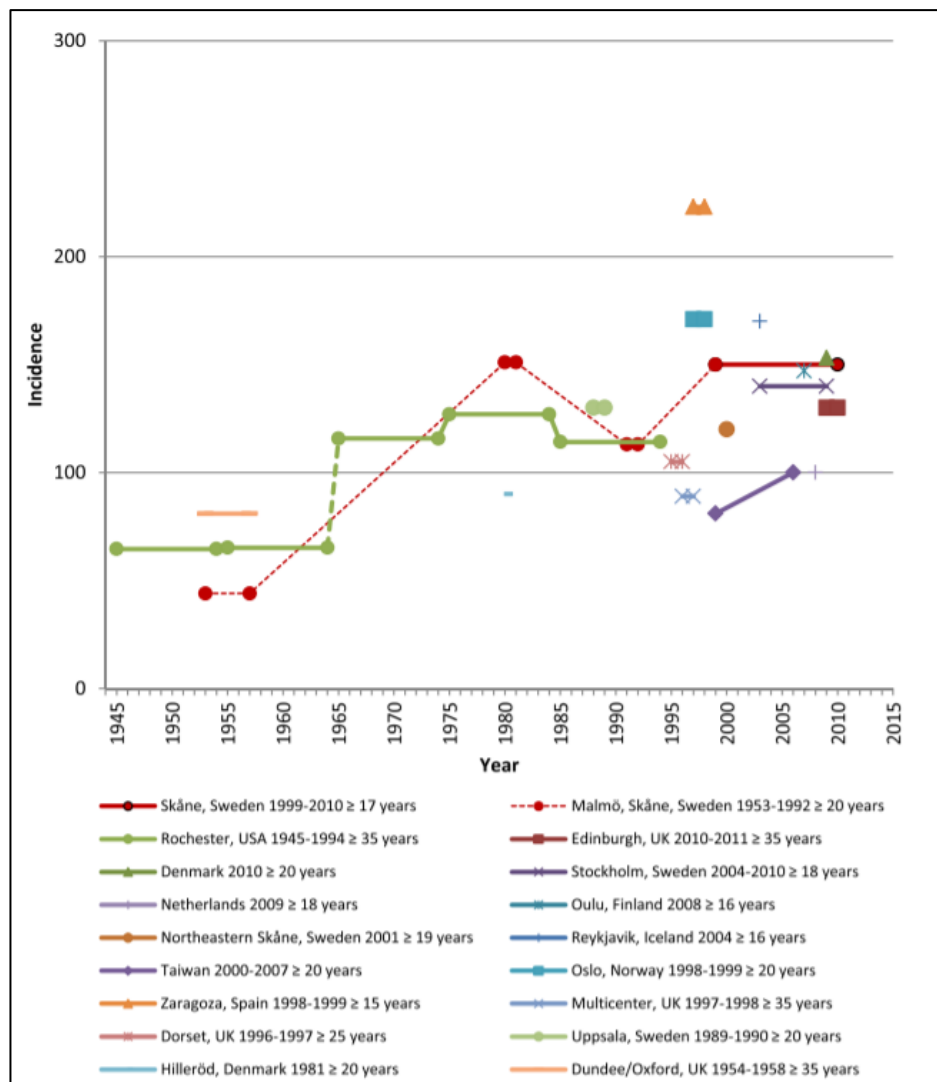


Figure 2.9: Reported incidence of distal radius fractures in men per 100 000 py over the last six decades [15]

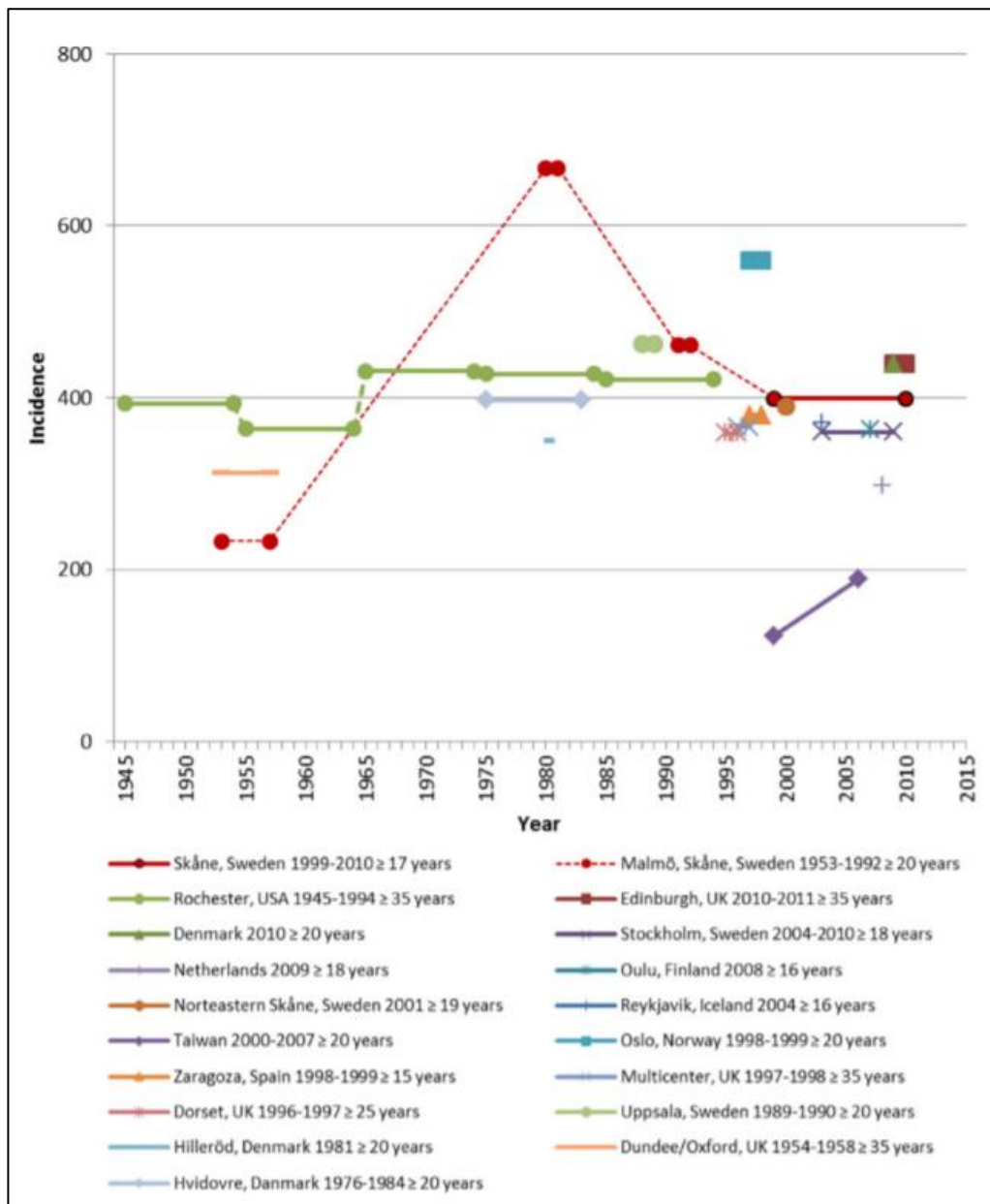


Figure 2.10: Reported incidence of distal radius fractures in women per 100 000 over the last six decades [15]

2.3.2 Risk Factors

There are multiple risk factors associated with DRFs. The most notable are age, gender, and lifestyle. The graph shown by Figure 2.11 shows a bimodal distribution of DRFs in which incidence rates for adults aged 50 and above and children aged 18 are higher than middle-aged adults. This distribution pattern is seen across all countries globally [16]. In children and young adults, sports, physical activity, and motor vehicle accidents are the most frequent causes of DRFs. In the age group above 65, women are 5 times more likely to sustain this injury than men, as Figure 2.11 also indicates [16]. Furthermore, elderly women are 50% more likely to experience a clinically significant decline in function post-injury than those without the injury. The differences in peak bone mass, risk of osteoporosis and muscle strength between men and women are likely the underlying causes for this increased risk for women. There are also seasonal factors associated with the increased risk of a sustaining DRF. Countries far from the equator where winters typically bring snow and ice present a higher risk of falling for the elderly. In contrast, countries near the equator have seen higher rates of DRFs in summer, hypothetically due to the risks associated with tropical storms [16].

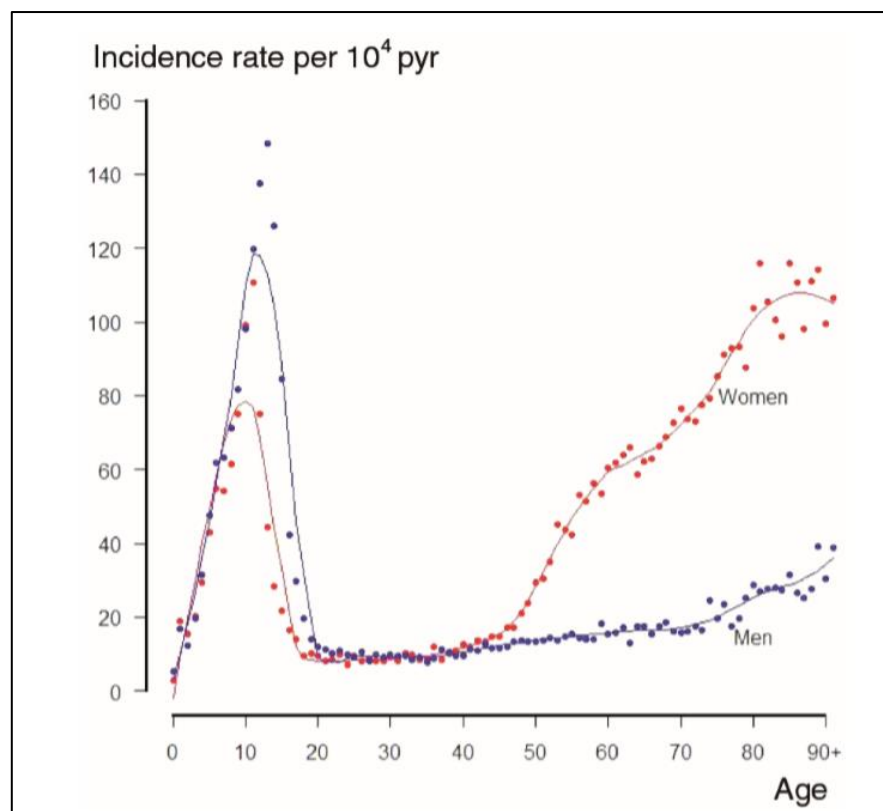


Figure 2.11: Comparison of DRF incidence between men and women by age in Stockholm, Sweden, 2004–2010 [17]

2.3.3 Treatment and Bone Healing

There are a multitude of factors affecting the type of treatment received for a DRF and therefore many treatment options. Depending on the severity of the fracture, surgery may be necessary. A fracture resulting in bone displacement requires the surgeon to re-align the bone fragments in a procedure known as a reduction. If the bone can be re-aligned without any incision this is called a closed reduction. Once the bone is realigned a cast is applied for about six weeks to allow the bone to heal [14].

Open surgery for DRF is required if bone displacement cannot be aligned through closed reduction. The procedure is called an open reduction as an incision is made to access the displaced bone fragments. There are multiple ways in which the bone can be held in place after surgery, for example, a cast, metal pins, plate and screws or an external fixator. An open fracture (where the bone pierces the skin) which often occurs in high energy trauma will require surgery as soon as possible. External or internal fixators are used to secure the bone in this case. Figure 2.12 illustrates a typical treatment protocol for distal radius fractures [14].

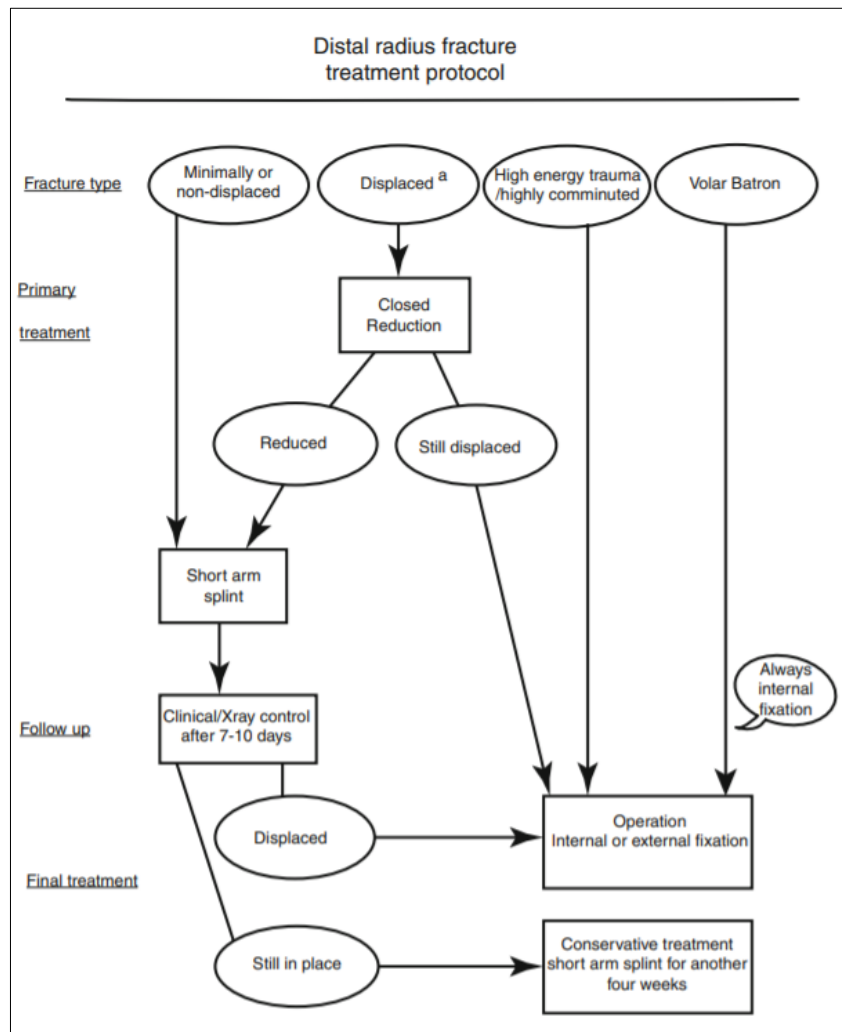


Figure 2.12: A standard treatment protocol for distal radius fractures [18]

Techniques for the immobilization of broken limbs have been around for millennia. It was not until the 19th century that Plaster of Paris was first used to immobilise fractured bones. It is still widely used today as it is inexpensive, non-toxic and is easily applied. The chemical composition of Plaster of Paris is calcium sulphate and water. Before being mixed with water, the calcium sulphate is first heated to 120°C to allow partial dehydration. Once mixed with water it hardens and sets within about 5-15 minutes [19]. As a recent alternative to Plaster of Paris, fibreglass casts or glass-reinforced plastic casts are often used. These fibreglass casts are three times stronger and only one third of the weight of traditional plaster casts. Additionally, fibreglass casts produce better x-ray images than plaster casts [20]. Fibreglass casts are, however, not used in severe fractures as it does not accommodate for swelling [19]. The images shown by Figure 2.13 are examples of fibreglass and plaster casts applied to the right forearm.



Figure 2.13: Images of fibreglass cast (left) and plaster cast (right) [21, 22]

Orthopaedic surgeons are trained in a technique called three-point fixation when applying casts. The plaster is moulded in such a way that pressure is applied at the fracture site and two other points to ensure the bone is kept straightened during immobilization [23]. This technique is illustrated by Figure 2.14.

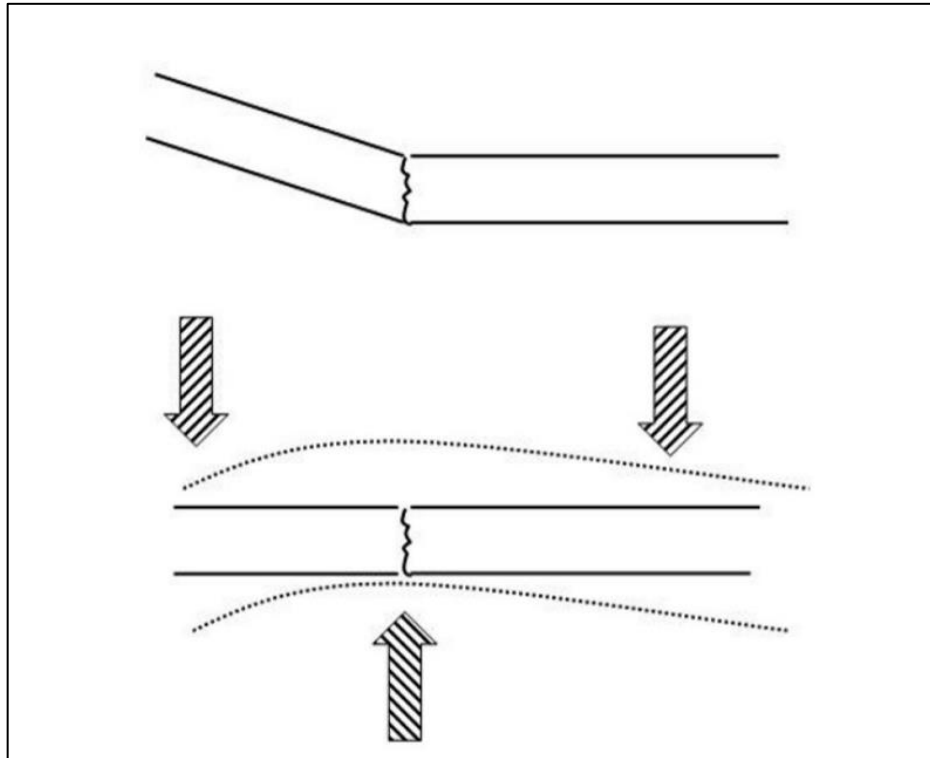


Figure 2.14: An illustration of the three-point fixation technique applied to a fracture [23]

The orientation of the pressure points are flipped depending on the type of fracture that has occurred. Additionally, the patient will have their wrist positioned in such a way so as to accommodate the pressure points and correct bone alignment. An example of this is shown by Figure 2.15.

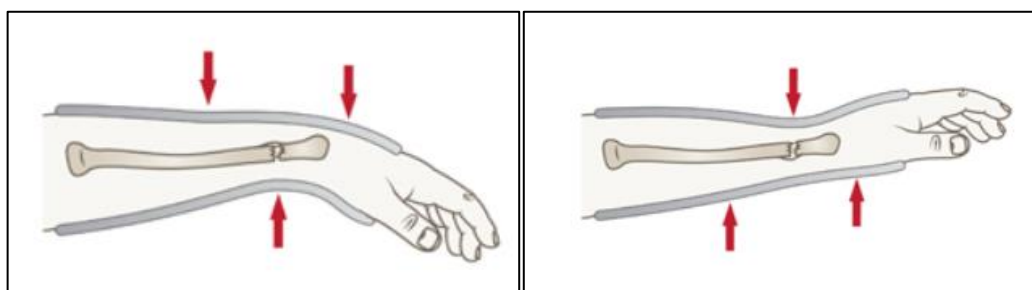


Figure 2.15: Three point fixation applied to a Colles's fracture (left) and Smith's fracture (right) [24]

Bone fractures are classified as either simple or compound depending on the amount of soft tissue damage surrounding the fracture. In simple fractures, the bone does not pierce the skin or surrounding tissue, whereas in compound fractures one or more parts of the bone penetrate the adjacent tissues and skin. Simple fractures typically take between two to three months to heal but can vary significantly depending on the age and bone health of the individual. The mechanism by which a bone heals after a fracture can be described in four stages, also shown by Figure 2.16.

1. **Formation of a fracture haematoma** – After a fracture, blood vessels inside the bone are ruptured causing bleeding. Clotted blood then forms a fracture haematoma
2. **Formation of a fibrocartilaginous callus** – During this stage there is an increase in osteoblasts (bone-matrix forming cells) in the periosteum and endosteum near the fracture site. This gives rise to regenerated blood vessels which permeate the fracture haematoma. The fracture haematoma develops into a connective tissue called a procallus. A special type of connective tissue producing cell within the procallus is called a fibroblast. These cells produce collagen fibres which assist in reconnecting the broken bones. A uniform cartilaginous tissue develops from the secretions of chondroblasts in the procallus. Eventually the procallus forms into a fibrocartilaginous (soft) callus which lasts for at least 3 weeks.
3. **Formation of a hard callus** - Osteoprogenitor cells near the fibrocartilaginous callus develop into osteoblasts and produce primary trabeculae bone. The fibrocartilaginous callus is subsequently replaced by this bone over the course of a few months, forming a hard (bony) callus
4. **Bone remodelling** – In the final phase of fracture repair, bone is remodelled as callus material is removed by osteoclasts (bone absorbing cell) over a period of 3 to 4 months. Compact bone replaces trabeculae bone, usually leaving a slight thickening around the fracture site [9].

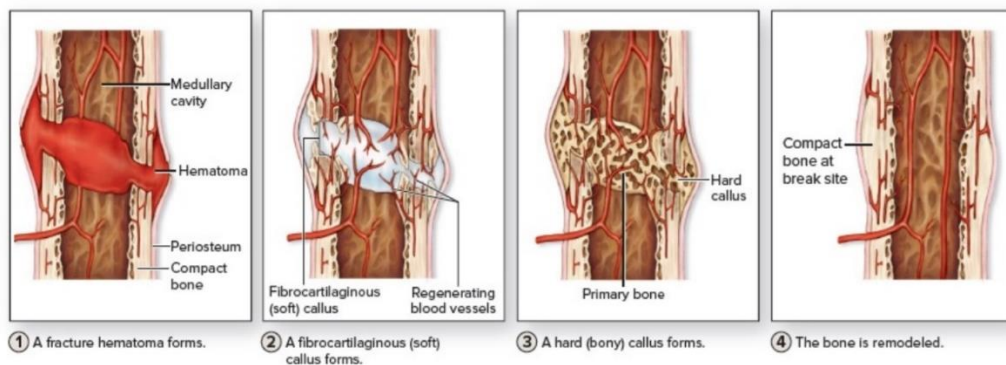


Figure 2.16: The four stages of bone fracture repair [9]

2.3.4 Complications and Disadvantages Associated with Cast Immobilization

There are several medical risks associated with cast immobilization. Long periods of immobilization can increase the risk of Deep Vein Thrombosis, especially in lower limb cases [25]. A more serious complication known as Compartment Syndrome can occur when increased pressure in a confined space limits blood circulation and tissue function. During the first application of a cast there is often a lot of swelling at the site of the fracture. Once the swelling has subsided it can then leave the cast loose and in an unfavourable position, requiring the reapplication of a new cast – a cost and time implication. Other potential risks include pressure sores, venous congestion, joint stiffness in the arm and shoulder, cartilage degradation and muscle atrophy [19].

Furthermore, tendon adhesions in the wrist is another possible complication which may arise during plaster cast immobilization. A tendon adhesion occurs when tendons bind to one another, preventing them from moving in isolation. The result is that a patient will have limited or no range of motion in the wrist or fingers. This complication can occur when patients excessively limit their finger and hand motion during immobilization or if the cast was poorly applied [26]. Finally, traditional plaster casts can feel heavy and cumbersome for a patient and are often a source of poor hygiene and bad odour. The medical methods and technology of cast immobilization have not changed in centuries and therefore newer, cheaper, and better methods are required to address the increase in incidence of distal radial fractures.

2.3.5 Rehabilitation and Prognosis

Inadequate rehabilitation following a DRF may result in unsatisfactory functional outcomes and decreased quality of life. Rehabilitation programs vary depending on several factors such as age, activity level, bone quality and injury severity. The common aim of rehabilitation, however, is to restore range of motion, dexterity and strength in the patient's wrist and fingers at a level of performance near or equal to that prior to the fracture. It has been shown that full grip strength is usually only achieved between 12 and 24 months after the DRF, with hand dexterity also being effected [27].

The chances of complete recovery can be improved by starting mobility exercises as soon as possible and preferably during the immobilization period. Unfortunately, fewer than 10% of patients are referred to therapy during immobilization [28]. Additionally, patients who do undergo therapy programs often do not comply with recommended exercises to be practiced at home as they may be weary and over-cautious of getting re-injured. A study has shown that early rehabilitative interventions may assist in

quicker recovery of digit range of motion during immobilization [2]. Furthermore, there is evidence to suggest that early rehab interventions can reduce the number post-immobilization therapy visits [28]. To address these issues, research has already been undertaken to test the validity and reliability of using a wearable activity monitor to quantify arm activity in adults who have sustained a DRF [29].

Tendon gliding exercises are commonly prescribed to a patient with an immobilized wrist as they may help restore finger range of motion and prevent tendon adhesions [3]. As the name implies, the different exercises isolate individual flexor tendons and allow them to 'glide' over each other. Figure 2.17 illustrates these exercises and are named (from left to right) as straight hand, hook fist, full fist, flat fist (also called straight fist), and thumb flexion. Some physicians have also discussed the potential use of passive finger motion in very early stages of DRF rehabilitation. Passive finger motion is where the fingers on the hand of the fractured wrist are flexed and extended using only the non-injured hand i.e. finger motion is not actively initiated by the muscles in the forearm of the injured wrist. The speculated reason for passive finger motion as an early stage rehabilitative intervention is that it might promote tendon and joint mobility without causing excessive strain to the soft callus tissue as referred to by the second image of Figure 2.16 [30].

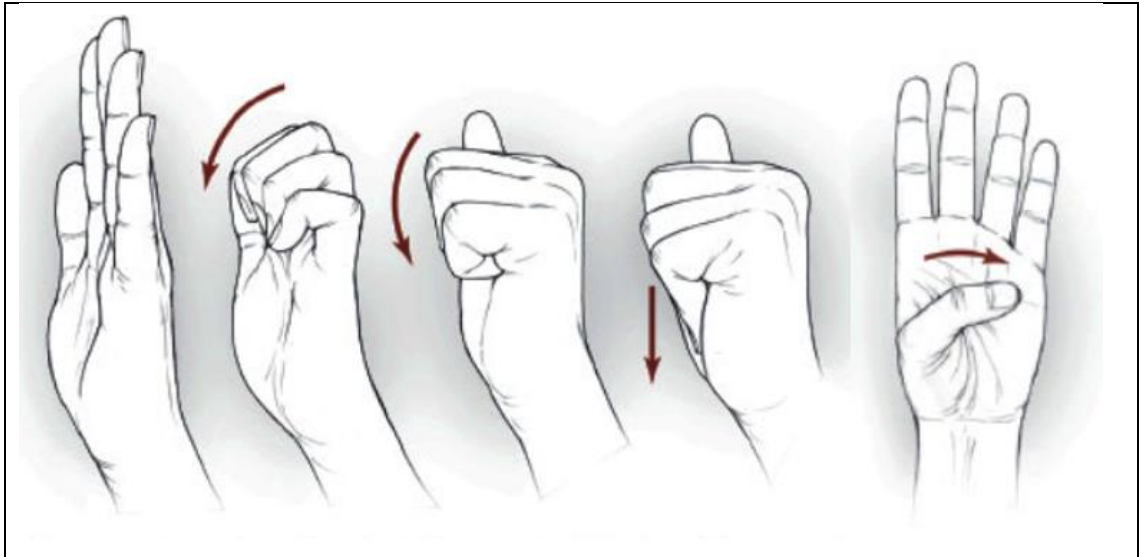


Figure 2.17: Tendon gliding exercises recommended for DRF patients [31]

Clinical outcomes for DRFs are commonly measured objectively through radiographic parameters, wrist, and finger range of motion (ROM) and grip strength. While these are important benchmarks for successful clinical outcomes, emphasis on patient-rated outcome measures are regularly becoming a standard part of rehabilitation as patients are more interested in their ability to execute everyday functional tasks [28]. Therefore, two commonly utilized patient-rated functional outcome systems for DRFs are the DASH (Disabilities of Arm, Shoulder and Hand) and PRWE (Patient-Rated Wrist Evaluation) scale questionnaires [28, 32]. These questionnaires employ a range of questions or statements in which a patient is asked to rate the difficulty or ease with which they can perform certain functional tasks, such as turning a key or using a knife to cut food [33]. Correlations between patient-rated measures and clinical measures have been shown to be inconsistent, which therefore necessitates the use of both outcome measures to provide an overall complete perspective on rehabilitation success [28].

2.3.6 The Zero-Cast Wx Solution

Surgisplint Ltd, a start-up company based in Auckland have developed a novel wrist-brace called Zero-Cast Wx for patients who have suffered a DRF. This plastic injection-moulded wrist brace is an adjustable orthosis which has been designed to replace plaster and fibreglass casts typically used to immobilize a DRF. Zero-Cast Wx consists of two clamping plates, the volar and dorsal plate, a hand bridge, and C-arm as shown by Figure 2.18. The injection-moulded plastic and foam lining materials make it lightweight, breathable and waterproof. Zero-Cast Wx comes in sizes 2,3 and 4 for both left and right wrists [1].



Figure 2.18: An illustration of Zero-Cast Wx components [1]

As referred to in subsection 2.3.4, a common problem seen in patients who have worn a plaster cast for up to eight weeks is that they lose mobility and function of the joints and tissues near the fracture site. This is mainly caused by cast immobilization which does not allow the patient to maintain hand function and ROM. The Zero-Cast Wx system has been designed to solve this problem by immobilizing the fracture site securely with three-point fixation while still enabling the patient to have significant hand function and ROM, features not afforded by either traditional plaster or fibreglass casts.

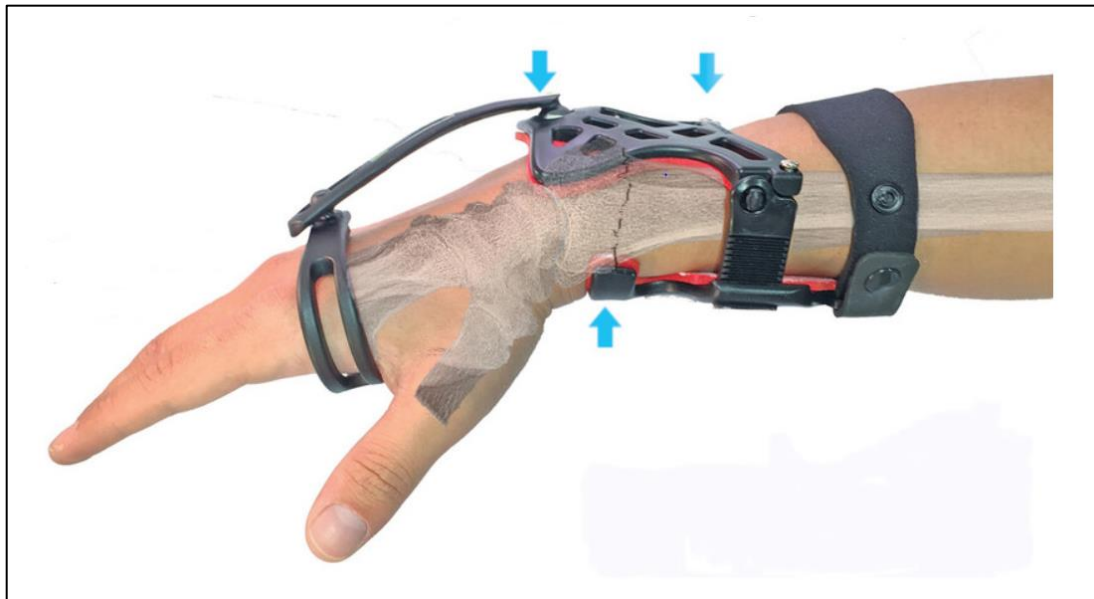


Figure 2.19: Three-Point Fixation applied in the Zero-Cast Wx [1]

2.3.7 Proposed Smart Enhancements to Zero-Cast Wx

Although Zero-Cast Wx offers many benefits such as being waterproof and lightweight, two immediate opportunities for further improvement have been identified by the Surgisplint team. The first is to produce a more objective method of how tight the brace is to be fitted. At present, there is a general fitting protocol which trained clinicians are recommended to follow. This protocol involves two stages which determine the fit of the brace, the ratchet arm fit and the dorsal tilt fit. During the ratchet arm fit, the clinician guides the ratchet arms of the dorsal plate through the slots of the volar plate. This step is illustrated by Figure 2.20.



Figure 2.20: Image showing the dorsal plate fitted to the volar plate via ratchet arms [34]

The proximal end of the dorsal plate is said to be adequately fitted when there is sufficient skin 'spill-over' and when the proximal strap is higher than the dorsal plate. An example of a good fit as defined by the Surgisplint guidelines is shown by Figure 2.21. Once a good fit has been achieved, the ratchet arms are locked into place by rotating the volar plate locking screws to the 'locked' position as shown by Figure 2.22.

A potential problem with using skin 'spill-over' as a measure of fit quality is inconsistent pressures across patients. There are inherent differences in skin and soft-tissue thickness among men, women, and children. These differences are attributed to body fat, water retention and muscle mass. A patient with high body fat and water retention for example, is likely to show skin 'spill-over' before the correct fitting pressure is obtained. Furthermore, any localized swelling and inflammation due to the fracture may also exacerbate the problem of using skin 'spill-over' as an indicator of a good fit.

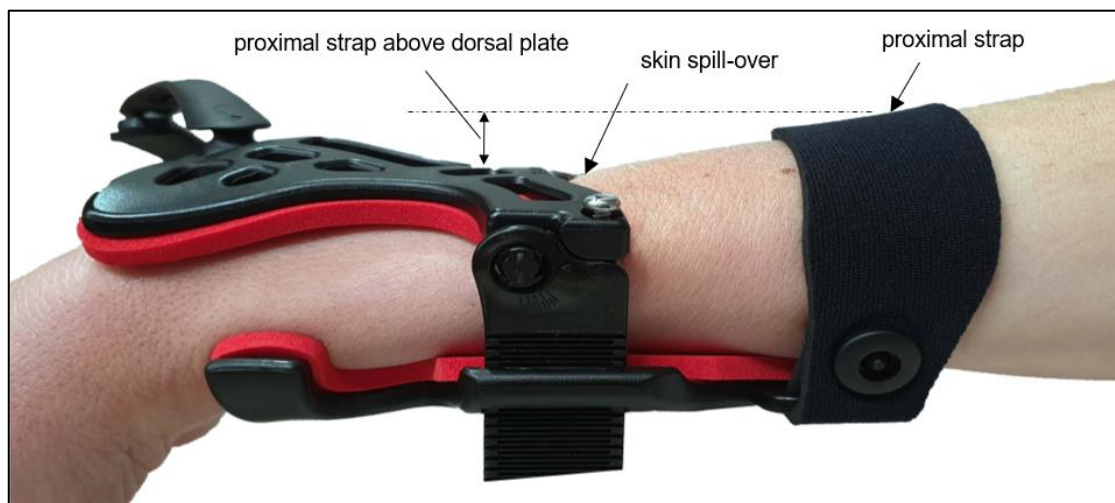


Figure 2.21: Image showing a correctly applied ratchet arm fit as per current fitting guidelines [34]



Figure 2.22: Image of volar plate locking screw [34]

The dorsal tilt fit is the second stage of the brace application. It involves tightening two ratchet arm screws that control the tilt angle of the dorsal plate which in turn increase fitting force at the distal end of the wrist. This is illustrated by Figure 2.23.

The protocol for the dorsal tilt fit is to tighten the ratchet arm screws until they are flush with the surface of the dorsal plate. A problem with this protocol is that there may be significant variations in applied pressure across patients due to varying forearm morphology. Similar to the ratchet arm fit, this could be caused by a combination of soft-tissue and wrist circumference variations. In addition to these two fitting protocols, clinicians also have to rely on the subjective feedback of the patient, many of whom will have vastly different comfort and pain thresholds. In light of these observations, this project investigated possible ways of quantifying the brace fitting force, thereby giving clinicians a more objective measure of classifying fit quality. Another possible benefit of having the fitting pressure data is that it could inform the physician if any swelling occurs in the days and weeks following the application of the brace.

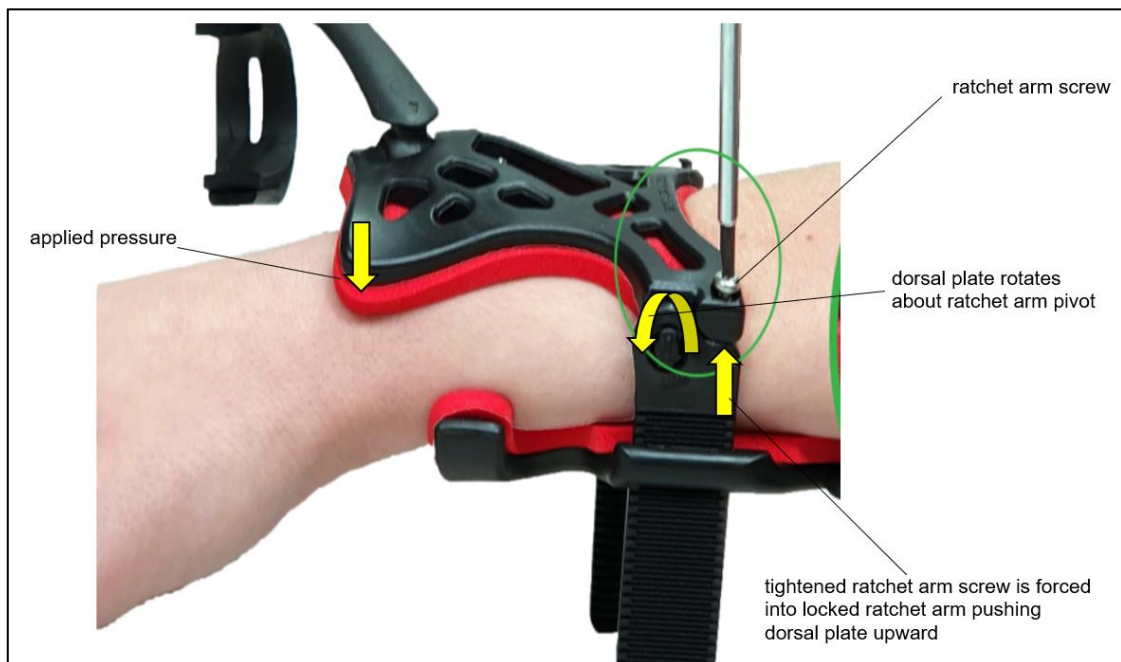


Figure 2.23: An image illustrating the dorsal tilt fit

The second development opportunity investigated by this project involves the potential use of Zero-Cast Wx as an early rehabilitation tool for DRF patients. As subsection 2.3.5 alluded to, there may be considerable benefit to a DRF patient if early rehabilitation is initiated, as it may mitigate the risks associated with immobilization such as joint stiffness, muscle weakness and tendon adhesions.

As section 1.2 briefly mentioned, the team at Surgisplint have expressed their interest in developing an electronically integrated proof-of-concept (POC) brace which could record and classify rehabilitative hand motion artefacts and remotely transmit this data for clinical analysis. Such a device could provide clinicians with new insights into the patient's progress, while possibly also being used to collect evidence for better rehabilitation methods. Furthermore, a virtual rehabilitation solution for DRFs could save substantial costs for both clinician and patient in the future.

2.4 Smart Wearable Technology

The following subsections will briefly look at the critical technologies and methods which have allowed wearable health and medical devices to emerge in the consumer market. In particular, the literature on hand motion recognition technology will be looked at in some detail as it guided the decisions made in later stages of this project.

Biomedical engineering has seen rapid developments in the area of smart wearables for the purpose of gathering and monitoring physiological data over recent years. These developments can be attributed to improvements in small-scale electronics, lower manufacturing costs, and the increasing prevalence of mobile computing. In 2017 the annual growth in wearable devices was 17% with over 300 million devices in sales, and projections have been made for over 500 million in sales by 2021. It should be noted, however, that most of these wearable devices were consumer products for general health and well-being. These devices mainly include smart-watches, fitness trackers and body-worn cameras, all of which provide data and measurement accuracy of insufficient quality for medical grade applications [35]. While no formal definition for a *smart wearable medical device* has been established, there is certainly an emergence of such devices that broadly fit this description. Separately defining the constituent terms of a *smart wearable medical device* can provide a contextual definition. A *Smart wearable* can be defined as an integrated biomedical sensor that can be worn on or implanted in the body, providing near real-time digital feedback of some physiological parameter/s for the purpose of monitoring and enhancing health or well-being. The diagram shown by Figure 2.24 illustrates the concept of a *smart wearable*, also commonly referred to as *wearable biomedical sensors* [36, 37].

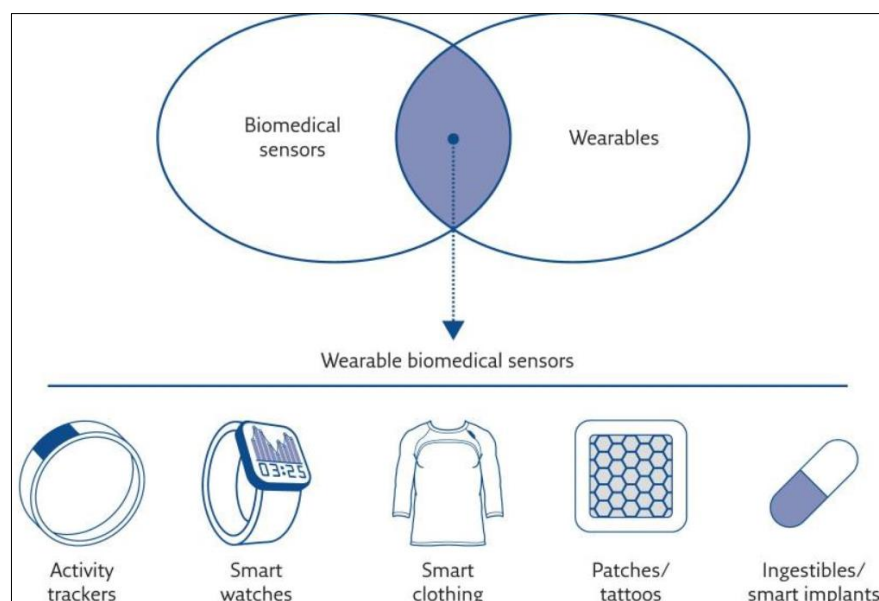


Figure 2.24: Examples of smart wearable devices [36]

A *medical device*, broadly speaking, is a machine, contraption or instrument that is used for the diagnosis, treatment, monitoring or prevention of a disease or physical condition [35, 36]. Figure 2.25 shows several illustrations of common medical devices found in most hospitals and clinics. Combining these separate definitions provides a contextual understanding for the term *smart wearable medical device*.

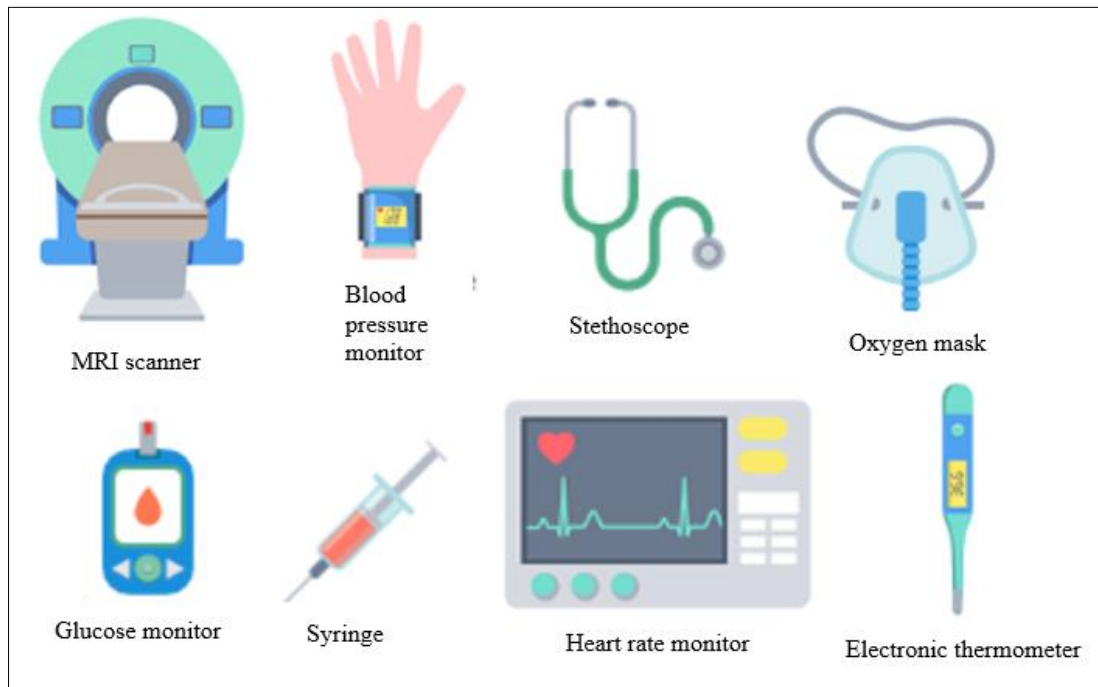


Figure 2.25: Illustrations of common medical devices [38]

The following subsection considers some of the fundamental technologies that are common to both *smart wearables* and *medical devices* which have enabled their successful design and manufacture.

2.4.1 Sensors, digital communication, and signal processing

One of the most valuable technologies which has allowed us to accurately get information about our environment is a sensor. A sensor is a device that detects a physical property by responding to an input stimulus. The input stimulus, referred to as the measurand produces a functionally related output. Sensors are often interchangeably used with transducers, however, there are important differences. A transducer, more accurately, is a device that converts one form of energy to another. Typically, the term ‘transducer’ is used to refer to devices such as sensors, actuators, and transistors.

A sensor usually consists of two components: a sensitive element and transducer. The sensitive element can interact with the measurand and in doing so changes the functioning of the transducer. The transducer then produces an electrical signal which is transformed into digital information via a data acquisition system. Subsequently, this information is processed into a meaningful format and stored for analysis and action to be taken [39]. Figure 2.26 shows a schematic diagram of a typical sensing system.

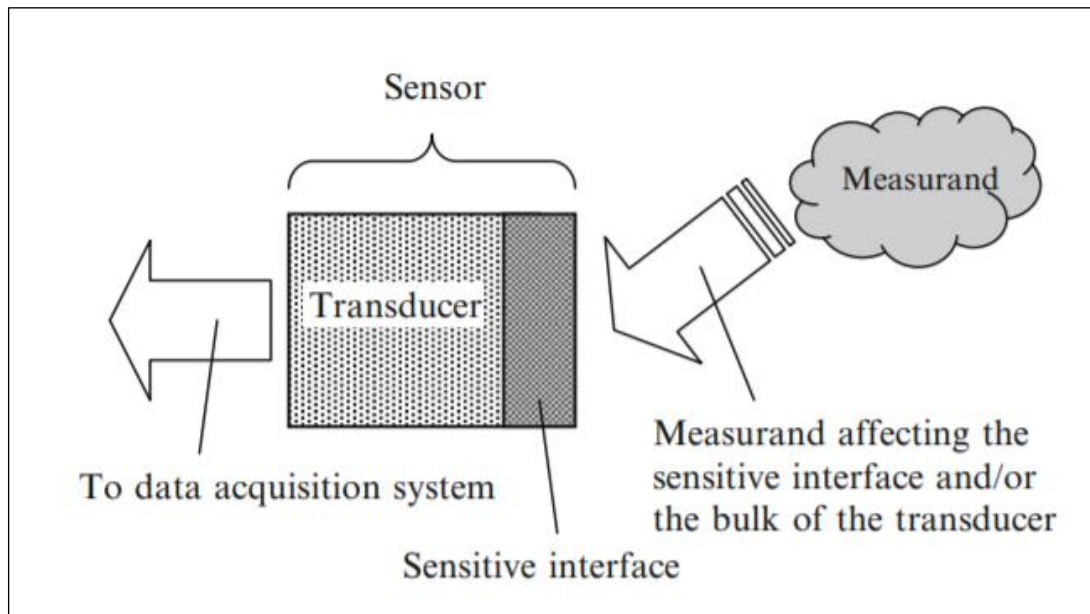


Figure 2.26: A schematic diagram of a sensing system [39]

A signal is a piece of information or data expressed as a time-based function. This information is typically expressed as a series of amplitudes over regularly spaced intervals of time via a communication system. Digital communication systems form the foundation for almost all modern electronic devices through which signals are received and transmitted. Digital communications is a vast and complex subject and therefore only the fundamental concepts will be summarized in this review.

Figure 2.27a shows a block diagram of typical communication system regardless of its application or configuration. The three primary elements of all communication systems are the transmitter, channel, and receiver. The input transducer, which could be a microphone for example, converts the information source output into an electrical signal that varies with time. The transmitter then converts this electrical output into a form which can be sent through a physical channel such as a cable. The transmitter often changes the signal characteristics of the input transducer to match those of the channel via a process known as modulation. Additionally, the transmitter performs other functions like signal filtering and amplification. Since the channel is a physical medium, the signal is degraded in various ways through noise, interference, and distortion, for example. The receiver performs multiple functions, primarily demodulation, filtering, and amplification of the signal. The output transducer, for example, a speaker, converts the receiver output into a form appropriate for the information sink [40].

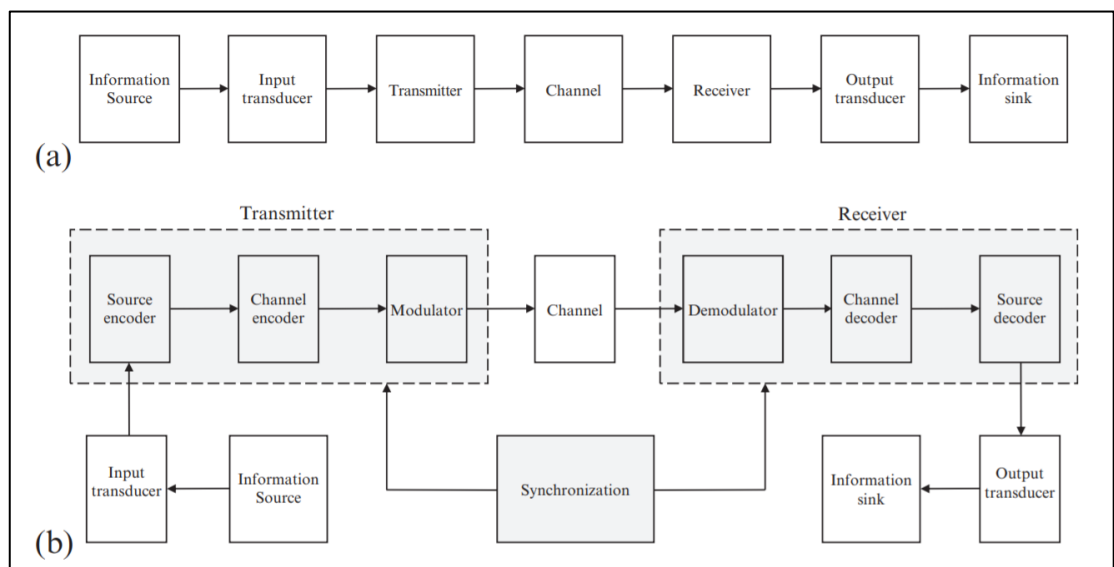


Figure 2.27: Block diagrams of a) communication system and b) digital communication system [40]

Signal processing is a scientific technique within the field of digital communications that analyses and processes signals in order to obtain meaningful information. This technique is essential in science and engineering as many signals cannot be utilised or comprehended due to interference such as noise. A signal can be classified as analogue, discrete or digital as shown by Figure 2.28. Most natural signals are analogue signals which are continuous functions of time. To process analogue signals digitally, an analogue to digital converter (ADC) is required which allows the signal to be passed to a digital signal processing unit (DSP). The output of the DSP are passed to a digital to analogue converter (DAC) which is used to convert the modified signal to analogue form again [41]. This is illustrated in the block diagram shown by Figure 2.29.

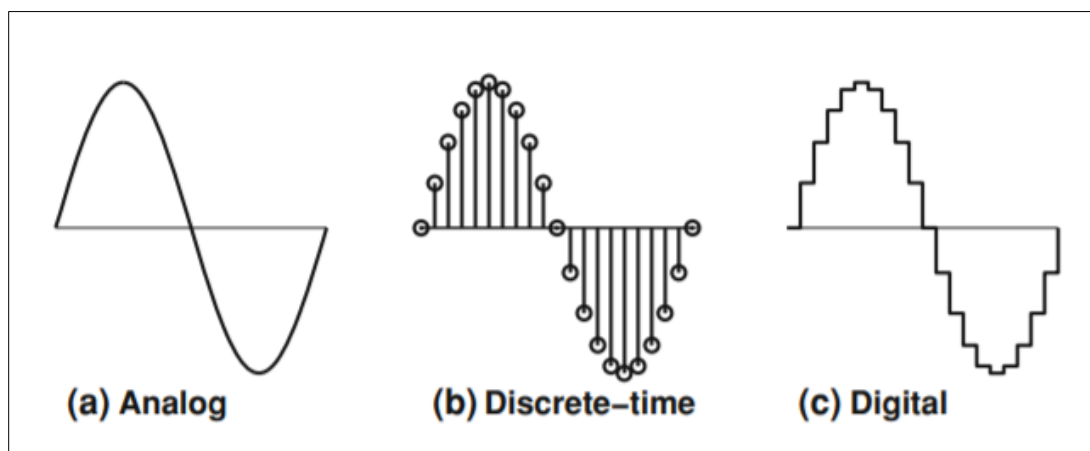


Figure 2.28: A sinusoidal signal represented in three forms [41]

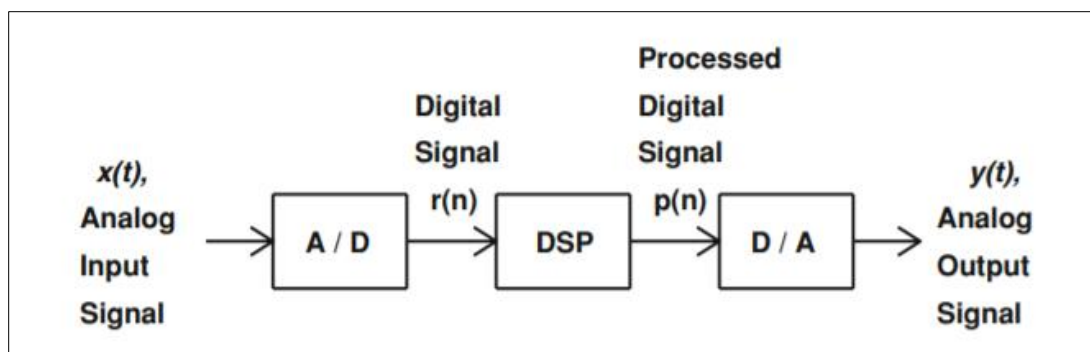


Figure 2.29: A block diagram showing a typical signal processing system [41]

2.4.2 Machine Learning

Machine learning (ML) is an applied science that combines knowledge from the fields of computer science and statistics to infer patterns from input data in order to make predictions about new unseen data [42, 43]. For example, consider the image recognition problem of recognizing a dog or cat in a photograph. A large dataset of cat and dog images, with each image correctly labelled or tagged, is an example of what we want a computer to 'learn'. In order for an ML algorithm to do this, it has to 'learn' a model or a set of rules from a labelled dataset so that it can make correct label predictions on a new dataset. This technique is called supervised machine learning and is used in a wide range of applications today.

Research on solving complex problems with machine learning was fairly slow until the rise of the internet, advances in data storage technology and computing power. These advances allowed for very large datasets to become available and subsequently the development of ML solutions. Examples of practical ML applications now include text recognition for smartphones, speech recognition, driverless vehicles, and gesture recognition devices. There are various machine learning models or techniques, all of which have specific dataset requirements. The block diagram shown by Figure 2.30 is a breakdown of the various machine learning techniques [44, 45].

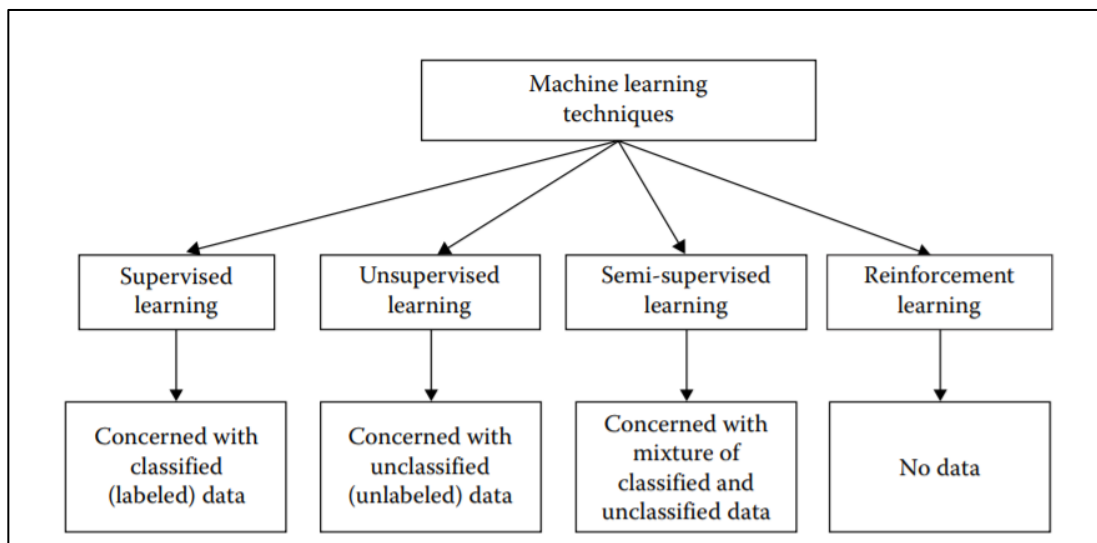


Figure 2.30: Block diagram of machine learning techniques [44]

Supervised learning

Supervised machine learning is a model where a labelled dataset is provided from which associations can be made between the datapoints and their corresponding labels. Thus, when a new datapoint is passed to the algorithm, it can predict the correct label or answer [43]. The example of cat and dog images referred to earlier is an example of supervised learning.

Unsupervised learning

In unsupervised machine learning the model is given a dataset without any labels. Given a large enough dataset, the algorithm identifies common characteristics between data and forms groups known as clusters [43]. Revisiting the example of cat and dog images, the algorithm would be given a dataset of cat and dog images without any of the images labelled. The algorithm would only be able to identify two distinct categories without knowing either as 'cats' or 'dogs'.

Semi-supervised learning

A semi-supervised learning model uses a dataset containing labels for some datapoints. Clusters will be formed for similar datapoints by the algorithm and it will then use the few labelled datapoints to label other datapoints in the same cluster. This learning model can provide time-saving benefits as not all datapoints are required to be labelled [43].

Reinforcement learning

The reinforcement learning model is a fast-developing and specialised area of ML where there are changing situations and large state spaces. For example, situations such as games like chess and backgammon or autonomous vehicles require that the algorithm constantly changes in response to feedback data from the environment [43].

Machine learning problems can broadly be separated into three categories:

1. Classification – where an object or idea is to be classified into two (binary) or more categories (classes). For example, image recognition of a cat or dog or classifying email as spam or not.
2. Clustering – a method whereby a large unlabelled dataset are grouped into clusters, such that points in each cluster have common properties.
3. Prediction – models built to forecast the future value or state of something based on historical data. For example, using consumer trends to predict sales output of a new product [43-45].

This project seeks to solve various classification problems (classifying correct brace fits and various hand motion artefacts). The remainder of this subsection will therefore look at classification and its associated algorithms in some more detail.

Classification

Classification is a supervised learning technique where a labelled dataset is used to train an algorithm that can be used to classify unseen data into two or more categories. The model trained from the labelled data is known as a classifier. Classifiers can either be binary classifiers (two classes) or multi-class classifiers. The previously mentioned algorithm of identifying cats or dogs is an example of a binary classifier. In the example graph shown by Figure 2.31, the axes represent *features* of a dataset. This could be height and length in the example of classifying dogs and cats. The data points are said to represent feature vectors in a two-dimensional space [43].

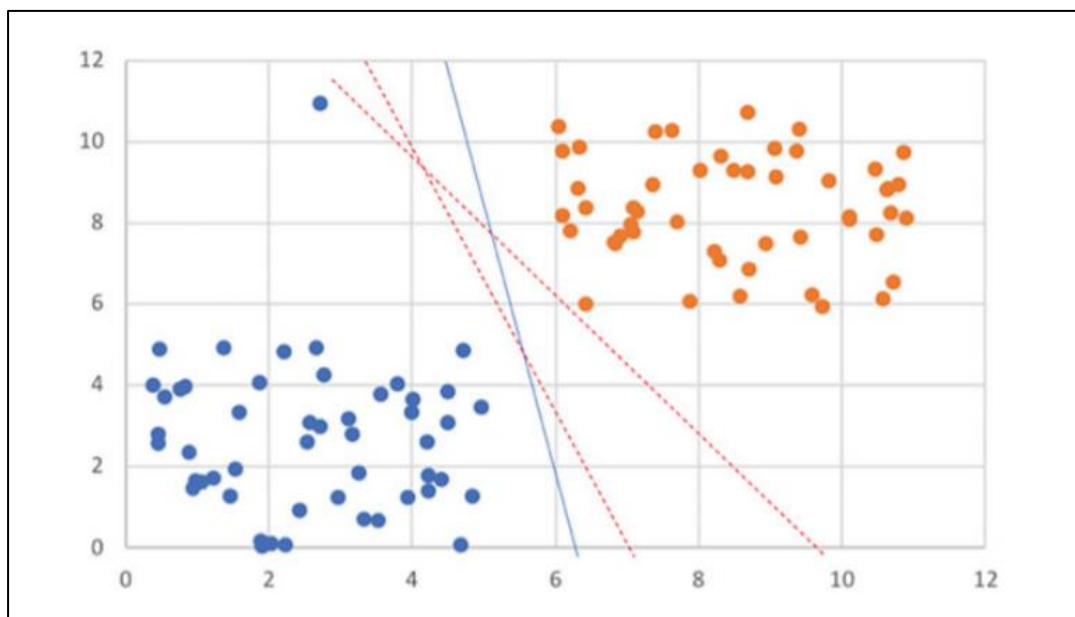


Figure 2.31: A graphical illustration of a binary classifier showing multiple linear decision boundaries [43]

In many problems the dataset cannot be separated by a linear boundary. In such cases supervised learning algorithms known as support vector machines (SVMs) can classify the data with a non-linear boundary. This is illustrated by Figure 2.32. Multiclass classifiers can be created by combining multiple independent binary classifiers. In the example shown by Figure 2.33, the classifier has a horizontal and vertical decision boundary separating four classes of data. The classification algorithms used in this project will be discussed further in Chapter 5 and in more detail in Appendix B.

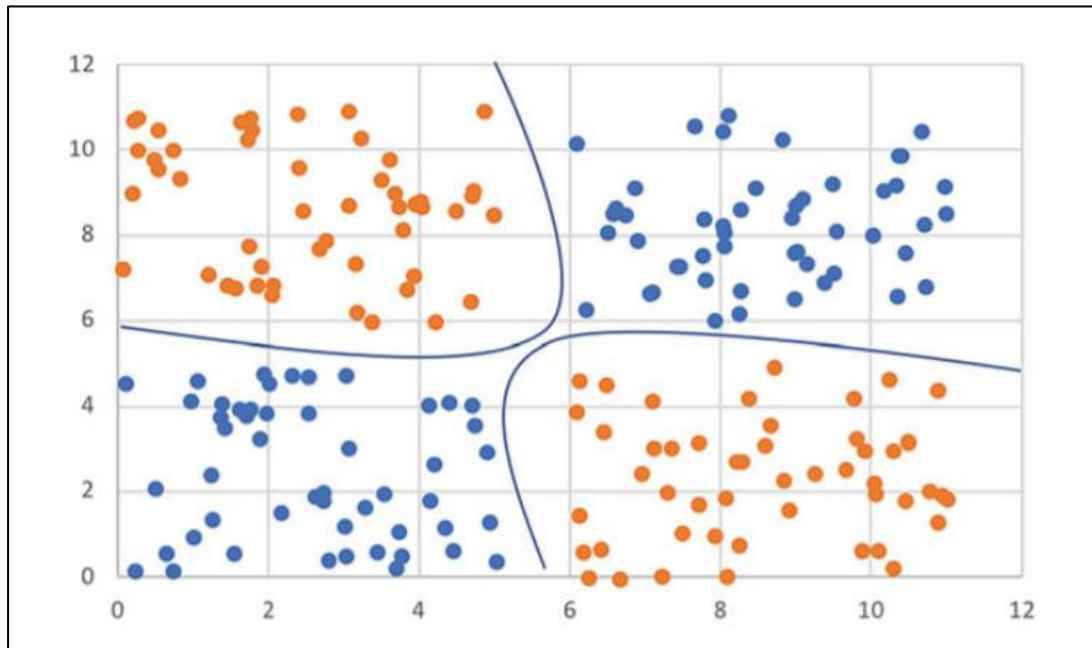


Figure 2.32: A graphical illustration of a non-linear decision boundary [43]

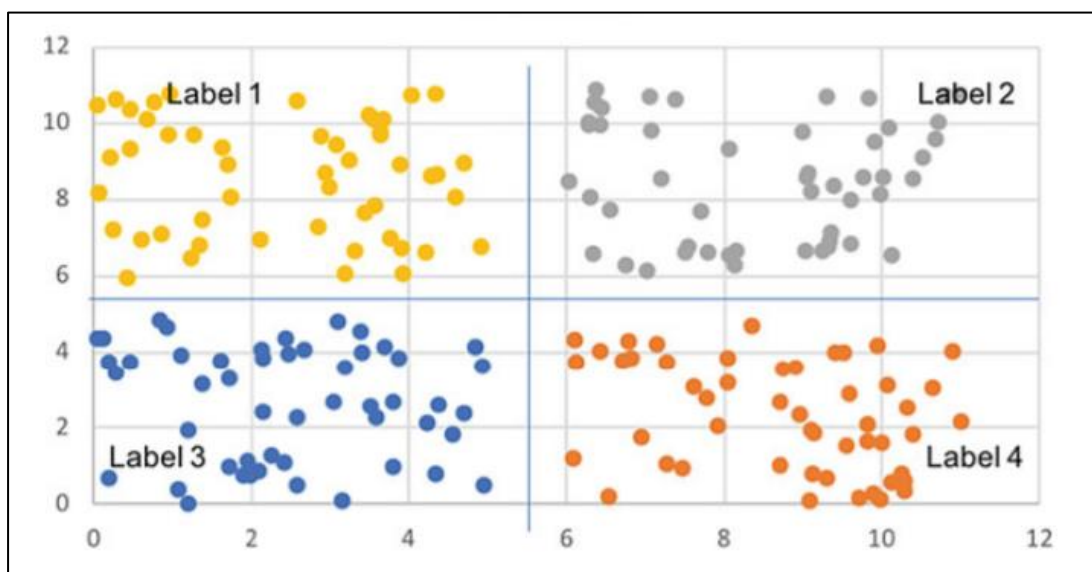


Figure 2.33: A graphical illustration of a multiclass classifier using two linear decision boundaries [43]

2.4.3 The Internet of Things

The internet of things (IoT) is a system of interconnected devices that are digitally tagged with a unique identifier and that can communicate with each other over a network without requiring physical interaction between a human and computer. A 'thing' in the internet of things refers to an object or physical host on which the computing device is attached. An IoT system consists of internet-enabled smart devices that retrieve, transmit and act on data from their environment [46]. These systems are used in almost all industries from manufacturing, medicine, and agriculture to name a few, and serve to improve efficiencies and performance. As an example, the IoT in a building automation system may acquire data from CO₂ sensors in offices, which is then sent to the building management system that signals a fresh air fan to increase power when a threshold point is reached.

2.4.4 Examples of Smart Wearable Medical Devices

Wearable devices of medical-grade quality for the purpose of monitoring, diagnosing, and managing illnesses are still in the infancy stages of development. The reasons for this lie in the inherent challenge of designing products which meet strict medical requirements, and which can produce data that provides clinicians with valuable and actionable insights on the patient's condition [35, 36]. As the world's elderly population increases, so will our need to change the way we treat and manage disease and chronic conditions. Leveraging the power of micro-electronics, big data, the IoT and ML may provide the answer in revolutionizing the healthcare industry [37]. The challenge, however, is seamlessly integrating sensors with non-invasive and wearable products or clothing, a necessary task to be undertaken if medical-grade wearable devices are to become a reality. Fortunately, this could be achieved in the near future as advances are being made in smart-sensors with flexible and non-toxic materials [47].

The examples shown by Figures 2.34, 2.35 and 2.36 illustrate the various applications and current developments in smart wearable medical technology. A key feature common to all of these devices is that they enable the clinician to monitor the patient's condition remotely through dedicated app software and cloud-based data storage.



Figure 2.34: TracPatch, is a smart wearable medical device for tracking patient rehabilitation post-knee surgery [48]



Figure 2.35: E-vive uses app-controlled muscle stimulation for patients who have undergone knee surgery [49]



Figure 2.36: CarbonHand is a grip enhancing device for patients with orthopaedic or neurological problems [50]

2.4.5 Medical Device Regulation

There is an important distinction between a health or wellness device and a medical device. Medical devices usually need to conform to strict regulations set out by a regulating body. Manufacturers of any medical devices require that their product be registered and regulated by a national or regional body that govern the design, manufacture, and use of such devices. In the United States, for example, a branch of the Federal Drug Administration (FDA) called the Centre for Devices and Radiological Health (CDRH) regulates companies that manufacture, package, or import medical devices that are sold. These devices include medical and non-medical radiation-emitting products. Before any new product can be marketed and sold, the engineers and manufacturers need to determine if their product is regulated by the FDA or if similar products are regulated [51]. They recommend following two steps to achieve this:

1. Determine if the product meets the definition of a medical device in accordance with Section 201(h) of the Food, Drug and Cosmetic act
2. Determine if a suitable product classification exists for the product

The FDA defines a medical device as:

“An instrument, apparatus, implement, machine, contrivance, implant, in vitro reagent, or other similar or related article, including a component part, or accessory which is:

1. *recognized in the official National Formulary, or the United States Pharmacopoeia, or any supplement to them,*
2. *intended for use in the diagnosis of disease or other conditions, or in the cure, mitigation, treatment, or prevention of disease, in man or other animals, or*
3. *intended to affect the structure or any function of the body of man or other animals, and which does not achieve its primary intended purposes through chemical action within or on the body of man or other animals and which does not achieve its primary intended purposes through chemical action within or on the body of man or other animals and which is not dependent upon being metabolized for the achievement of its primary intended purposes. The term "device" does not include software functions excluded pursuant to section 520(o).”*

If the device is regulated or requires regulation, then it will be classified into one of three classes, class I, II or III, which increase with regulatory control. The device and company then need to comply with numerous requirements throughout the product lifecycle [51]. Medical devices distributed in Europe are similarly regulated by the

European Commission (CE). Medical devices in the European Union are currently regulated by three separate directives. These directives are:

1. Active implantable medical devices
2. Medical Devices
3. In vitro diagnostic medical devices

As of May 25th, 2017, two new regulations on medical devices and in vitro diagnostic medical devices have been implemented to keep up to date with the advances made in science and technology. These regulations will eventually replace the three directives in 2022 [52].

2.4.6 Hand Motion and Gesture Recognition Technologies

The human hand is one of the most complex anatomical structures, providing sophisticated motor functions which help us complete a broad range of tasks. With the largest number of degrees of freedom compared to any other human body part, the hand epitomizes what it means to be human in many ways. There has been considerable research interest in the human-computer interface over the past two decades. In particular, research on hand motion and gesture recognition has garnered much attention due to the vast number of applications [53]. For example, being able to accurately map forearm muscle activation to hand motion would allow hand amputees to control robotic hands. Measuring hand motion or tremors in patients with neurological or musculoskeletal conditions could provide physicians and physical therapists with valuable insights on rehabilitation, disease progression and prognosis [53, 54]. Furthermore, the applications in the commercial sector are growing rapidly given the rise in popularity of smart wearables for smartphones, gaming and controlling computer peripherals. Various techniques and methods for quantifying and classifying hand motion have been developed throughout numerous studies. The following subsection explores recent literature on hand motion recognition technology and considers the pros and cons associated with some of them.

a) Surface Electromyography

Electromyography is a technique for measuring bioelectric signals generated by contracting muscles. Surface electromyography (sEMG) is a non-invasive method of detecting these signals by using adhesive skin electrodes. An EMG signal correlates with the force applied by a muscle and hence can be used to predict the motion and/or position of associated limbs. Tenore et al [55] demonstrated a 90% classification accuracy of individual finger flexion and extension motion using 32 electrodes on the forearm. You et al [56] achieved an accuracy of 97.75% in classifying finger flexion

using only four electrodes. Figure 2.37 shows a smart wearable called the MYO armband which was used by Zhang et al [57] to classify five hand gestures with an accuracy above 98%.

A number of other studies have shown impressive accuracy in distinguishing between a large number of gestures using many electrodes. The technique has positive implications for research in robotic prostheses. There are limitations, however; accuracy diminishes with reduced surface area and improper positioning of electrodes; a restriction which presents a challenge in integrating this technique with wearables [58, 59]. Furthermore, it is challenging to distinguish individual signals from deeper lying muscle tissue.



Figure 2.37: Zhang [57] used the MYO armband – an sEMG based device for real-time classification of five gestures with an accuracy of 98.7% (image [60])

b) Force Myography or Pressure Distribution Mapping

Force Myography (FMG), also referred to as Pressure Distribution mapping (PDM) is a non-invasive technique that uses force sensors to detect force patterns produced by changes in limb contour when underlying muscles and tendons are contracted or relaxed. Each force pattern corresponds to a unique movement or position of the limb relative to a default state. This data can then be used to predict limb positions or motion by training a machine learning algorithm [61-63]. This technique typically makes use of an array of Resistive Polymer Thick Film Sensors (RPTF), also simply referred to as Force Sensing Resistors (FSR) which are devices that exhibit a decrease in resistance with an increase in applied force [64]. The use of FSRs in hand motion or gesture recognition provide a low-cost and simpler alternative to other methods. Dementyev and Paradiso [65] demonstrated an 80% classification accuracy for five gestures in their wrist-worn device called WristFlex as shown by Figure 2.38. WristFlex used 15 FSRs to measure pressure changes in the circumference of the wrist. Li et al. [61] used an array of 32 FSR's to classify up to seventeen finger motions with an accuracy above 99%. A challenge with this method is in producing repeatable cross-session results as changes in wrist orientation and the strap positioning affect accuracy.



Figure 2.38: The WristFlex prototype used 15 FSRs in a custom Velcro wrist strap [65]

c) Electrical Impedance Tomography

Electrical Impedance Tomography (EIT) is a non-invasive technique that produces a cross-sectional impedance distribution of an object using impedance measurements from oppositely paired surface electrodes. Changes in hand position result in a change in the interior structure of the arm as muscles and tendons contract. These differences can be determined using EIT. This method was used by Zhang and Harrison [66] in their prototype wrist-worn device, Tomo shown by Figure 2.39. It used eight copper electrodes to classify ten hand gestures with 92% accuracy.

d) Near Infra-Red Diffuse Tomography

A similar technique to EIT uses infrared emitters and receivers to generate an impedance image of an interior structure. McIntosh, Marzo and Fraser [58] used this technique in their wrist-worn device, SensIR shown by Figure 2.40. The device was constructed of fourteen emitter-receiver pairs, from which 196 measurements could be taken to generate a light transmission image. SensIR could detect twelve gestures with 93% accuracy.

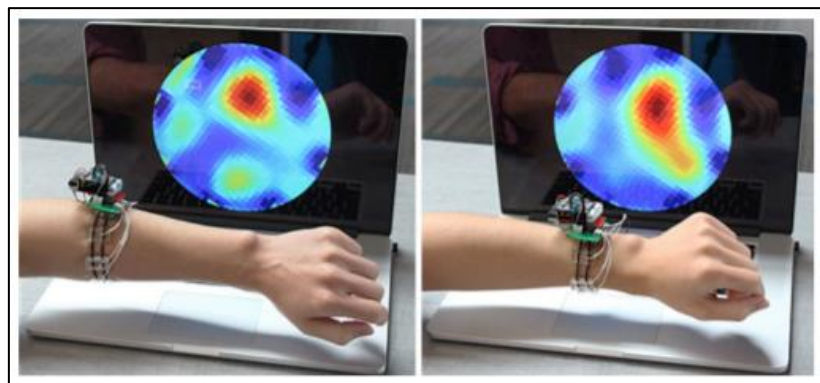


Figure 2.39: Tomo shown worn on the forearm and wrist with generated impedance images [66]

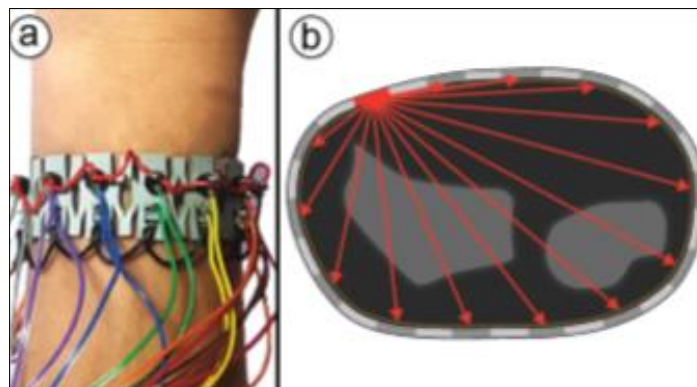


Figure 2.40:a) The SensIR wrist-worn device shown left b) One emitter on while all receivers capture the light level [58]

e) Optical Techniques

Optical methods utilise a camera to capture 2D and 3D hand pose. Cameras sensitive to various light spectra have previously been used. Figure 2.41 shows Digits, a wrist-worn device that uses an infra-red camera to generate a full 3D pose of the user's hand. Rather than employing a classifier algorithm, Digits uses a series of image processing techniques which are incorporated with a detailed kinematic model of the hand shown by Figure 2.42. Accuracy is calculated based on the error between simulated joint angles and actual joint angles.

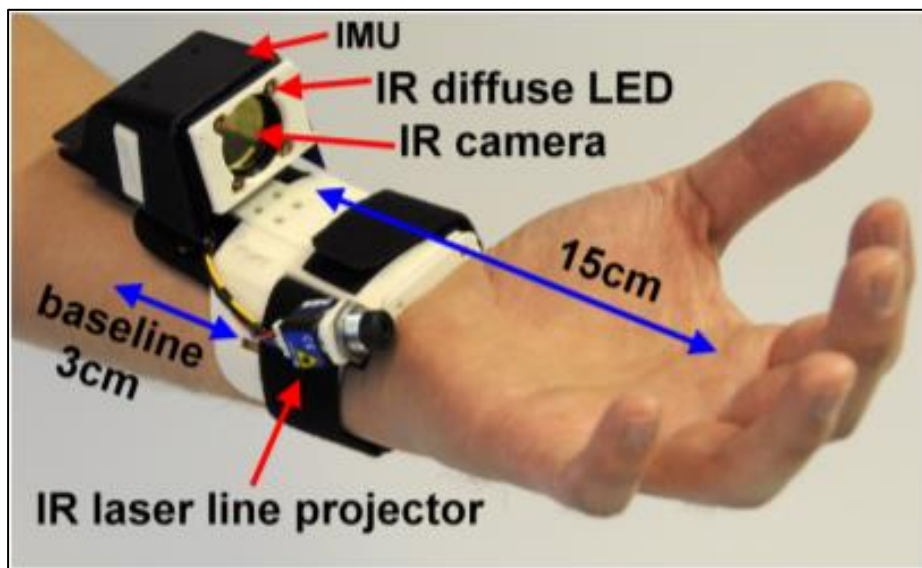


Figure 2.41: Main hardware components shown in the Digits wrist brace [67]

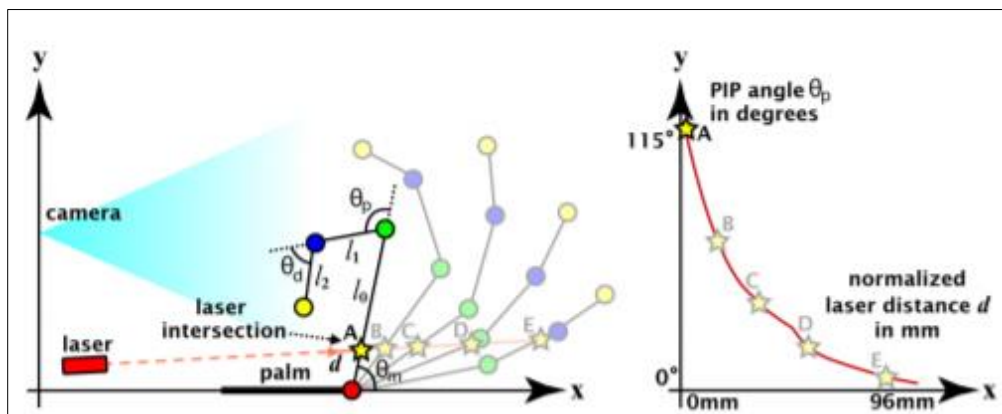


Figure 2.42: A forward kinematics model for a single finger with intersecting laser used in Digits brace [67]

f) Sonomyography (ultrasound)

Ultrasonic imaging is a technique in which pulses of sound waves are emitted into tissue with differences in reflections being measured. The time taken for sound to be reflected is proportional to the depth, and the magnitude of the reflections indicate the type of tissue because of differences in acoustic impedance [59]. Sonomyography is a technique in which the morphological variations of muscles or other human tissues are detected during movement [68]. McIntosh et al. [59] combined this technique along with an image processing and neural network algorithm to classify ten discrete hand gestures with an accuracy of above 98%. Their device setup is shown by Figure 2.43. There are, however, a number of limitations in this method that currently prevent it from being a wearable solution. For example, gel is needed on the skin surface for the transducer to transmit sound effectively which makes this technique challenging to implement in an everyday wearable. While hydrogel pads could be used as an alternative coupling option, the large power requirements of portable ultrasound devices would limit total user time, making this option currently impracticable for most applications.

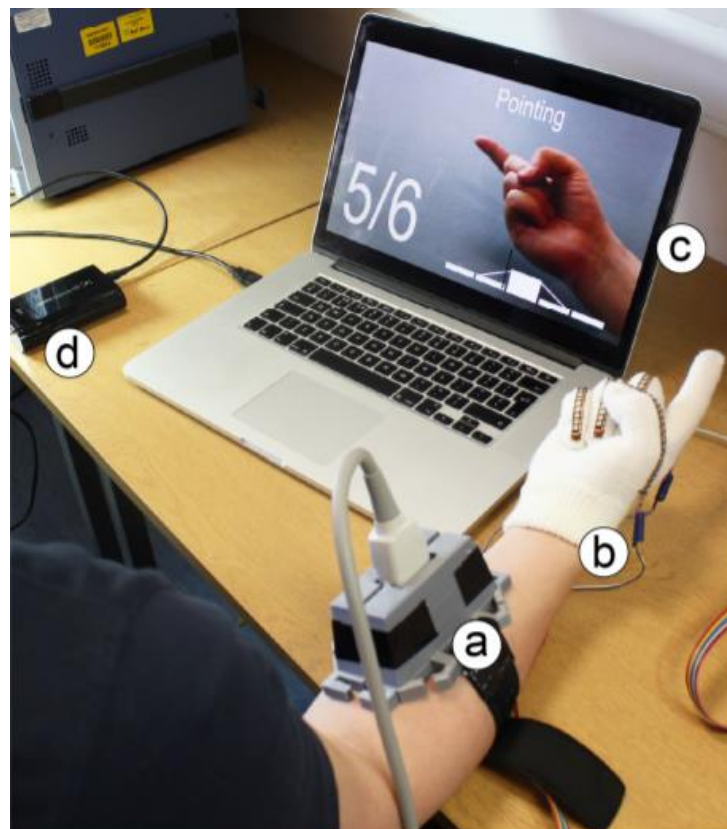


Figure 2.43: An example of Sonomyography and image processing to predict hand gestures [59]

g) Optomyography

The novel technique of detecting and measuring the displacement of skin due to muscle activity is known as Optomyography. Muhammad and Raghavendra [69] were the first to use two IR photoelectric sensors to measure near-infrared rays being reflected from the surface of the forearm while moving the hand into various gestures. This method was later further developed by Muhammad and Raghavendra using a more advanced data acquisition setup and five sensors, shown by Figure 2.44 [70]. In both studies, the resulting signals were only visually inspected to infer the relationships between skin surface changes and hand gesture. Further work is required to apply machine learning methods in order to assess the accuracy and feasibility of this technique in wearable devices.



Figure 2.44: The forearm band set up with five embedded infra-red sensors [70]

h) Mechanomyography

Mechanomyography refers to the use of multiple sensing techniques for measuring low-frequency mechanical signals during muscular contraction. These sensors include the use of inertial measurement units (IMU), laser sensors and microphones which can be attached to the skin [71]. IMUs are more commonly used due to their lower cost and ease of integration with wearables. Wen et al. [72] used a smart-watch with an embedded IMU, as shown by Figure 2.45, to classify five hand gestures with an accuracy of 87%. Ding et al. [71] achieved a recognition accuracy of 94% for individual finger-tapping using an IMU, two auto-event annotation algorithms and three classifiers.



Figure 2.45: Gesture recognition using only a smart watch in the Serendipity system [72]

2.5 Closure

In this chapter a literature review was undertaken that primarily focused on the topics of distal radius fractures, the associated treatment, and complications of DRFs, the Zero-Cast Wx system and smart wearable technology. Several other topics were also briefly discussed to provide background and supporting information. The next chapter reports the first stage design of a POC embedded technology system that can be integrated with Zero-Cast Wx for the purpose of obtaining fitting force and hand motion artefact data.

Chapter 3: Design and Testing of a Proof-of-Concept Embedded Sensor System in the Zero-Cast Wx Brace

3.1 Introduction

This chapter discusses the first stage design of a POC embedded technology system that can be integrated with Zero-Cast Wx for the purpose of obtaining fitting force and hand motion or position data.

Justification is provided for the use of Force Myography in the Zero-Cast Wx brace system. This includes the undertaking of a design selection for various force sensing resistors that could be embedded in the brace for the dual purpose of obtaining fitting force and various hand motion or position data. Additionally, the hardware and circuitry required for data acquisition is reported. Finally, the validation of the embedded sensor system is reported via a single-user test in which the user performed a predefined sequence of hand rehabilitation exercises while the data was sampled and recorded. This stage of the design was limited to wired components only.

3.2 Force Myography Applied in the Zero-Cast Wx Brace

Subsection 2.4.6 described a hand gesture recognition technique using Force Sensing Resistors (FSR) known as Force Myography (FMG). This section discusses why this technique was employed in this project, and why FSRs were chosen to apply this technique. A decision matrix was utilized to select a suitable FSR model and the method by which it was integrated with the Zero-Cast Wx brace is discussed. Following this is a brief report of a self-performed test that samples force data from a sequence of hand mobility exercises.

3.2.1 Justification

FMG was selected for this project because it is a non-invasive technique that can be used for the dual application of detecting force due to volar and dorsal plate clamping as well as force exerted due to changes in wrist circumference when the fingers are moved. No other technique was identified that could provide this dual functionality. Additionally, the minimal circuitry and signal processing required in this technique made it favourable in terms of cost and time savings.

3.2.2 Resistive Polymer Thick Film Sensors

FSR and Flexiforce® sensors as shown by Figure 3.1 are polymer thick film sensors which change in electrical resistance when a force is applied to the active surface area.

They account for 55% of sensors used in FMG publications, making them the most popular single element RPTF sensors for this application [62]. While there is no study that compares the performance of these two sensors in FMG applications, the FSR is better on force repeatability and response time based on the technical data provided by the manufacturers [62]. It was also found that FSR sensors are cheaper than Flexiforce sensors. Based on this information it was decided that the FSR range of sensors would be used in the FMG application of this project.



Figure 3.1: a) FSR sensors and b) Flexiforce sensor [62]

Interlink Electronics was originally founded on the invention and commercialization of the FSR and are currently the premium manufacturer of the device [73]. The Interlink Electronics FSR 400 series shown by Figure 3.2 is a family of seven single zone Force Sensing Resistors designed for human machine interfaces such as automotive electronics, medical devices, robotics, and industrial systems [64]. Table 3-1 summarizes the mechanical properties of the FSR 400 series by Interlink Electronics.

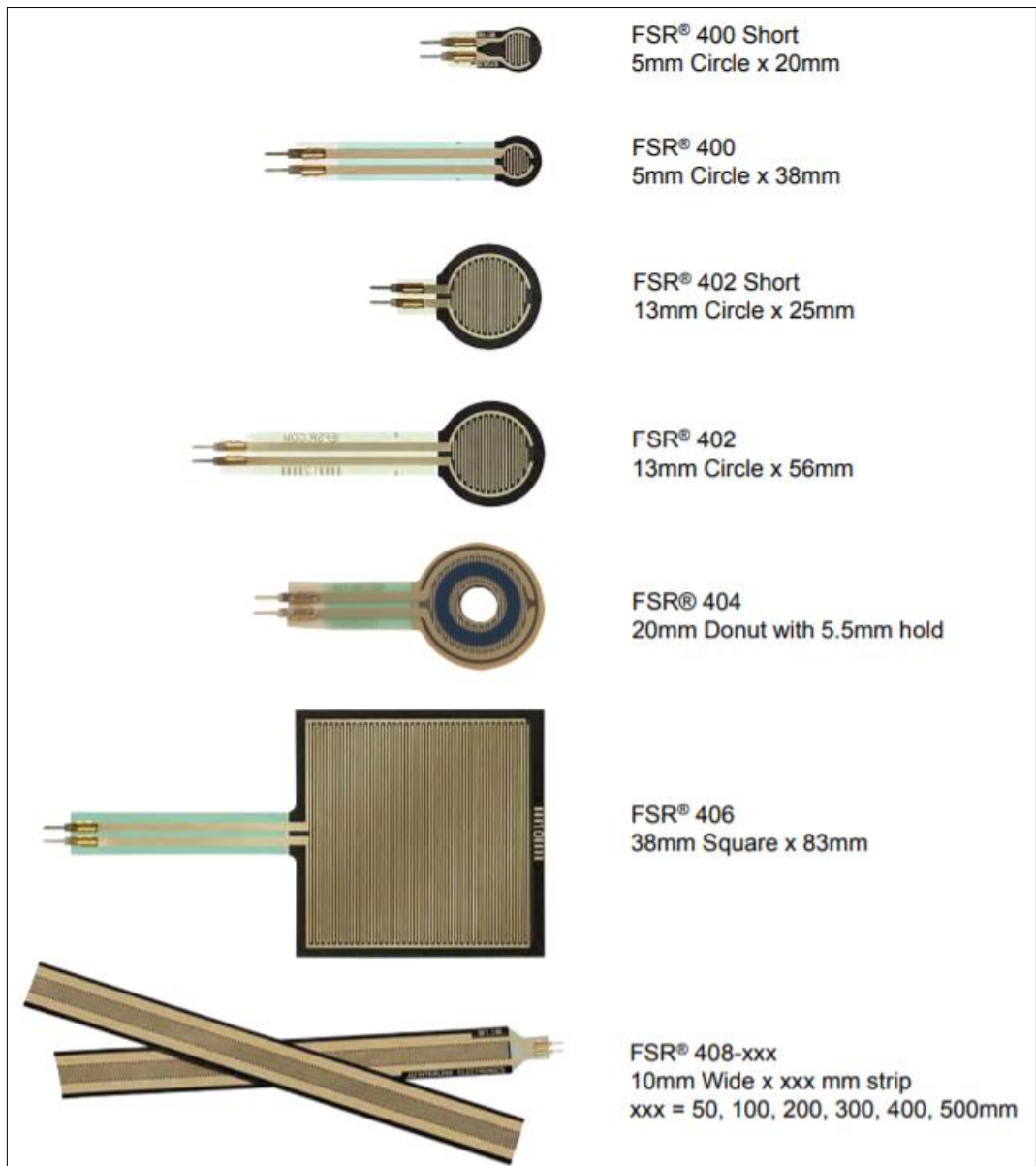


Figure 3.2: The FSR 400 Series by Interlink Electronics [74]

Table 3-1: Mechanical specifications of FSR 400 series [74]

Metric	Value
Actuation force	~0.2 N min
Sensitivity	~0.2N – 20N
Force resolution	Continuous (analog)
Force repeatability (single part)	+/- 2%
Force repeatability (part to part)	+/- 6% (Single Batch)
Non-actuated resistance	>10 Mohms
Operating temperature performance Cold: -40°C after 1 hour Hot: +85°C after 1-hour Hot Humid: +85°C 95RH after 1 hour	-5% average resistance change -15% average resistance change +10% average resistance change
Tap durability Tested to 10 Million actuations, 1kg, 4Hz	10% average resistance change
Static load durability 2.5kg for 24 hours	-5% average resistance change

3.2.3 FSR 402 Design Selection

As all seven models of the FSR 400 series exhibit identical mechanical and electrical properties, the factors contributing to the selection of a particular model were cost, size, and geometry. These factors were used in a weighted decision matrix to decide on the most suitable FSR to use in the Zero-Cast Wx brace. The requirements and justification for the selection criteria is summarized in Table 3-2.

To select the most suitable FSR in the Zero-Cast Wx application, the selection criteria and various FSR models were entered into a decision matrix as shown by Table 3-3. A reverse ranking method was used to evaluate each FSR model on each criterion. Criterion weightings were reverse ranked which reflected their relative significance specific to this project. The ranking values for the weightings and scores were reached after consulting with the Surgisplint team. The weighted score for each category was calculated by multiplying the weighting by the rank score. The total score for each FSR

was then calculated by adding the weighted scores from each category. The FSR with the highest combined score was then selected.

Table 3-2: FSR selection criteria with design requirements/constraints

Criterion	Justification	Requirement/constraint
Size and Geometry	This was considered the most significant criterion as it directly affects where and how the sensors will be located and how many will be needed to detect both fitting force and forces exerted by changes in wrist circumference.	The FSR should be easily fitted between the plastic plate and foam pad without impeding the function of the brace. Maximum width: 50mm Maximum length: 100mm
Cost per unit	Funding was limited due to the nature of this project (a master's thesis). Achieving the desired objective at a lower cost would also be commercially beneficial to Surgisplint	<\$10 per unit Cheaper units will score higher

Table 3-3: Decision matrix for FSR Selection

FSR 400 Series		Size & Geometry	Cost	Total
		Weighting	3	2
400 short	Score	5	4	
	Total	15	8	23
400	Score	4	6	
	Total	12	12	24
402 short	Score	7	2	
	Total	21	4	25
402	Score	6	5	
	Total	18	10	28
404	Score	3	2	
	Total	9	4	13
406	Score	2	3	
	Total	6	6	12
408	Score	1	1	
	Total	3	2	5

Based on the results of the decision matrix, FSR 402 was selected to be used in the first phase of the embedded technology design. The dimensions and geometry of the 402 model is shown in Figure 3.3.

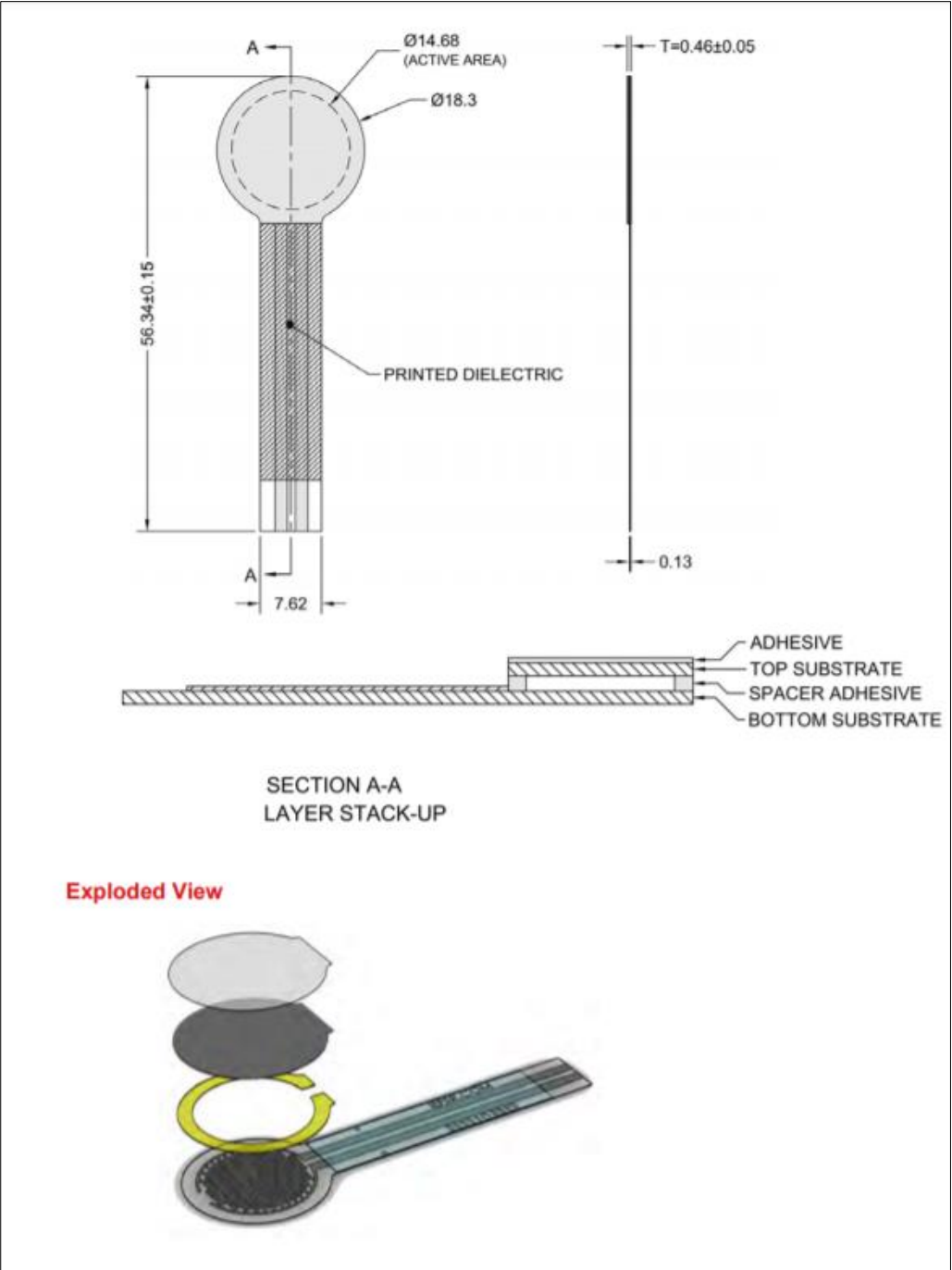


Figure 3.3: Mechanical data of FSR model 402 [73]

3.2.4 FSR 402 Circuit Design

There are several electrical interface options recommended by Interlink Electronics. The FMG application in this project only required a simple force-to-voltage conversion which could be achieved by a voltage divider circuit as shown by Figure 3.4 [64]. A potential drawback of this circuit, however, is the non-linear voltage response which may create a source of error between actual force magnitude and sensor reading. While this was acknowledged, research has shown that linearity is not a significant factor for gesture prediction, so long as the force patterns vary among gestures [62].

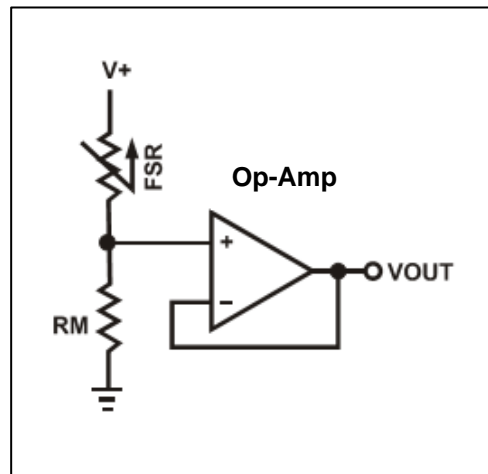


Figure 3.4: FSR connected in voltage divider circuit [64]

In the circuit shown, one end of the FSR is connected to a power supply, $V+$, and the other end to a pull-down resistor, R_m (measuring resistor), which is connected to ground. The point between the FSR and pull-down resistor is connected to the analogue input of a microcontroller for sampling. The use of an operational amplifier as a buffer to limit the circuit load is optional but not essential during POC design stages. The total current in the circuit is denoted by I_{tot} . As the applied force on the FSR increases, the voltage across it decreases. The derivation for V_{out} follows from Ohm's law:

$$I_{tot} = \frac{V+}{R_{FSR} + R_M}$$

Equation 3-1: Ohms Law applied in FSR Circuit

$$V_{out} = I_{tot} R_m$$

(constant current for resistors in series)

Substituting the expression for I_{tot} in the above equation gives

$$V_{out} = \frac{R_M V+}{R_{FSR} + R_M}$$

Equation 3-2: FSR voltage divider circuit

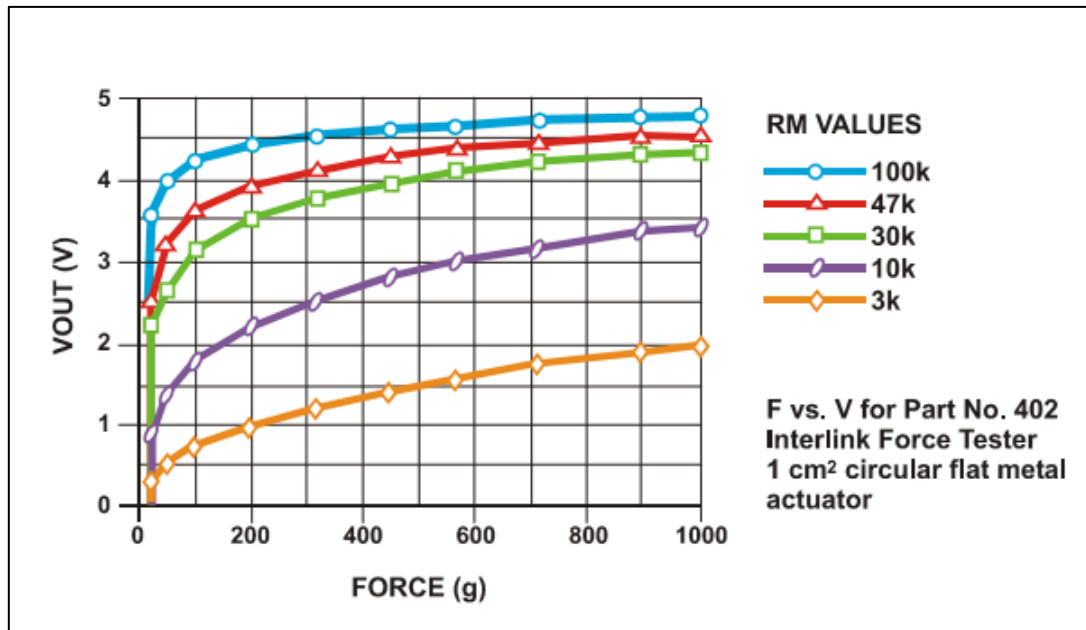


Figure 3.5: A series of curves for applied force vs output voltage using standard R_M values [73]

A series of Force vs. V_{out} curves is shown by Figure 3.5 for an FSR 402 in a voltage divider configuration with various values for R_M . A simple analysis was carried out to select a resistor value for R_M assuming a 5V power supply as recommended by Interlink Electronics. The resistor value for R_M was selected based on the highest obtainable sensitivity over the operating force range (i.e. largest voltage change per change in unit force). Having the highest possible sensitivity in this application would allow for higher accuracy in detecting changes in wrist contour. From the results presented in Table 3-4, this was observed to be a resistor value of 10k Ω . This was therefore the resistor selected to be used in the embedded FSR circuit.

Table 3-4: Approximate FSR 402 sensitivity and current drawn with various R_M values

Resistor value (k Ω)	Approximate sensitivity (V/N)	Current (mA)
3	0.14	1.67
10	0.19	0.50
30	0.13	0.17
47	0.10	0.11
100	0.06	0.05

3.2.5 FSR 402 Integration with Zero-Cast Wx

A critical decision that was made early on in this project was whether to mount the FSR array in either the dorsal plate or volar plate. This was done by carefully considering the spatial, geometrical, and practical limitations imposed by the current Wx design, along with the functional anatomy of the wrist. Firstly, it was observed that FSR sensors could only be installed on either the dorsal or volar plate, but not both. Since all FSRs would be contained in a single circuit, it was more practicable for all electronic components to be located on one of the plates. If FSRs were to be mounted on both plates, that would result in some wiring being exposed, as the dorsal and volar plates are two separate units.

Secondly, the largest flat surface area on which to test an FSR configuration was required. FSRs perform optimally on hard, flat surfaces [64]. Figure 3.6 and Figure 3.7 show that the volar plate provides an overall larger and flatter surface on which to mount FSR sensors and electronic components. Finally, the anatomy of the wrist was also taken into consideration. Anatomically, the tendons on the dorsal side of the wrist are closer to the skin than tendons in the volar side. It could therefore easily be assumed that these tendons would have a large impact on changing wrist contour when the fingers are flexed and extended. In most individuals, however, the tendons in the volar side of the wrist protrude more prominently than the dorsal side, despite lying deeper in the wrist (Figure 2.6). This is likely because of the confined space in the carpal tunnel which means that volar-side tendons are bundled together and bulge outwards when any of the connected muscle tissue is contracted. Based on these factors, it was decided that the dorsal plate was the best component of the Zero-Cast Wx brace to be integrated with the FSR array.



Figure 3.6: Photograph comparing total surface area between dorsal plate (left) and volar plate (right)



Figure 3.7: Photograph comparing surface curvature between dorsal plate (left) and volar plate (right)

Subsection 2.3.4 of the literature review discussed how complications such as tendon adhesions, joint stiffness and muscle atrophy are often attributed to prolonged cast immobilization. Physiotherapists recommend that patients practice a series of hand exercises known as tendon gliding exercises to lower the risk of these complications. As part of the initial first phase of the embedded design, four rehabilitation exercises were selected to test the application of FMG in the Zero-Cast Wx brace system. The exercises selected were namely, extended hand, hook-fist, flat fist, and thumb flexion, all shown by Figure 3.8 **a**, **b**, **c**, and **d** respectfully, and were personally recommended by the Surgisplint consultant physiotherapist.

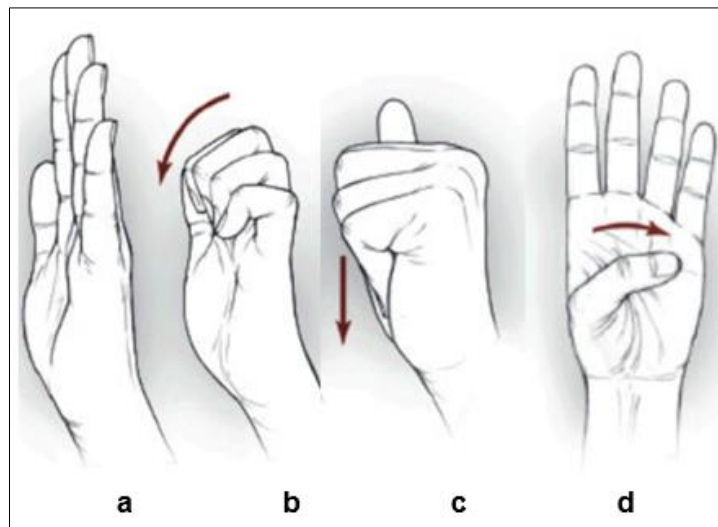


Figure 3.8: Tendon gliding exercises selected to test FMG in Zero-Cast Wx

The objective here was to extract FSR force patterns that are unique to each tendon gliding gesture. This would be the first successful step in developing a hand gesture recognition system using embedded technology in the Zero-Cast Wx brace.

Prior to the integration of the FSR array with the volar plate, it was necessary to take a more detailed look at the functional anatomy of the wrist during the execution of the exercises. This exercise assisted with the initial placement of the FSR test array.

As shown by Figure 2.6 in the literature review, there are nine flexor tendons which pass through the Carpal Tunnel in the volar side of the wrist. Four tendons converge into the Flexor Digitorum Superficialis (FDS) muscle, four to the Flexor Digitorum Profundus (FDP) muscle and one to the Flexor Pollicis Longus (FPL) muscle, all shown by Figure 2.3. The FDS tendons pass directly over the FDP tendons. These muscles and tendons function by flexing (curling inwards) the fingers, thumb, and wrist.

Similarly, as shown by Figure 2.2, the dorsal side of the wrist has four Extensor Digitorum Tendons that converge into the Extensor Digitorum Muscle. This muscle along with the Extensor Digitorum Minimi (little finger) and Extensor Indicis (index finger) muscles and their respective tendons work together to extend (straighten) the fingers. The Extensor Pollicis Longus and Extensor Pollicis Brevis muscles and tendons function to extend the thumb, also shown by Figure 2.2.

The function-specific wrist and forearm anatomy of the tendon gliding exercises are presented by Figures 3.9, 3.10, 3.11, and 3.12.

a) **Muscles:** Extensor Digitorum, Extensor Digitorum Minimi, Extensor Indicis, Extensor Pollicis Longus, Extensor Pollicis Brevis

Function: Extending fingers and thumb in 'straight hand' gesture

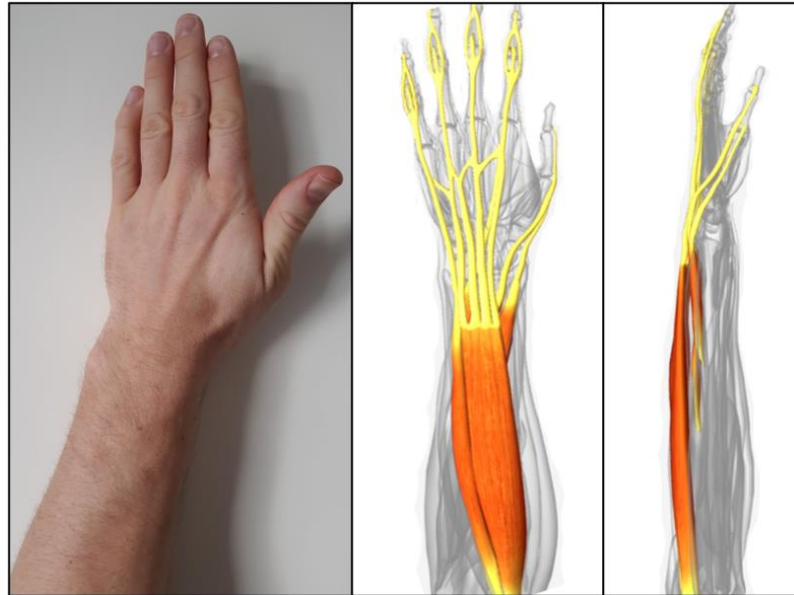


Figure 3.9: Extensor muscles and tendons contracted and isolated in 'extended hand' gesture

b) **Muscle:** Flexor Digitorum Profundus

Function: Flexing of the fingertips or bending occurring at the proximal and distal interphalangeal joints resulting 'hook-fist' gesture.

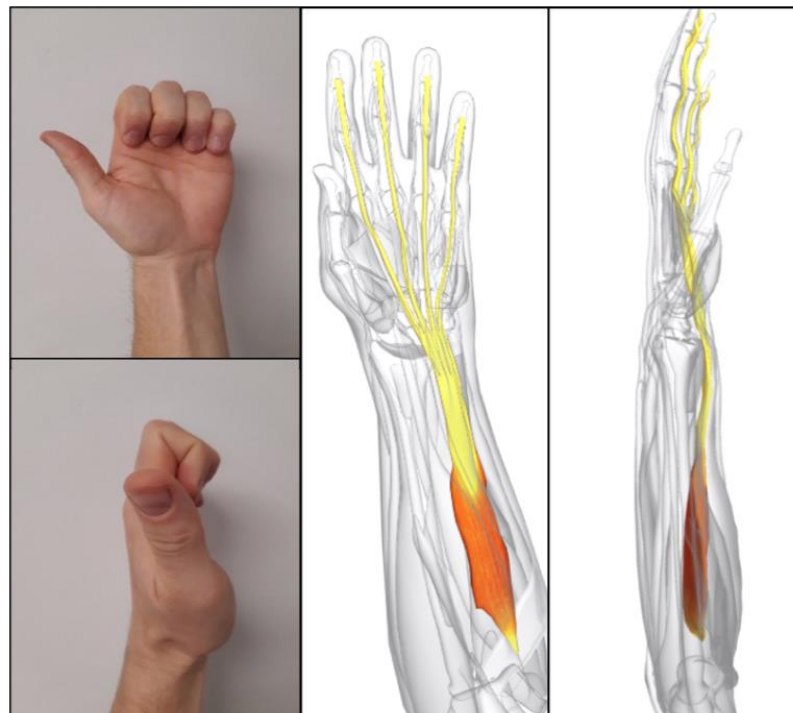


Figure 3.10: FDP muscle and tendons contracted and isolated in 'hook-fist' gesture [75]

c) Muscle: Flexor Digitorum Superficialis

Function: Flexing of the fingers with fingers flat against the palm. Bending occurs at the metacarpophalangeal and proximal interphalangeal joints in in the 'flat-fist' gesture

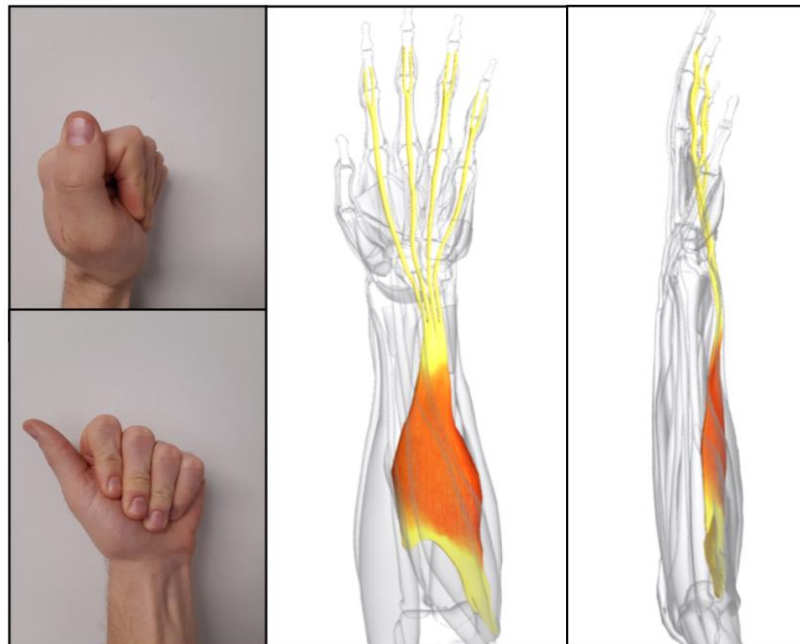


Figure 3.11: FDS muscle and tendons contracted and isolated in 'flat-fist' gesture [75]

d) Muscle: Flexor Pollicis Longus

Function: Thumb touching the base of the little finger in 'thumb flexion' gesture

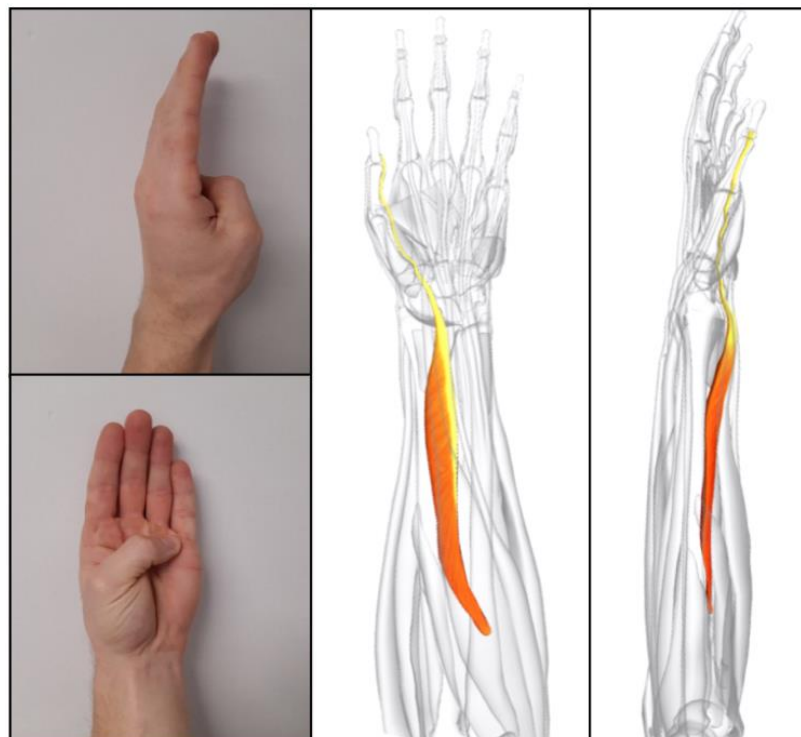


Figure 3.12: FPL muscle and tendon contracted and isolated in 'thumb opposition' gesture [75]

Using the functional anatomy of the tendon gliding exercises, a simple sensor array was selected which could potentially detect both fitting force and the tendon gliding exercises. Figure 3.13 shows the FSR array that was tested on a single user. FSR position 1 and 2 were located to detect forces exerted by the flexor tendons. Since the tendons are all closely situated to each another it was anticipated that all three FSRs would be triggered to some extent for each type of hand gesture. The desired outcome, however, was to have the FSR array detect a unique force pattern for each hand motion. FSR position 3 was located in line with the locking ratchets as an initial attempt to detect fitting force.

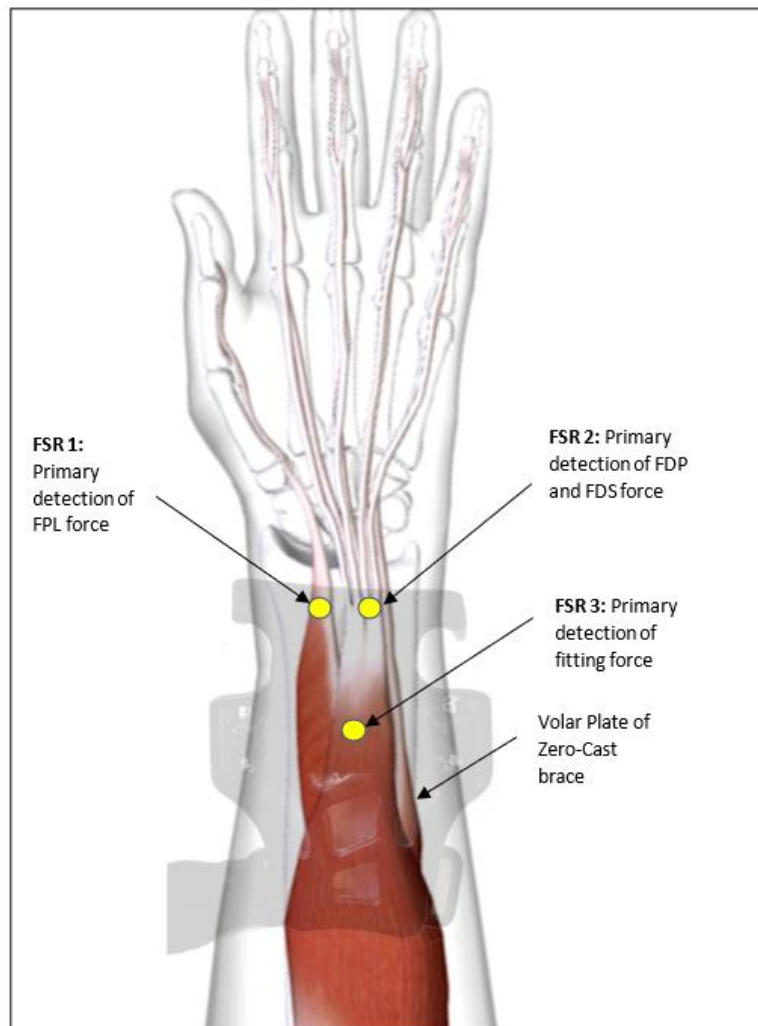


Figure 3.13: Anatomy guided FSR array in the left volar plate of Zero-Cast Wx

3.2.6 Volar Plate Modification, Circuitry and Software used for Data Acquisition

Modified Volar Plate

The FSRs used require a firm and flat surface to measure force effectively. It was therefore necessary to make some minor alterations to the plastic volar plate to be used for the initial test. The volar plate of the testing brace was modified by removing the foam lining and filling the ventilation gaps with an epoxy filler. Once hardened, the filler was sanded and painted to provide a hard and smooth surface on which to mount the FSRs. The image shown by Figure 3.14 compares the modified volar plate of size four left, to that of unmodified size four right.

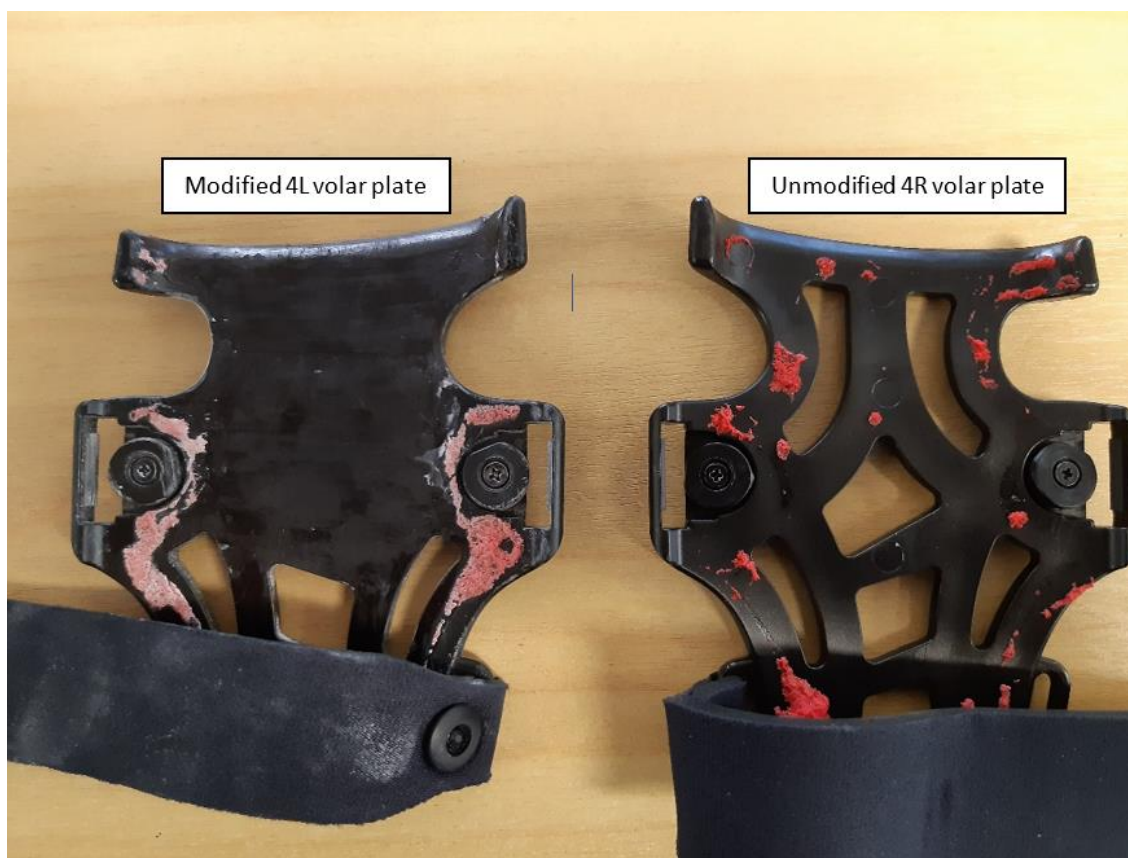


Figure 3.14: Photograph comparing the modified volar plate with an unmodified volar plate (foam liners removed)

Electronic Hardware and Circuitry for Data Acquisition

For POC use, an Arduino Uno was selected to sample force data as it is a relatively inexpensive microcontroller and has all the required functionality for testing the FSR array. It is also easily programmed using the Arduino IDE (Integrated Development Environment). Table 3-5 highlights some of the key specifications of the Arduino Uno. Figure 3.15 and Figure 3.16 show the Arduino pin diagram and circuit schematic for FSR data sampling, respectively.

Table 3-5: Arduino Uno Specifications

Feature	Details
Microprocessor	ATmega328P – 8-bit AVR family microcontroller
Input voltage	7 – 12 V
Operating voltage	5V
Analogue input pins	6 pins
Digital I/O pins	14
Clock speed	16 MHz
Flash memory	32 KB

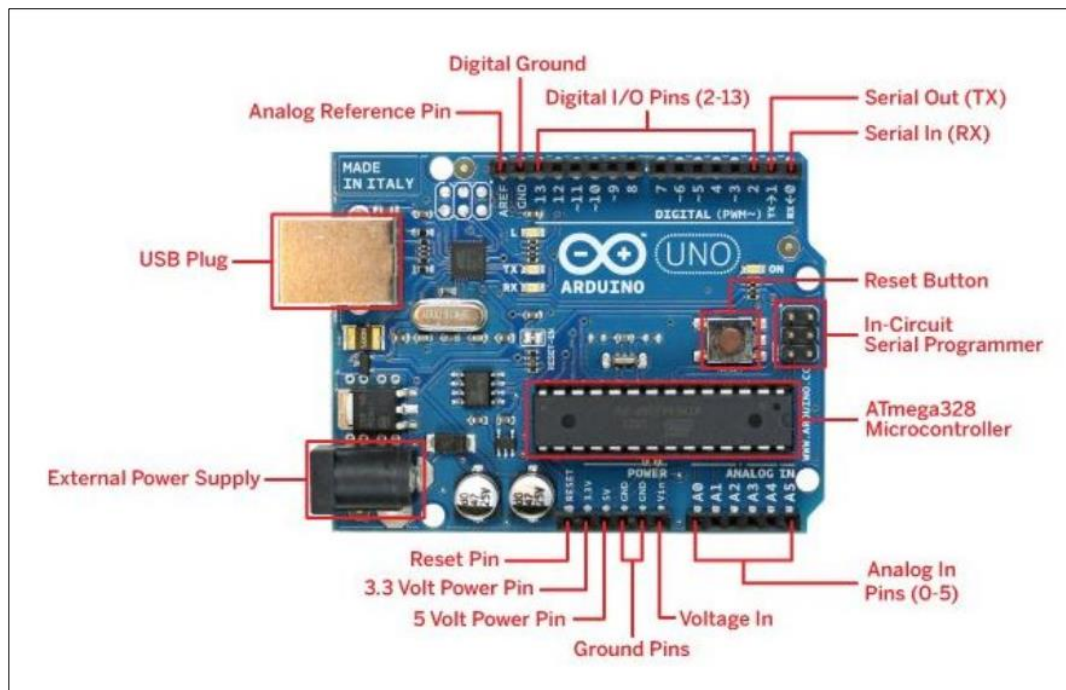


Figure 3.15: Arduino Pin Diagram [76]

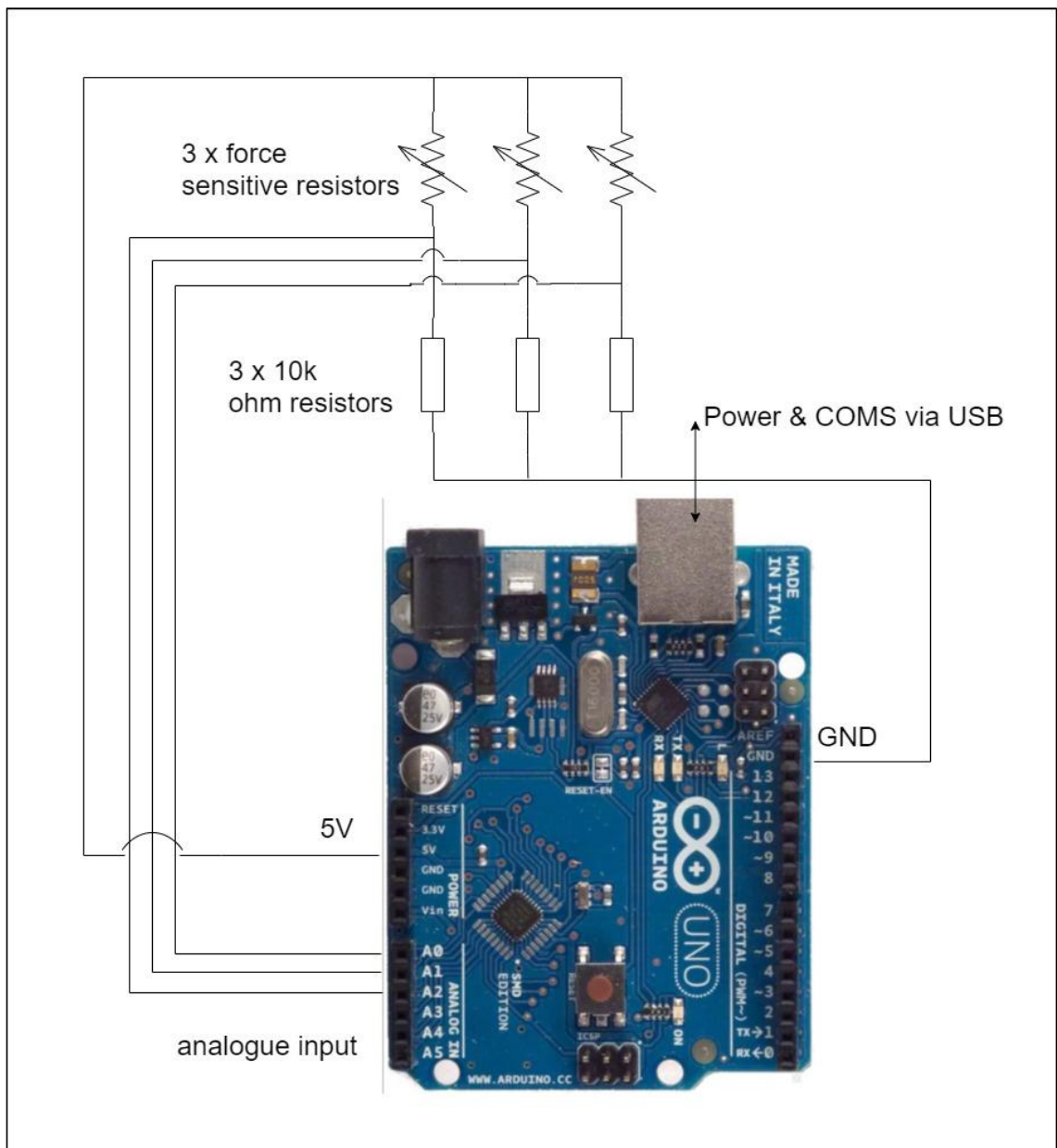


Figure 3.16: Full schematic circuit for FSR force sampling using Arduino Uno

Software

The Arduino IDE was first used to program the Arduino Uno to sample FSR voltage data. The Arduino IDE is a C-based platform and incorporates a suite of built-in functions specific to Arduino hardware. The code to sample FSR voltage data from the three analogue inputs is shown in Appendix A-1. Using the Arduino IDE is insufficient for signal sampling and processing. The platform is typically only used for executing repeatable tasks on the Arduino.

National Instrument's LabVIEW software was combined for this application, to extract and plot the sampled FSR data from all three analogue inputs. This was achieved using a specialized add-on package called LINX, which allows Arduino hardware to communicate with LabVIEW. Additionally, a simple graphical interface could be created to see the FSR voltage in near real-time as well as a combined time-plot after the program has been aborted. A study on sampling rates for upper limb FMG applications suggests a minimum sampling rate of above 84Hz [77]. The default sampling rate in the LINX package was 125Hz which was maintained throughout this research. LabView also allows the data to be extracted easily into a .CSV format for further analysis. Refer to Appendix A-2 for the LabView code used for voltage sampling.

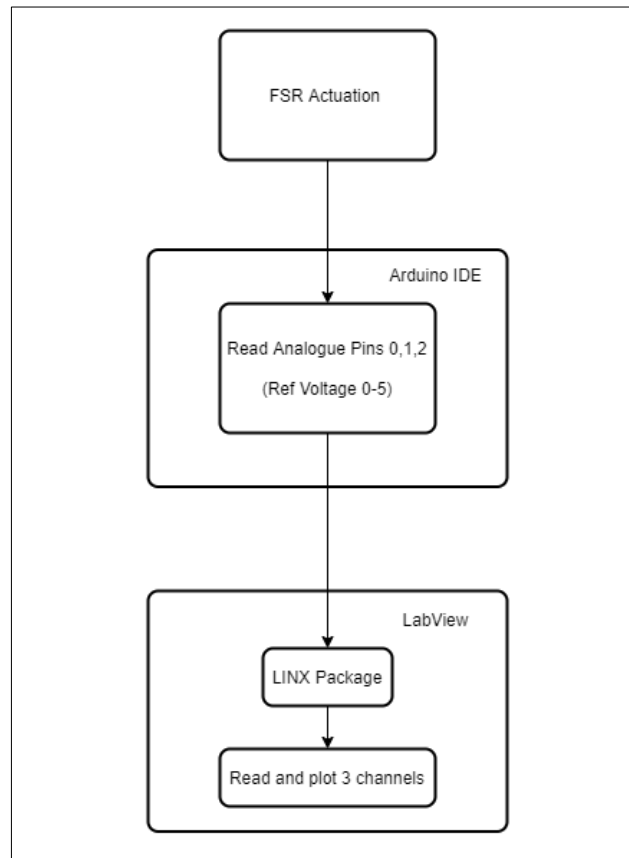


Figure 3.17: High level data flow and process execution

Hardware Setup

The modified (4L) volar plate was fitted with three 402 FSRs as shown by Figure 3.18. The full test setup is shown by Figure 3.19.



Figure 3.18: Photograph of modified volar plate (4L) with fitted FSR 402 sensors

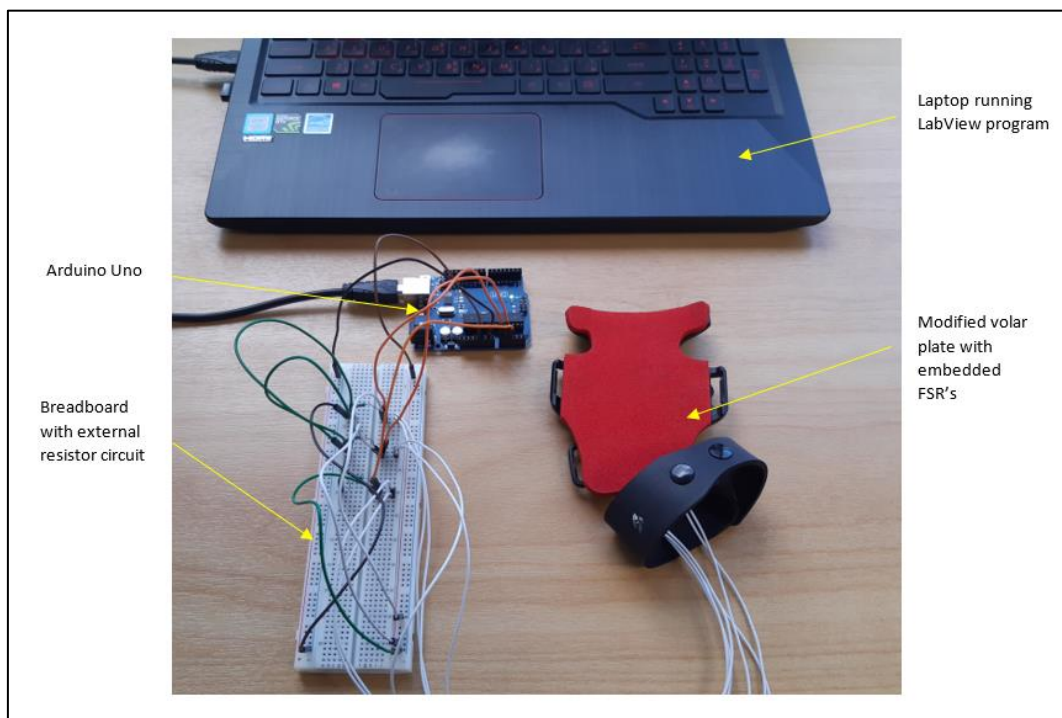


Figure 3.19: Full test setup with modified volar plate and wired circuitry

3.2.7 Test Results

The 4L Zero-Cast Wx with embedded FSRs and connected circuitry was then used in a self-performed experiment. The brace was fitted according to the standard Zero-Cast Wx fitting protocol. After fitting the brace, the user placed their elbow on a desk with the forearm at 90 degrees to the desk surface with the hand kept in a relaxed state as shown by Figure 3.20.



Figure 3.20: Participant fitted with modified test brace placing forearm at 90 degrees to desktop

With the LabView program sampling voltage readings, the participant performed the sequence of hand gestures corresponding to the tendon gliding exercises, as shown by Figure 3.21. These were the relaxed, hook-fist, flat-fist, and thumb flexion positions with each being held for approximately three seconds. It should be noted that although the relaxed hand position was not designated as tendon gliding gesture, it was selected as a default position and also served as a preliminary indication of the viability for detecting fitting force using FMG.

From Figure 3.22 it can be seen that each gesture corresponds to unique FSR amplitudes for this specific fit, which was the objective of this stage of the project. These initial results showed that FMG is a viable technique when applied in the Zero-Cast Wx brace. Additionally, it also provided the confidence to move onto the next phase of the design which was creating a wireless system and using the data from a single user to train a machine learning algorithm that can distinguish between different hand positions.

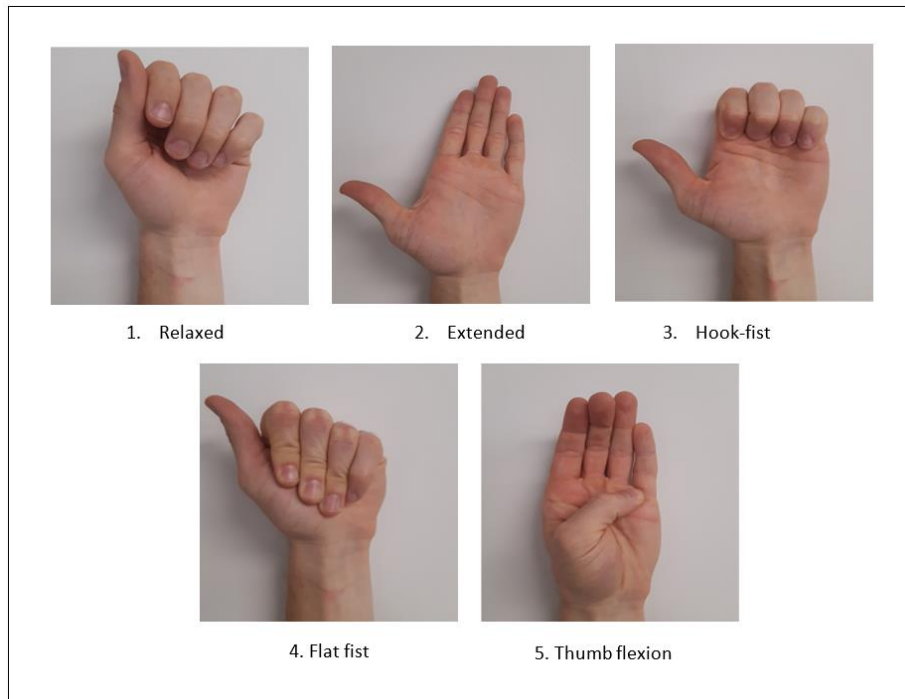


Figure 3.21: Sequence of gestures performed during data sampling

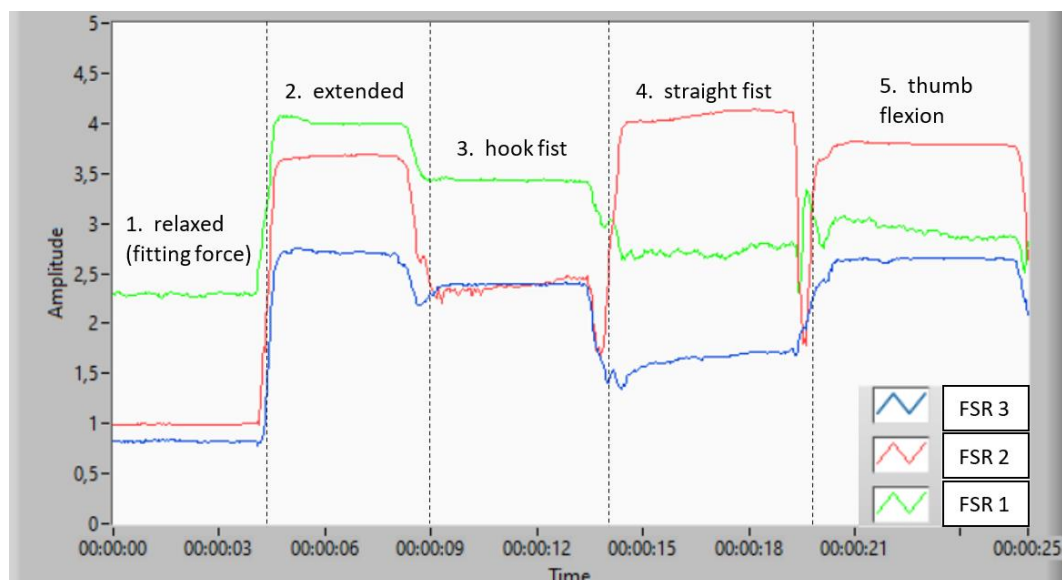


Figure 3.22: Graph showing sampled FSR data for successive hand gestures

It should also be mentioned that the emphasis of obtaining unique FSR amplitudes for various hand gestures was intentional during this stage of the project. The application of FMG and machine learning to classifying 'fitting force' would be focused on during the multi-user study and is discussed later in Chapter 6. Hand gesture recognition is a more complex task than fit classification and this stage of the project intentionally focused on extracting useful data early on which would help progress more quickly during later stages. It was considered a better approach to obtain more fitting data from multiple users, before drawing any conclusions on the plausibility of classifying fitting force.

3.3 Closure

In this chapter justification was given for applying the FMG technique in the Zero-Cast WX brace with FSR sensors. A methodological design approach to selecting a suitable FSR sensor was used and the integration process and choices made were described in detail with the aid of functional anatomy and the guidance of Surgisplint's expert clinicians. Furthermore, it was discussed and justified why tendon gliding exercises were used to test the application of FMG in the Zero-Cast Wx brace and the process and tools used for data acquisition were described. The embedded sensors and connected circuitry were used in a self-performed test to assess the feasibility of using the FMG technique in the Zero-Cast Wx system. In the following chapter, the second phase of the embedded design process is reported. The investigation and design selection of various electronic components and the design of an attachable enclosure for creating a final proof-of-concept embedded system is reported.

Chapter 4: Design of a Wireless Proof-of-Concept Force Myography System in the Zero-Cast Wx Brace

4.1 Introduction

In this chapter the second phase of the embedded technology design is reported which details the design of a wireless POC force myography system that can be integrated with the Zero-Cast Wx brace. This includes a design selection of various electronic components, required circuitry with circuit layout design and the design of an enclosure for all components which could be attached to the volar plate of the Zero-Cast Wx brace.

4.2 Electronic Component Selection and Protoboard Layout Design

In this section a design selection process is used to identify the most suitable electronic components to be used in the wireless POC embedded design. A schematic of the full embedded circuit is illustrated and used to explain the layout design of the FSR circuitry on a solderable protoboard.

4.2.1 Wireless Microcontroller Design Selection

A microcontroller with multiple analogue inputs and wireless transmission capability was required. Four readily available microcontrollers which could be applied in Zero-Cast Wx were assessed using various selection criteria. These criteria were used in a weighted decision matrix to decide on the best microcontroller. The requirements and justification for the selection criteria is summarized in Table 4-1.

Table 4-1: Microcontroller selection criteria with design requirements/constraints

Criterion	Justification	Requirement/constraint
Size	This was considered a significant criterion as it should be easily integrated with the existing Zero-Cast brace design	Microcontroller size was limited by the Zero-Cast brace size and geometry. Higher score given to smaller devices.
Cost per unit	Funding was limited due to the nature of this project. Achieving the desired objective at a lower cost would also be commercially beneficial to Surgisplint	<\$50 per unit Cheaper score higher in decision matrix
Power Requirement (Input voltage)	The input power would be indicative of the overall power consumption of the device. It would also affect the battery selection.	No specific requirements/constraints. Microcontrollers with lower power supply and/or wide supply range would be favoured.
Analogue Inputs	The number of analogue inputs affect the total number of sensors which could be added to the circuit.	A minimum of two analogue inputs required to be eligible for selection. More analogue inputs will score higher in decision matrix as more sensors could be added

Table 4-2 shows the different microcontrollers that were considered to be used in Zero-Cast Wx. The table highlights some of the key specifications that were taken into consideration when allocating criteria scores in the decision matrix.

A weighted decision matrix with reverse ranking was used to evaluate each microcontroller. Each criterion was weighted with a reverse ranking number (higher reflecting greater importance) and each microcontroller was reverse ranked for each criterion. The ranking orders were determined after consulting with the Surgisplint medical and strategic team. The weighted score for each category was calculated by multiplying the criterion weighting with the assigned rank score. The total score for each microcontroller was then calculated by adding the weighted scores from each category. The microcontroller with the highest combined score was then selected for use.

Table 4-2: Microcontroller options considered for the Zero-Cast Wx brace

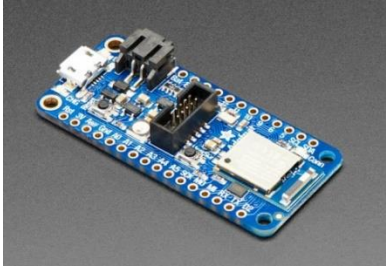
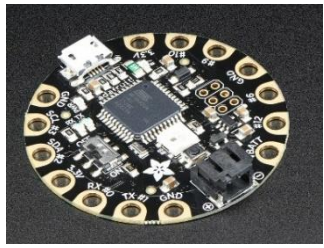
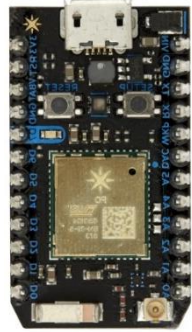
Microcontroller	Specifications/Features	Image
Adafruit Feather nRF52840 Express [78]	Size: 51 x 23 x 7.2 Mass: 6g 6 x analogue inputs BLE compatible 3.7V power supply ARM Cortex M4F processor at 64MHz	
Adafruit Flora [79]	Size: 45mm diameter x 7mm Mass: 4.7g 4 x analogue inputs ATmega32u4 processor at 8MHz 3.5V – 16V power supply External BLE module required	
Particle Photon [80, 81]	Size: 36.58 x 20.32 x 4.32 Mass: 3.7g 6 x analogue inputs ARM Cortex M3 processor at 120MHz Broadcom BCM43362 Wi-Fi chip 3.6V – 5.5V power supply	
Beetle BLE [82]	Size: 28.8 X 33.1 Mass: 10g 4 x analogue inputs ATmega328 processor at 16MHz BLE compatible 6 V – 8V power supply	

Table 4-3 shows the results of the decision matrix. The Beetle BLE (Bluetooth Low Energy) obtained highest score of 29 points, making it the most suitable microcontroller for use in the Zero-Cast Wx brace. The Beetle BLE is an Arduino based board with Bluetooth 4.0 that is one of the smallest Arduino BLE devices on the market, making it ideal for projects involving prototyping and wearable devices.

Table 4-3: Decision matrix for microcontroller selection

Microcontroller		Selection Criteria				
		Size	Cost	Input power (voltage)	Analogue Inputs	Total
	Weighting	4	2	1	2	
Adafruit Feather nRF52840 Express	Score	2	2	2	4	
	Total	8	4	2	8	22
Adafruit Flora	Score	1	3	4	3	
	Total	4	6	4	6	20
Particle Photon	Score	3	1	3	4	
	Total	12	2	3	8	25
Beetle BLE	Score	4	3	1	3	
	Total	16	6	1	6	29

4.2.2 FSR Sampling Schematic and Protoboard Layout Design

The circuit used for FSR force sampling in the Beetle BLE was almost identical to that of the Arduino Uno shown in Figure 3.16; with the exception of power being supplied by a battery and the inclusion of a switch. The schematic for the circuit is shown by Figure 4.1.

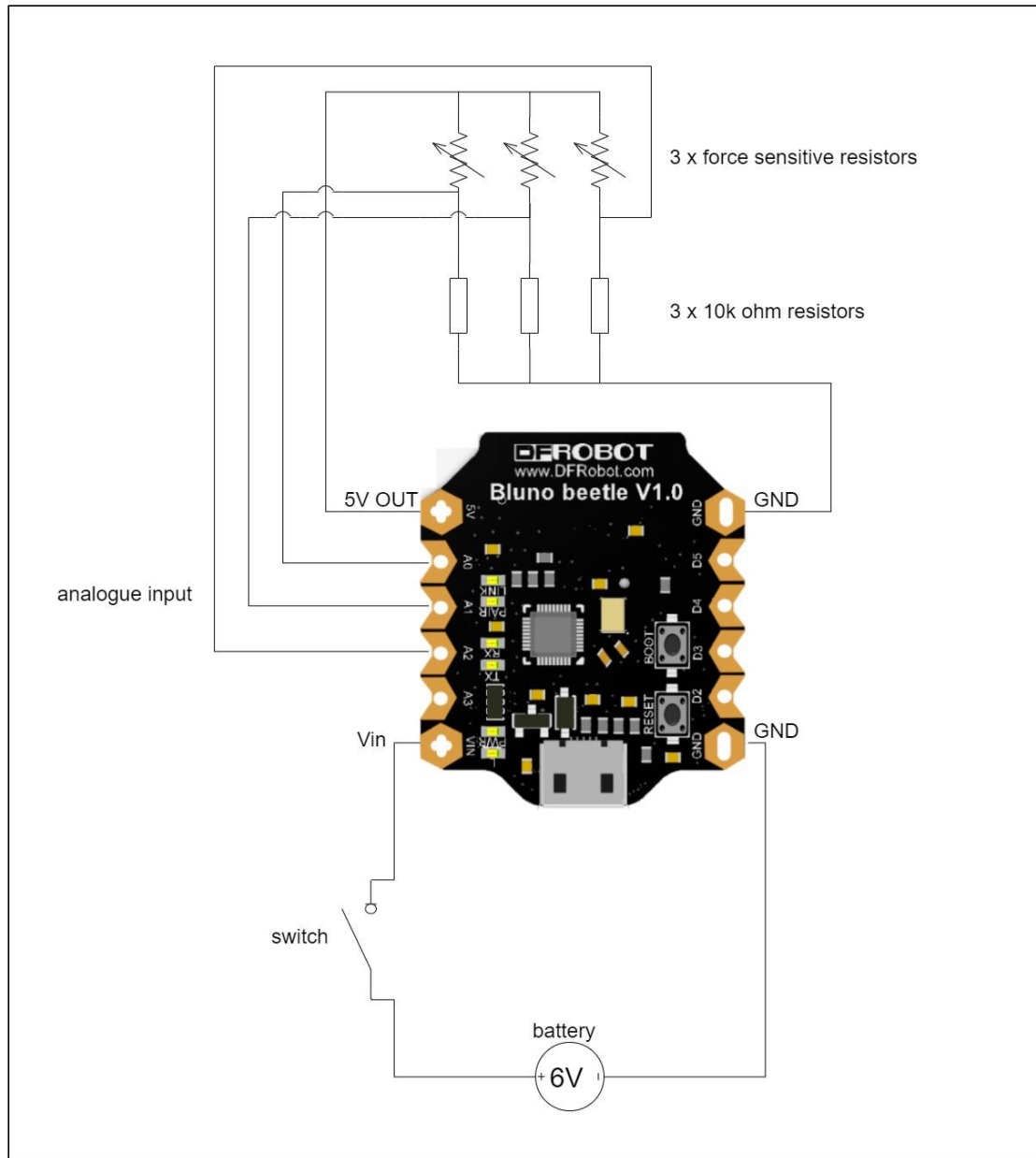


Figure 4.1: Full schematic circuit for wireless FSR force sampling using Beetle BLE

During the first stage of the embedded design, the 10k ohm resistors, R_M were connected on a solderless breadboard external to the Arduino Uno. In stage two, the resistors were required to be internally housed along with Beetle BLE. Using a solderable protoboard with electrically connected rails and header pins would more easily connect common points and reduce the amount of electrical wire required. The through-hole resistors were soldered on a square piece of protoboard and connected to the Beetle with header pins. The protoboard was cut down to a smaller size containing only the areas used for the resistors.

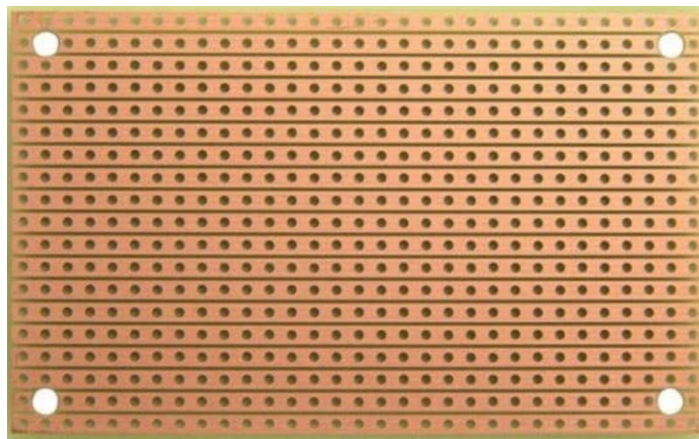


Figure 4.2: Image of solderable protoboard used for through-hole pull-down resistors

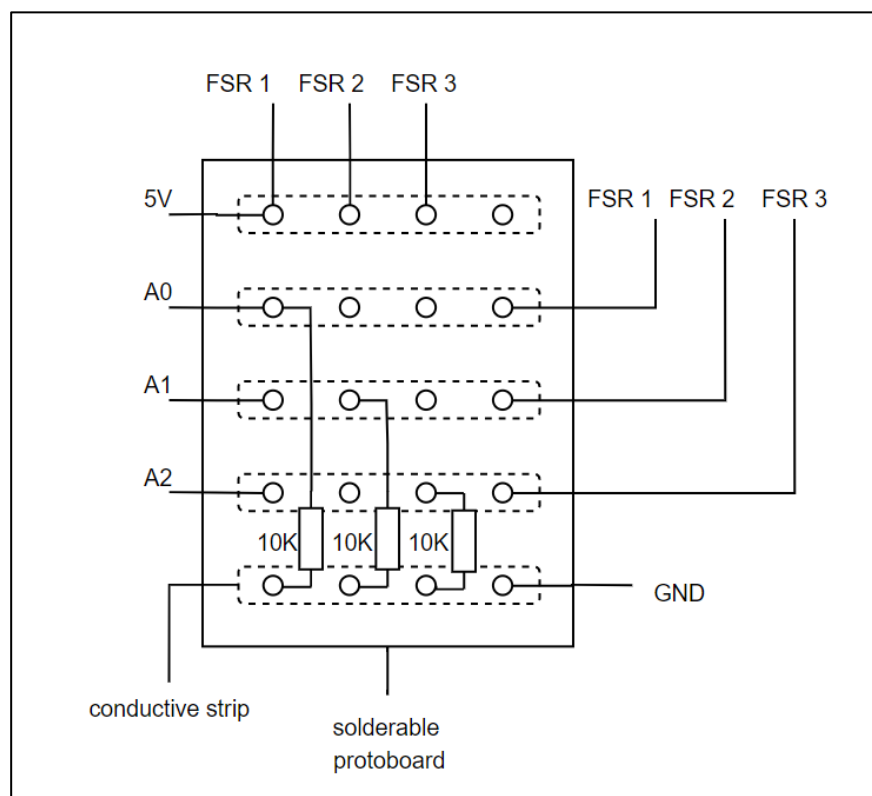


Figure 4.3: Schematic of protoboard and pull-down resistor layout

4.2.3 Battery and Switch Selection

The battery options for this project were limited due to the power requirements of the Beetle and the size constraints of the Zero-Cast Wx brace. The list of battery selection criteria along with justifications are shown in Table 4-4 below. Small batteries in the 6-8V range are uncommon and generally used only for specialized applications. A simple and practical solution first considered was to use a standard 9V battery and step down the voltage with a voltage divider circuit. The problem with this solution, however, was that a 9V battery was far too large to be considered a feasible option in the Zero-Cast Wx and this option would also require additional circuitry. Rechargeable lithium-ion battery were also strongly considered; however, they did not fulfil the voltage and size requirements for this project. The battery solutions shown in Table 4-5, were the only options considered to be the top contenders after conducting an online investigation. Each battery solution was evaluated in a weighted decision matrix shown in Table 4-6. The same scoring method for FSRs sensors and microcontrollers was used. The battery with the highest weighted score was selected.

Table 4-4: Battery selection criteria with design requirements/constraints

Criterion	Justification	Requirement/constraint
Voltage	This criterion was a minimum requirement as the Beetle BLE has specific power supply range.	6-8V Minimum requirement (not included in decision matrix)
Cost	Funding was limited due to the nature of this project (a master's thesis). Achieving the desired objective at a lower cost would also be commercially beneficial to Surgisplint	<\$10 per unit Lower overall cost scored higher in decision matrix
Size	The size of the battery contributes to the overall size of the electronics enclosure.	Battery should not exceed size of Beetle BLE –lower total volume scored higher in decision matrix
Capacity (mAh)	This directly affects how long the circuit can be operational for before the battery is replaced or recharged	Batteries with higher charge capacity will allow for longer use before replacement. Higher charges will score higher in decision matrix.
Units required	Multiple batteries at a lower voltage can be used in series if they are small enough	No more than two batteries in series to limit overall size and cost requirements. Fewer units will score higher.

Table 4-5: Batteries options considered for integration with Zero-Cast Wx Smart brace

Battery Solution & Description	Specifications	Image
1 X Exell L28PX Alkaline Used in cameras, garage door openers and small medical devices [83]	Voltage: 6V Capacity: 170 mAh Height: 25.2 Diameter: 13mm	
1 X Vinnic L1016 / Energizer A11 Typically used for a range of small devices such as garage door remotes and portable alarm systems [84, 85]	Voltage: 6V Capacity: 38mAh Height: 16mm Diameter: 10.3mm	
2 X CR2032 lithium coin Typically used in small portable electronic devices such as wrist watches, pocket calculators [86]	Voltage: 3V Capacity: 220 mAh Height: 3.2mm Diameter: 20mm	

Table 4-6: Decision matrix for battery selection

Battery		Selection Criteria				
		Cost	Size	Capacity	Units required	Total
	Weighting	2	4	1	3	
1 X Exell L28PX Alkaline	Score	1	1	2	3	
	Total	2	4	2	9	17
1 X Vinnic L1016 / Energizer A11	Score	3	3	1	3	
	Total	6	12	1	9	28
2 X CR2032 Coin battery	Score	2	2	3	1	
	Total	4	8	3	3	18

The circuit also required a very small and cheap switch solution - either a single pole single throw (SPST), single pole double throw (SPDT) switch or a latching type pushbutton that would power the circuit on and off with a single input action. Two possible switch options that met these criteria were found: a miniature single pole double throw (SPDT) sliding switch and miniature PCB latching push-button. Both options were cheap, however, we chose to use the mini slider switch without the need for a decision matrix because it is smaller in size and possibly has a lower risk of getting stuck when actuated.

Switch	Specifications	Image
SPDT micro slide switch	Switch type: Slide – single pole double throw Rated Voltage: 24V Rated current: 0.5A Mount type: PCB Height: 11.5mm Width: 10mm Depth: 2.5mm [87]	
PCB Mini Latching Tactile Push Button Switch	Switch type: latching push button Height: 12mm Width: 12mm Depth: 9mm [88]	

4.3 Electronic Enclosure Design

The primary purpose of the electronic enclosure in the POC design was to house all the components and provide adequate mechanical protection while being easily attachable to the exterior side of the Zero-Cast Wx volar plate. Minimizing the overall enclosure size while accommodating all components were prioritized over aesthetics for the purpose of developing a functional POC system. Although this initial design embodiment may be considered crude, it was foreseen that future iterations of the Zero-Cast Smart Brace would likely incorporate the components within the brace plates itself, thereby preventing any obtrusive parts and improving overall appearance. Details of the enclosure design are shown and described in the following subsections.

4.3.1 Part Assembly and Enclosure Features

The enclosure consisted of three components, the base, cover, and the battery cover which are all snap-fitted together as shown by Figure 4.4. All parts were modelled in Solidworks and 3D printed in the BioDesign Lab.

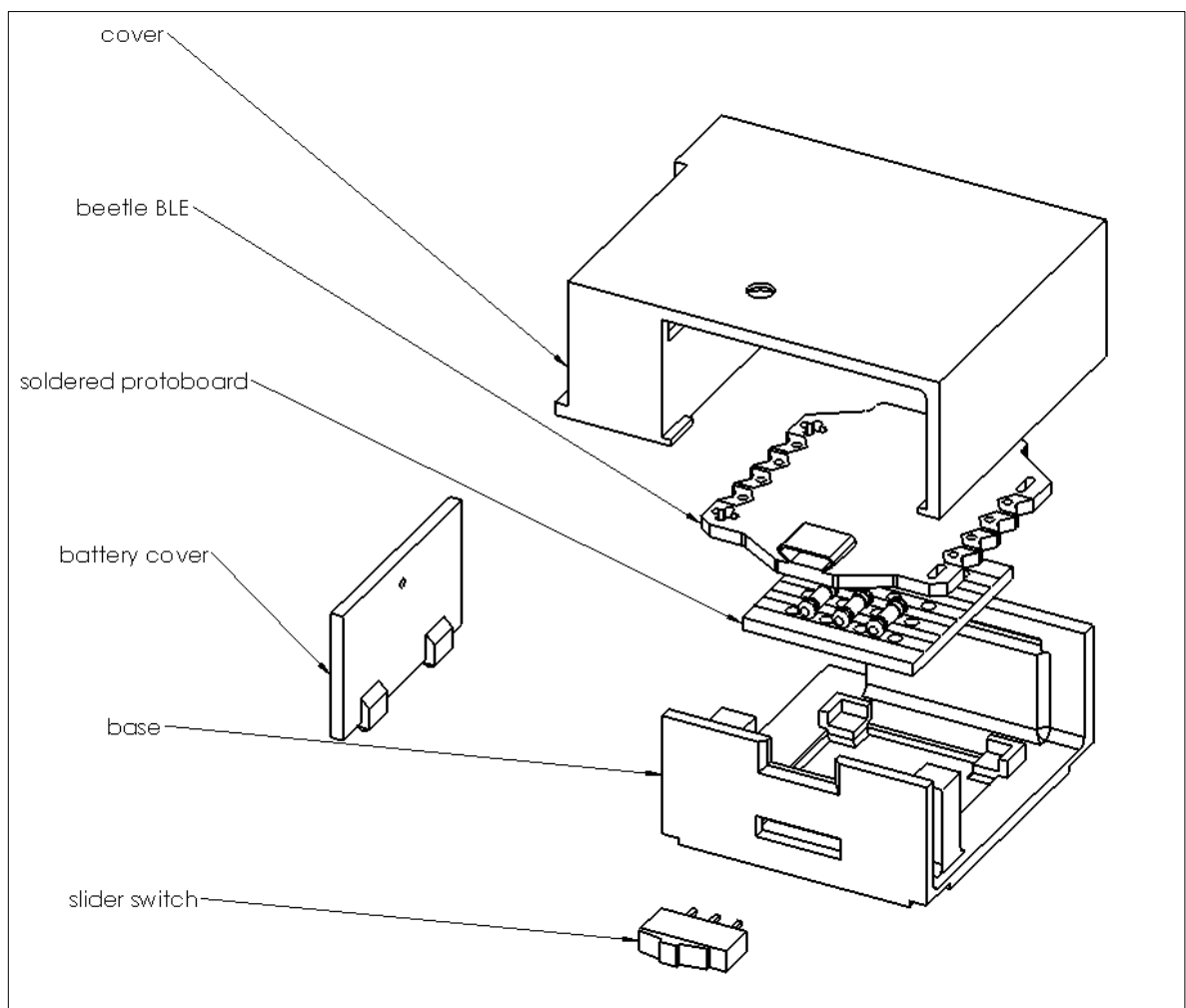


Figure 4.4: An exploded view of main components and enclosure

Figure 4.5 and Figure 4.6 show the main external features of the POC enclosure: A removable battery cover which allows the battery to be easily replaced, a slot to access the micro-USB port of the Beetle BLE, the slider switch to power the device, and a hole on the cover to show the light of the 'power on' LED.

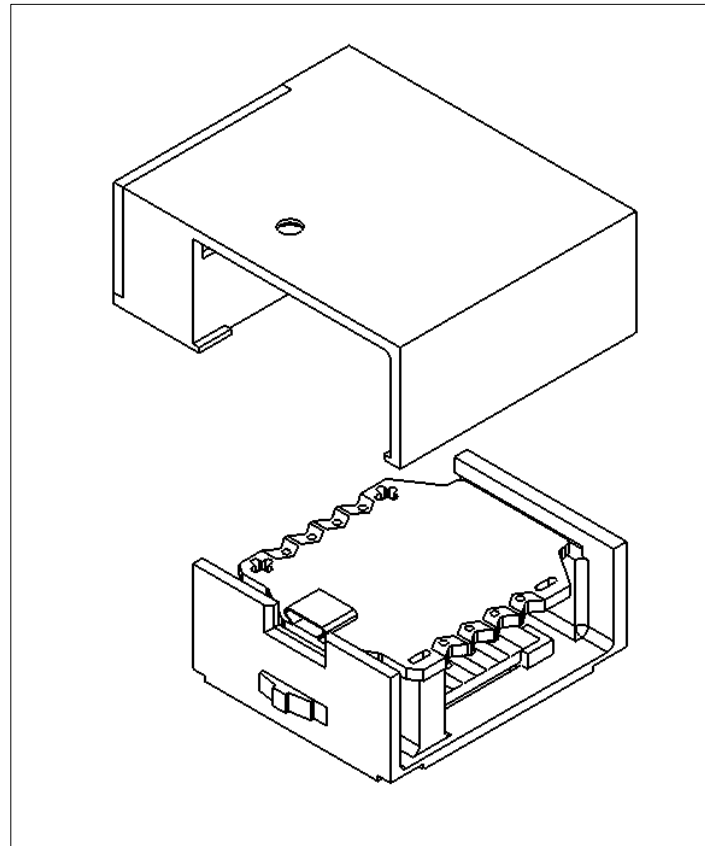


Figure 4.5: Partially assembled electronic enclosure

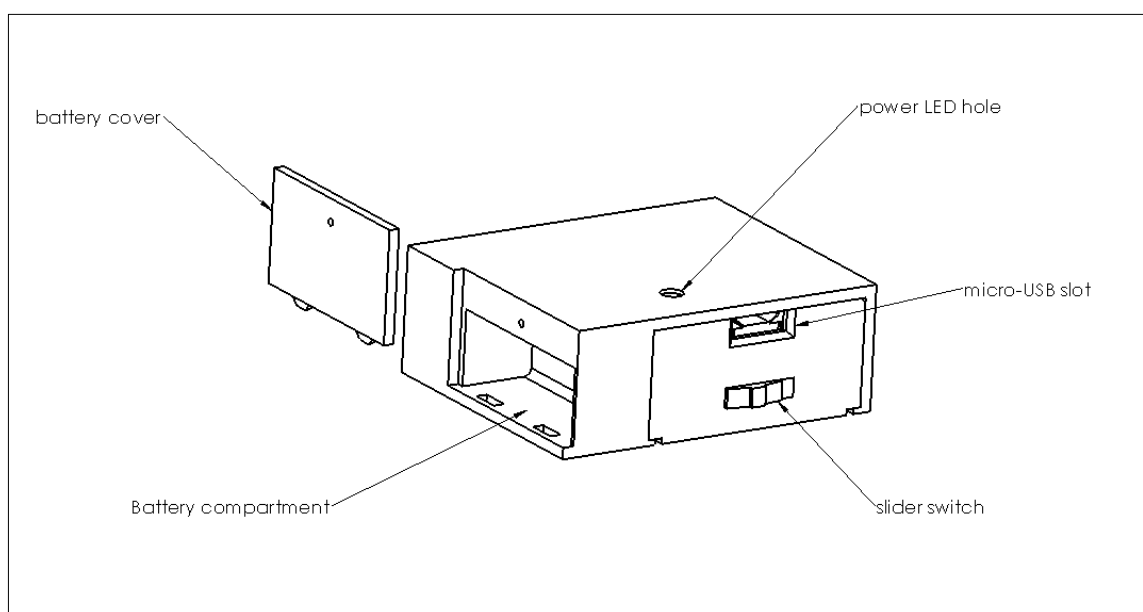


Figure 4.6: Assembled enclosure with battery cover removed

4.3.2 Design Details and Final Assembly Photographs

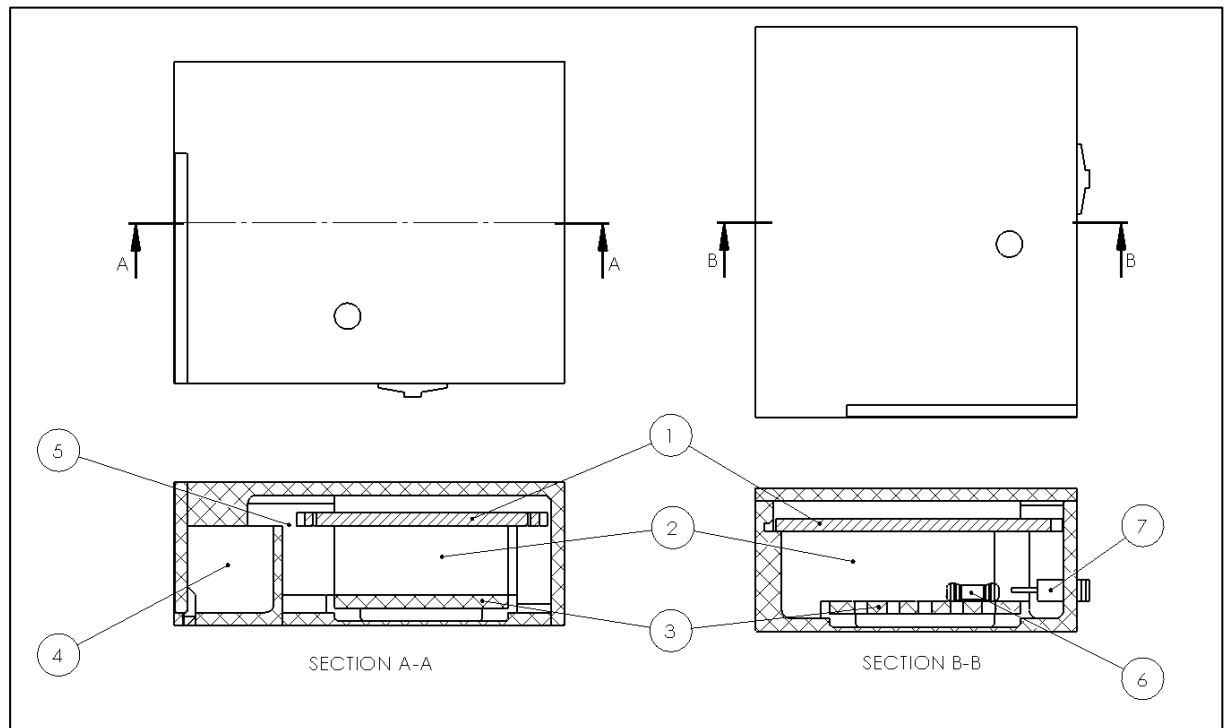


Figure 4.7: Section views of assembled enclosure with main components

1. Beetle BLE microcontroller – snap-fitted onto lip mount
2. Electrical wire compartment – provides space for electrical wire to pass from protoboard to Beetle and FSR sensors
3. Protoboard with header pins and through-hole resistors – snap-fitted onto raised corner mounts
4. Battery compartment – integrated with cover to keep electrically isolated and so that more space is available while electrical connections are being soldered in the base
5. Battery wire passage – a passage to feed the electrical wire from the battery to the Beetle and slider switch
6. Through-hole resistor – 10k ohm resistors soldered onto protoboard
7. Slider switch – snap-fitted into switch slot

Note: Electrical wire fed to FSR sensors pass through a slot at the back of the enclosure (top view with section A-A)

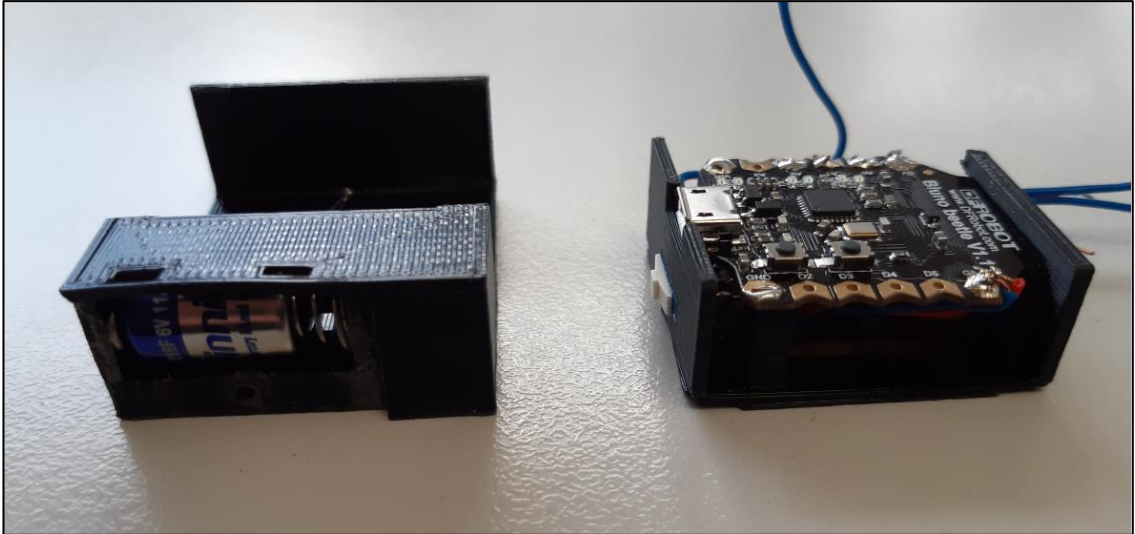


Figure 4.8: Image of cover with battery compartment (left) and base assembly (right)

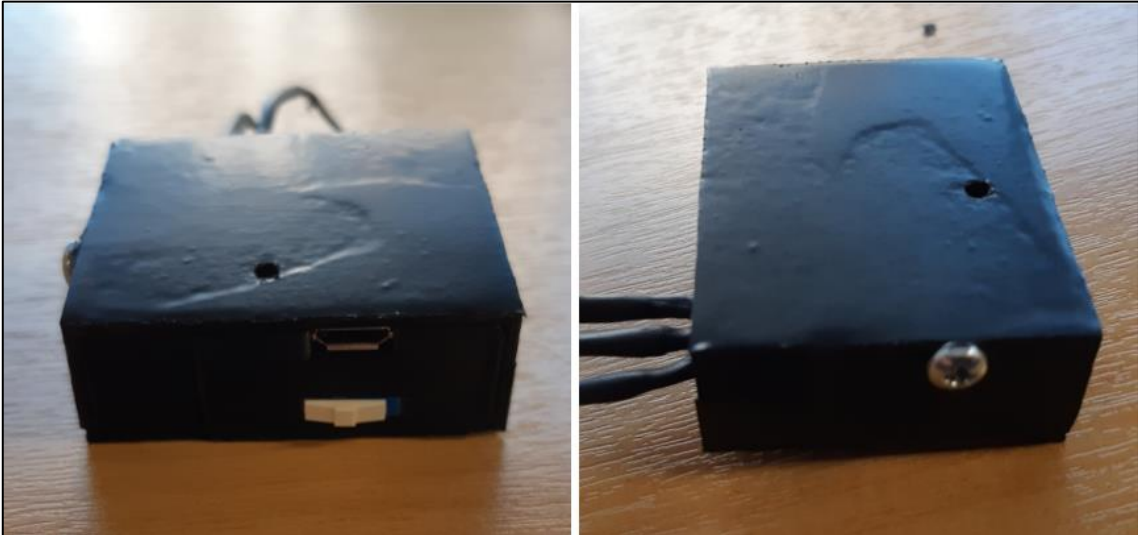


Figure 4.9: Images of fully assembled enclosure containing electronic components



Figure 4.10: Images showing the final POC wireless embedded FSR design in Zero-Cast Wx

4.4 Closure

This chapter documented the second and final stage of a POC embedded technology design in the Zero-Cast Wx brace system. A design methodology was implemented to select electronic components that met all specified requirements while also keeping within design constraints. An enclosure for the electronic parts was designed, 3D printed and assembled, which could now be used for training and testing machine learning algorithms. Chapter 5 looks at machine learning in more detail and investigates how this POC device could be used to apply a simple gesture recognition algorithm using data from a single user.

Chapter 5: Applied Machine Learning using Force Myography with the Zero-Cast Wx Brace

5.1 Introduction

In this chapter machine learning (ML) basics are covered in some more detail and the methods and tools of applying machine learning using embedded technology in the Zero-Cast Wx brace are discussed. A self-performed experiment for testing and demonstrating a simple hand gesture recognition algorithm is also reported.

5.2 Feature Engineering

Features, in the context of machine learning refer to the variables which help define what is being predicted or classified. Feature engineering can be defined as the process of transforming raw data into features which can then be used for training an algorithm. It consists primarily of three sub-processes: *feature extraction*, *feature scaling* and *feature selection* [89].

5.2.1 Feature Extraction

In subsection 2.4.2 of the literature review, the example of classifying photographs of dogs and cats was used. In this example, the ratio of the animals' body length to head width could be used as a feature by determining the number of pixels in the respective parts of the photograph. This is an example of feature extraction. It involves all the steps and transforms required to get raw data into usable features [89].

5.2.2 Feature Scaling

In many ML problems, datasets will often contain features that do not all have the same units or range. In order for ML models to be accurate, most of them require data which are scaled to have a common range. Although there are multiple ways of doing this, one of the most useful and popular ways are by min-max normalization or scaling. In this method the data are scaled to fall within a range of 0 to 1 [43, 89, 90]. This is achieved by implementing the formula:

$$x' = \frac{x - x_{min}}{x_{max} - x_{min}}$$

Equation 5-1: Min-Max data scaling

Where:

x' is the new scaled data point

x_{max} is the maximum value in the dataset

x_{min} is the minimum value in the dataset

x is the original data point

5.2.3 Feature Selection

It is usually unknown which features or combination of features will produce the most accurate classification algorithms. Features can be selected and tested manually or by using statistical selection methods to determine which ones are most relevant to the predicted class. Three of the most utilized feature selection methods include:

1. *Feature Correlation* - This selection technique evaluates the linear correlation between a feature and the class. A correlation coefficient (Pearson's) given between -1 and 1 indicates the degree to which the feature correlates with the class. Values close to 0 are considered to have a weak correlation with the class, while those close to 1 or -1 have stronger correlations [89, 90].
2. *Information gain* - This selection method evaluates the worth of a feature by measuring the information gain in relation to the class. Information gain is also referred to as entropy and is given as a value between 0 and 1. Features that contribute more information will have a higher information gain value and can therefore be selected over lower performing features [89, 90].
3. *Learner based* - A learner-based selection method involves evaluating the performance of a preselected classification algorithm on the dataset with different combinations of features selected. The subset of features yielding the best performance is then taken as the final selection. The algorithm used for testing various feature combinations is usually simple but powerful such as a decision tree. It is also worth noting that the algorithm used for feature selection does not have to be the same algorithm used for training the final model [89, 90].

Once the feature engineering process is complete, the data is compiled into table or matrix, which can then be used to train an algorithm. Figure 5.1 shows an algebraic formulation for a supervised machine learning dataset. The columns of the matrix represent the selected features and the rows are interchangeably referred to as observations, instances, or feature vectors. A single observation or instance corresponds to a labelled class value in the target vector [89].

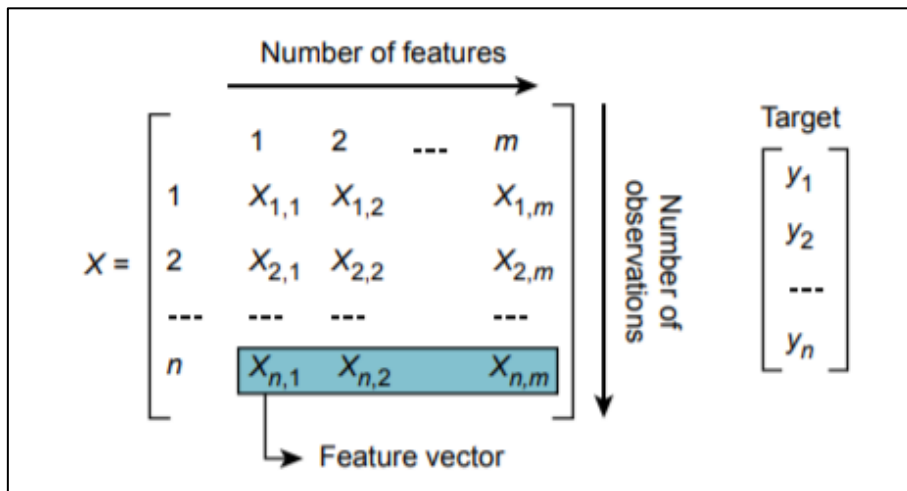


Figure 5.1: An algebraic representation of a supervised machine learning dataset [89]

5.3 Algorithm Training and Evaluation

In supervised machine learning, algorithm training is a process by which a function f is found that mathematically describes a set of mapped outputs to a set of input features. The main objective of machine learning, however, is to find such a function that can accurately map new unseen data. The best test for a machine learning algorithm is therefore to see how well it can generalize its function f to data that was not used to train it. Algorithm training itself, involves using a range of statistical techniques and steps which can be efficiently executed by a computer. The classification algorithms used in this project are briefly described in section 5.5 and in more detail in Appendix B [43, 89].

5.3.1 Cross-Validation

Trained algorithms are evaluated by testing their performance on a test dataset. In very large datasets where there are thousands of instances, a technique known as the *hold-out* method is typically used to evaluate algorithm performance. In this technique the whole dataset is split in two parts with one being used for training the algorithm and the other for testing it. This technique, however, does not work well on smaller datasets because the learned function may be biased toward the data it was trained on and may not perform well on unseen data [43, 89-91].

A better technique used with small datasets, is called *k-fold cross-validation*. In this technique the dataset is randomly split into k sets of equal size, with $k-1$ groups being used for training the algorithm and one group being used to test it. This is repeated k times or folds, so that each set is used $k-1$ times for training and once testing. The overall algorithm performance is then calculated by taking the average test

performance across all iterations. This technique is more clearly shown in Figure 5.2 where in each iteration non-highlighted blocks represent datasets used for training and the highlighted block represents the dataset used for testing. As the value for k approaches 2 (i.e. data split into two sets), the model performance becomes biased as the algorithm learns associations that are unique to the single training and test set. As k approaches N , the number of observations in the entire dataset, the model performance becomes highly variable because there is only one observation to test on for each iteration. This becomes especially pronounced when there are outliers in the data. Figure 5.3 illustrates the concepts of bias and variance and shows their relationship to model complexity [89, 90].

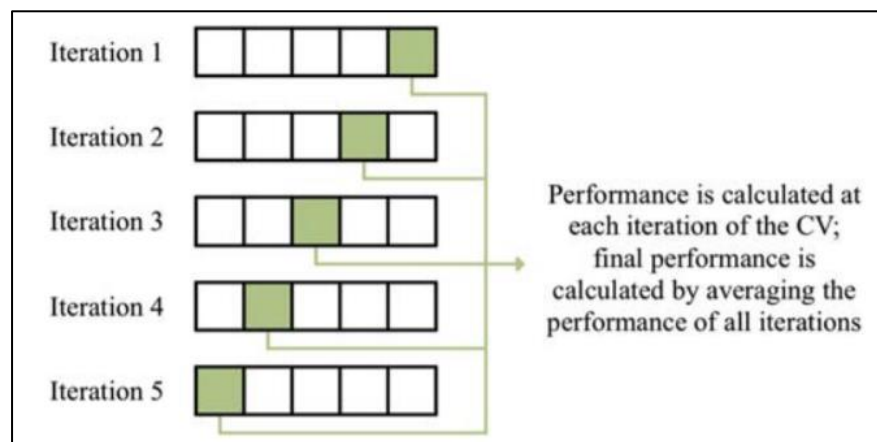


Figure 5.2: An illustration of the k -fold cross validation method with k equal to five [89]

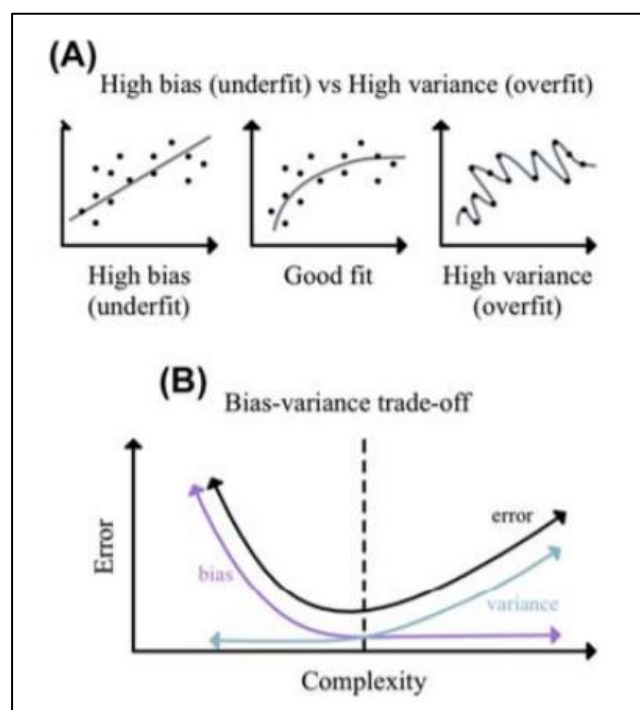


Figure 5.3: A) Examples of different levels of bias and variance in machine learning models B) The trade-off between bias and variance with changing model complexity [89]

Two of the most popular validation schemes in machine learning are 5-fold and 10-fold cross-validation. This is because they have been shown to produce a good trade-off between bias and variance in model performance. Another key concept which affects algorithm performance is *class balance*. Recall that a binary class classifier, is a supervised machine learning model that predicts two possible outcomes. A dataset is said to be balanced when there are an equal number of classes for the algorithm to train on. This may not always be possible in real world problems, but it does give one more confidence in the model when classes are balanced or close to being balanced. There are various methods for accounting for class imbalances, but this will not be explored in this thesis. Finally, stratified cross-validation is referred to when class the ratio in the training dataset is equal to the class ratio in the test set. This is the best method for evaluating algorithm performance on small datasets [89, 90].

5.3.2 Classification Accuracy

In classification problems, accuracy is commonly used as the main indicator of algorithm performance. It simply refers to the percentage of correct predictions made by an algorithm. In each iteration of *k-fold* cross-validation, the classification accuracy is defined as the percentage of correct predictions in the test set. This accuracy is averaged across all iterations to indicate the overall performance measure of the algorithm. In unbalanced datasets (unequal class sizes), it is sometimes more appropriate to assess the accuracy of each class. Using a confusion matrix is a standard way of understanding where an algorithm performs well and where it performs poorly. Figure 5.4 shows a confusion matrix for a simple binary (2-class) classifier. Classifier accuracy is therefore expressed algebraically by Equation 5-2. If only a confusion matrix is considered, then larger values in the matrix diagonal and smaller non-diagonal values indicate better overall algorithm performance [89].

$$Accuracy = \frac{TN+TP}{TP+TN+FN+FP}$$

Equation 5-2: Classification Accuracy

		Predicted labels	
		Negative	Positive
True labels	Negative	True Negative (TN)	False Positive (FP)
	Positive	False Negative (FN)	True Positive (TP)

Figure 5.4: Confusion matrix for a binary classifier [89]

5.3.3 Dataset Size

There are a number of factors that affect algorithm performance, one of which includes training dataset size. While there is no set rule for how large a dataset needs to be in order to train an algorithm, there are some general guidelines and statistical methods that can assist with this problem [92, 93]. A common method to predict the required size of a dataset in classification problems is to develop a learning curve with the available data. Here the classification accuracy is plotted against data size and a mathematical model can be fitted to the curve using a weighted nonlinear regression technique. The fitted model usually follows an inverse power law as shown by Figure 5.5. The model is then used to predict classification accuracy for larger datasets [93-95]. A challenge with this method is that it still requires some data to produce a sufficient portion of the learning curve so that a model can be fitted.

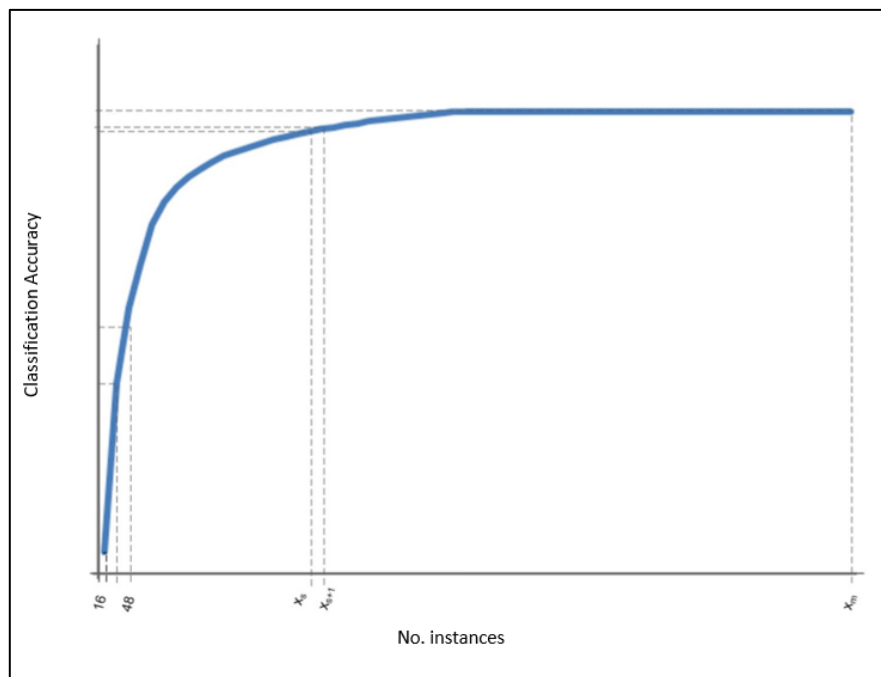


Figure 5.5: A generic learning curve for a classification problem

Therefore, when there is little to no data available, or when data is difficult or expensive to obtain other empirical rules have been developed to estimate the amount of data required. For example, the rule of 10 is a statistical heuristic which considers the relationship between model performance and the ratio of dataset size to feature. Here the amount of data required is estimated to be about 10 times the number of features used [96].

5.4 Using Waikato Environment for Knowledge Analysis

5.4.1 Background and Justification for Use

The Waikato Environment for Knowledge Analysis (WEKA) is an application software available for applied machine learning. The platform is written in JAVA and hosts a suite of machine learning tools which can be used to make predictive models from training data. WEKA is intended to be used as a tool by analysts across multiple disciplines and has the advantage of only requiring a basic understanding of statistics and data science.

While there are many other ML applications and platforms available, such as MATLAB, Simulink, and Python, they can be time and resource intensive due to specific coding requirements. WEKA was therefore primarily selected because it does not require any code to train and test the ML algorithms. The user simply has to import the data in a structured CSV format and then select one or multiple algorithms to train and test.

5.4.2 Interface and Primary Applications Used

WEKA has a simple and intuitive graphical user interface, easily accessible to users that are new to data science or machine learning. Figure 5.6 shows the WEKA start-up window with all its various applications. The *Explorer* and *Experimenter* were the only applications used for this project. They will be discussed briefly in this subsection.



Figure 5.6: Weka start-up window showing the various applications

Weka Explorer Application

The *Explorer* application allows the user to investigate their dataset in more detail. It provides more insight into the dataset through data transforms and visualizations. Additionally, the user can test out their dataset on selected algorithms before performing a controlled experiment with the *Experimenter* application. The interface is split into six tabs, each with a specific function. Only tabs used in this project will be reviewed. Figure 5.7 shows the *Preprocess* tab in the *Explorer* application with an imported dataset. This tab is where data is first loaded and where various filters can be applied to restructure data prior to any modelling. It also shows a summary of descriptive statistics for the dataset.

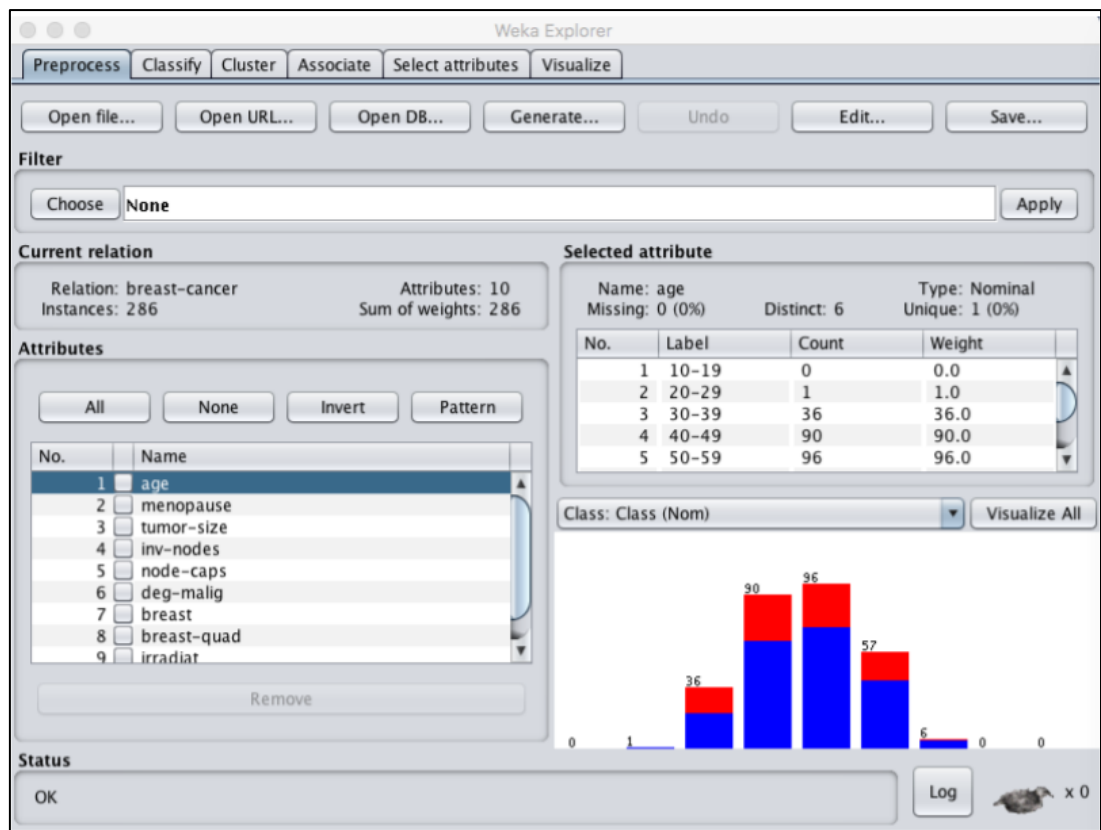


Figure 5.7: Screenshot of the Preprocess Tab in the Weka Explorer Application

The *Classify* tab shown by Figure 5.8 is for training and testing the performance of selected algorithms on the users' dataset. Selected algorithm results are shown in the *results list* pane and a detailed summary of the results are shown in the large *Classifier output* pane.

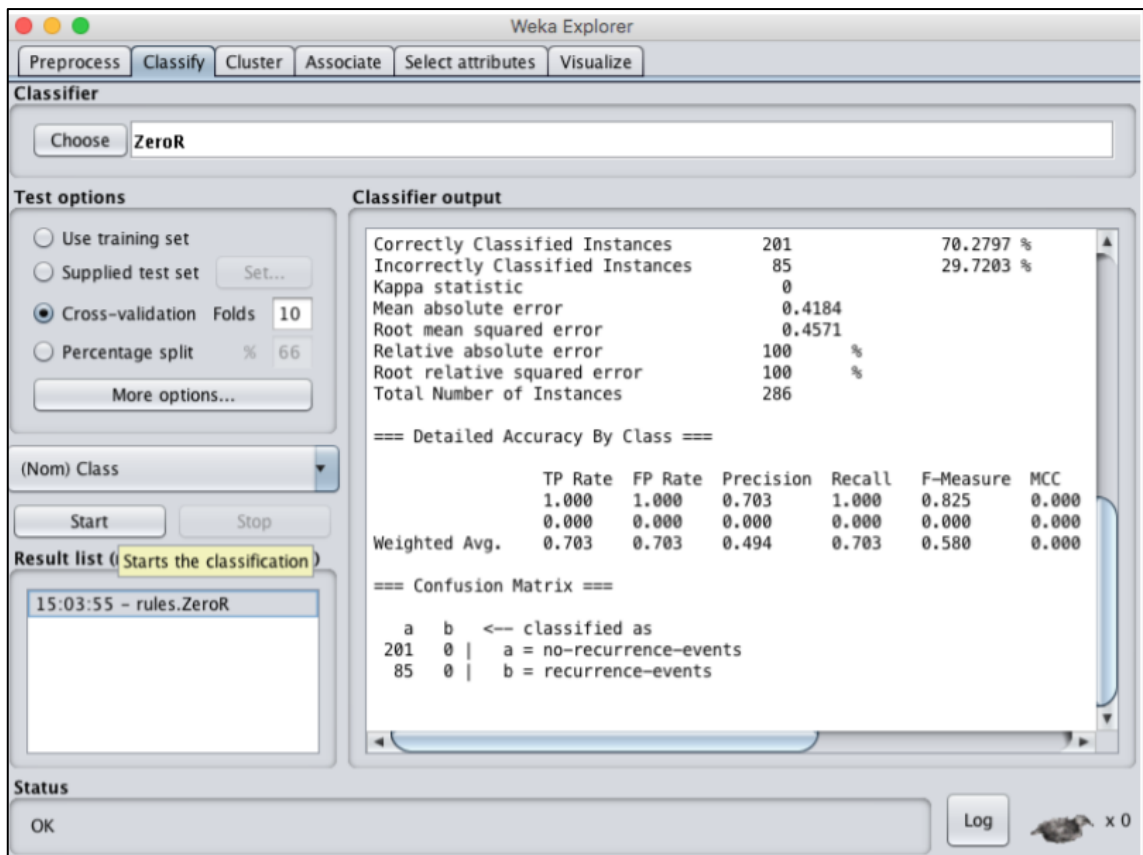


Figure 5.8: Screenshot of the *classifier tab* in the *Weka Explorer* application

The *Select attributes* tab is for carrying out a feature selection technique on the user's dataset in order to determine which features (variables) are most relevant to developing a classification model.

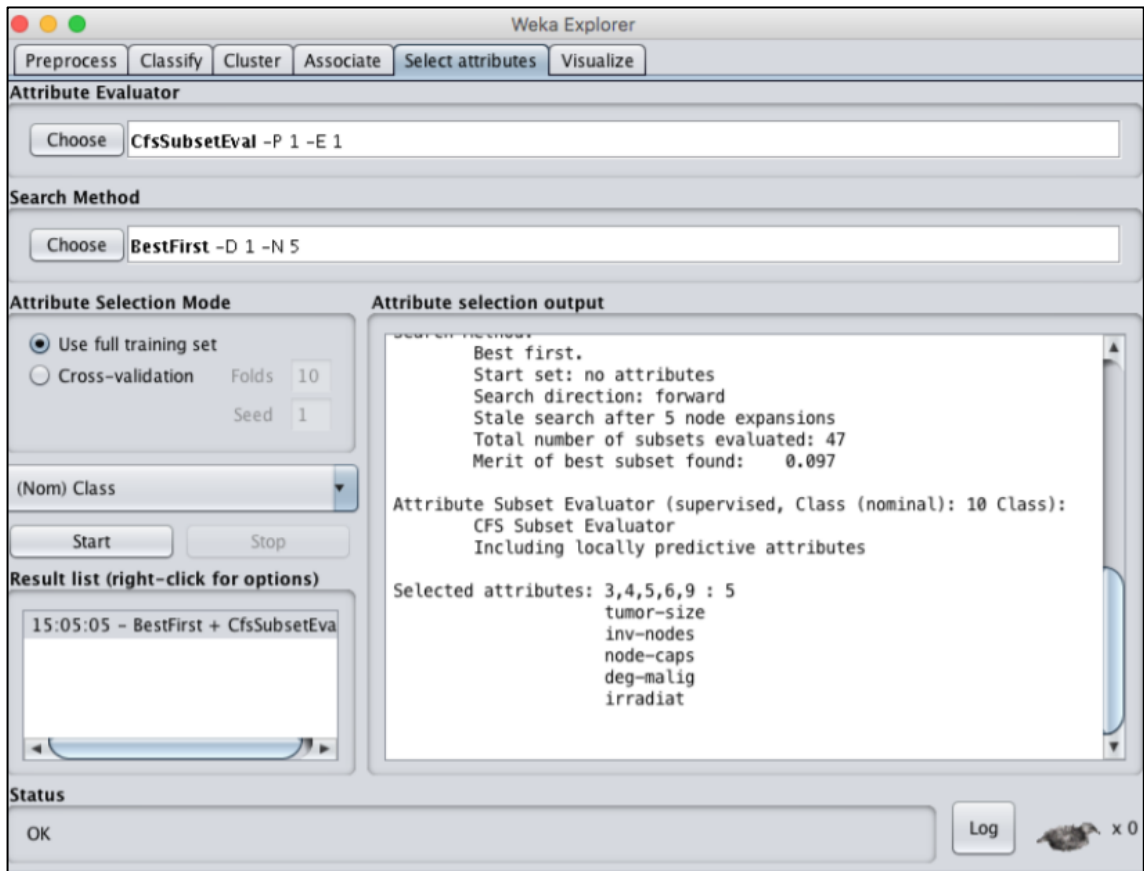


Figure 5.9: Screenshot of the *Select Attributes* tab in the Weka Explorer application

Weka Experiment Environment

The Weka *Experiment* application is used for creating and running controlled experiments. It is generally applied after the *Explorer* application has been used to examine and manipulate a dataset. Multiple versions of a dataset can be imported along with multiple algorithms in order to find a result that yields the best performance. This application is split into three tabs: the *setup*, *run* and *analyse* tabs. The *setup* tab is where the experiment is designed by importing different versions of the dataset and importing algorithms to be trained. The *run* tab is where the execution of algorithm training occurs and the *analyse* tab is where the results are interpreted using a suite of statistical techniques. More on this is described in chapter 6 when applied in the multi-user pilot study.

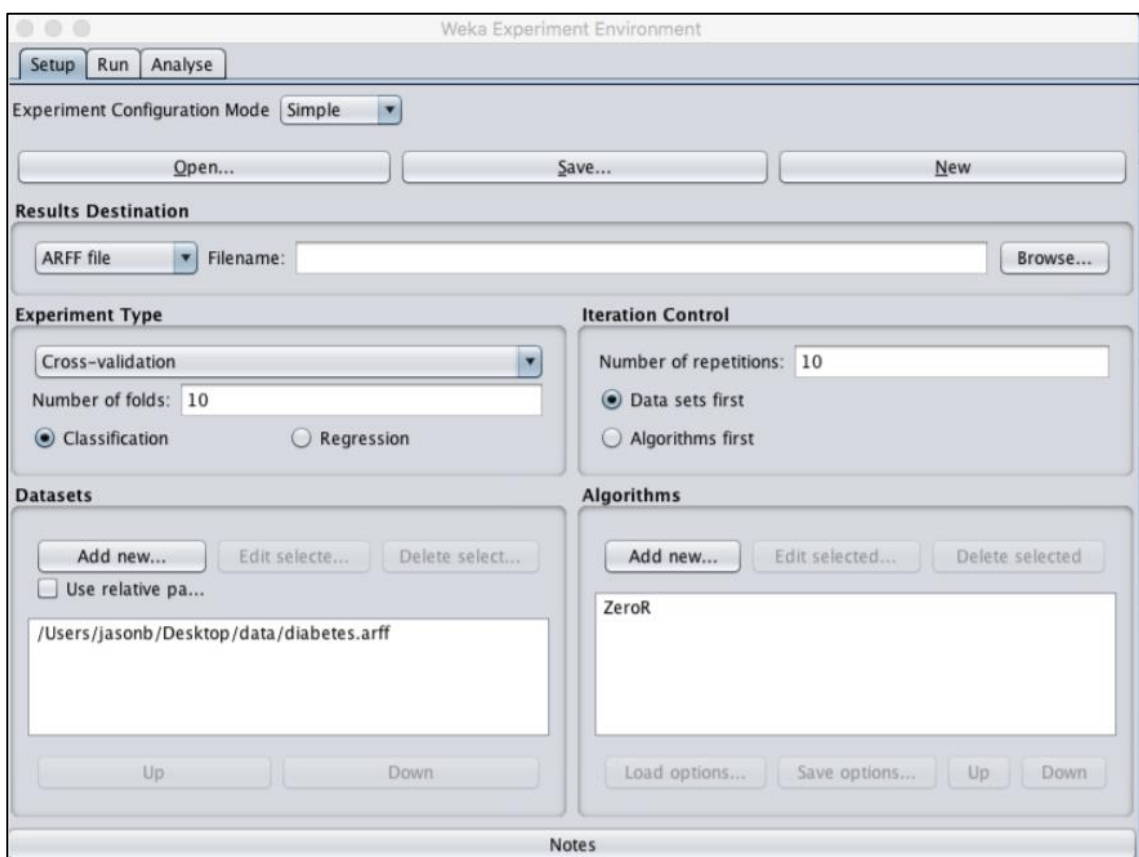


Figure 5.10: Screenshot of the *setup* tab in the Weka *Experiment* Environment

5.5 Machine Learning Algorithms for Classification Problems

A brief outline of the algorithms used in this project is discussed in this section. For a more detailed description of these algorithms please refer to Appendix B.

5.5.1 Logistic Regression

This algorithm produces a regression model through a linear combination of the input features which is then transformed with a logistic function (s-function). Although it is usually only applied to binary classification problems, the WEKA implemented Logistic Algorithm has been adapted to support multiclass problems.

5.5.2 Naïve Bayes

The Naïve Bayes algorithm uses a simplification of the Bayes Theorem in which the probability of each class occurring is calculated from the training data.

5.5.3 Decision Tree

A decision tree algorithm is made with a series of decisions based on feature values. The tree is usually structured with binary questions about features represented as nodes and decision paths represented as branches. The predicted class value is represented by the leaf node or terminal node in the tree structure.

5.5.4 K-Nearest Neighbours

In the K-Nearest Neighbours (KNN) algorithm, the k most similar data points are used from the training dataset in order to make a prediction for a class value. It is a simple algorithm that uses similarities between data to make predictions.

5.5.5 Support Vector Machines

Support Vector Machines (SVM) are traditionally used for binary classification problems, although WEKA does implement an extension tool to support multiclass classification. This algorithm works by finding the best way to separate data into classes with different types of boundaries.

5.5.6 Random Forest

Random forest is an algorithm which takes the average of an array of decision trees which are built from various parts of the training data. This algorithm typically performs better than a single decision tree as it reduces overfitting i.e. when the model is too closely correlated with the training data and therefore cannot accurately classify new data.

5.6 Machine Learning using WEKA and User-Specific FMG Training Data

5.6.1 Acquisition of Training Data

The POC embedded FSR system shown by Figure 4.10 in Chapter 4 was used to acquire training data for machine learning. The same data acquisition software described in subsection 3.2.6 was used. In this instance the data was being sampled wirelessly via Bluetooth with the Beetle BLE microcontroller and a BLE USB dongle. The POC brace was fitted to the left arm of the single user with the tightness of the fit recorded by measuring the ratchet arm lengths (screws on dorsal plate were kept flush with surface). The tendon gliding exercises along with the default relaxed position were set to be the class outputs in this self-performed ML experiment. During data collection the five gestures: relaxed, extended hand, hook fist, flat fist and thumb flexion (tendon gliding exercises shown by Figure 3.21) were performed in sequence. Each gesture was held for three to five seconds before transitioning to the next while data was sampled in LabView. After each complete sequence, the LabVIEW program was stopped, and the acquired data exported to Excel. The brace was removed and then reapplied to the wrist at the same measured fit as in the previous case. This was done to create some variability in the training data so that the learned algorithm did not become biased to any particular training set. A total of ten training sets were obtained, each time with the brace being removed and re-fitted.

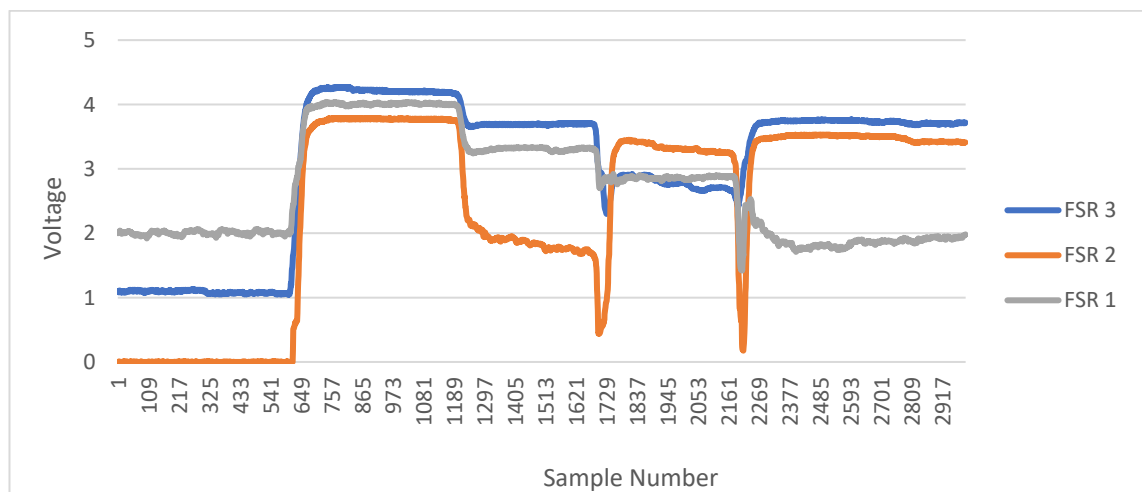


Figure 5.11: Plot of wirelessly sampled FSR voltage data during tendon gliding exercise sequence

5.6.2 Feature Extraction

After ten training datasets were obtained, the average FSR amplitude of each gesture was extracted as a feature. The average amplitudes were taken when voltage values had stabilized, and the hand was stationary at each gesture position. This step is more clearly shown by Figure 5.12. Each gesture therefore had ten examples for training an algorithm. This meant the entire training dataset consisted of 50 instances or observations: 5 class outputs and 10 training examples for each (relaxed position included as a class output). Table 5-1 shows a sample (15 observations) of the dataset that was imported into WEKA to train a simple classification algorithm.

Notes:

- feature scaling was not required in this experiment as features had same units and came from the same individual user
- All three features were used for this experiment, so feature selection was not implemented

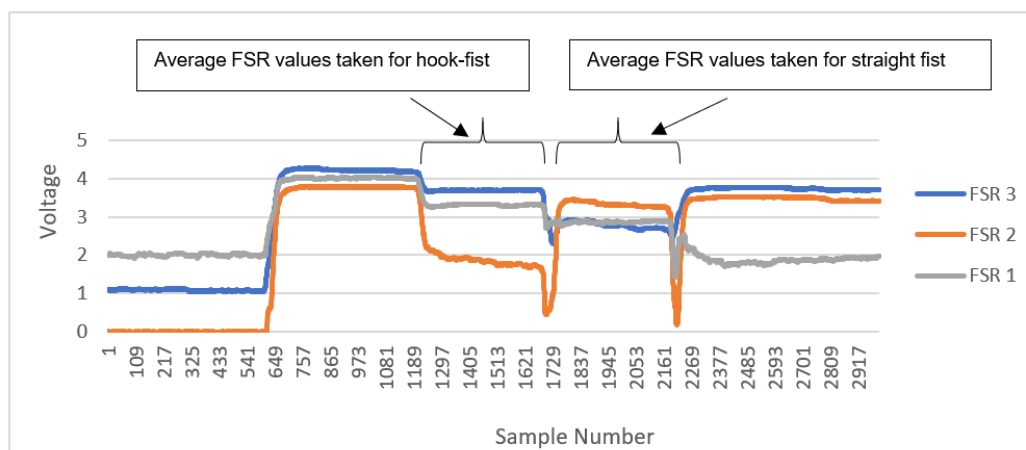


Figure 5.12: Example of feature extraction for tendon gliding sequence

Table 5-1: Sample of training dataset

FSR 1	FSR 2	FSR 3	Class
1.09	0.00	2.01	relaxed
4.22	3.77	4.01	extended
3.69	1.86	3.31	hook fist
2.79	3.34	2.86	flat fist
3.74	3.49	1.85	thumb
0.90	0.00	2.18	relaxed
4.20	3.73	4.07	extended
3.73	1.72	3.41	hook fist
2.94	3.02	2.96	flat fist
3.58	3.12	1.69	thumb
0.83	0.00	2.39	relaxed
4.20	3.97	4.23	extended
3.65	2.16	3.72	hook fist
2.59	3.31	2.99	flat fist

5.6.3 Algorithm Training and Evaluation with WEKA

The *WEKA Explorer* application was opened, and the training dataset was imported in the *Preprocess tab* as shown by Figure 5.7. In the *Classify* tab, a simple but powerful decision tree algorithm, abbreviated J48, was selected for this experiment. This algorithm was chosen because the output could be easily programmed into LabVIEW or other programming languages for real-time demonstration purposes. Using 10-fold cross-validation (WEKA uses stratified cross-validation by default) the algorithm performance was evaluated with the classification accuracy and the confusion matrix. The screenshot in Figure 5.13 shows that the algorithm performed exceptionally well with data from a single user. A classification accuracy of 92% was achieved and the confusion matrix shows that the algorithm only misclassified two instances in the worst performing class (two actual flat fist gestures were misclassified as thumb gestures)

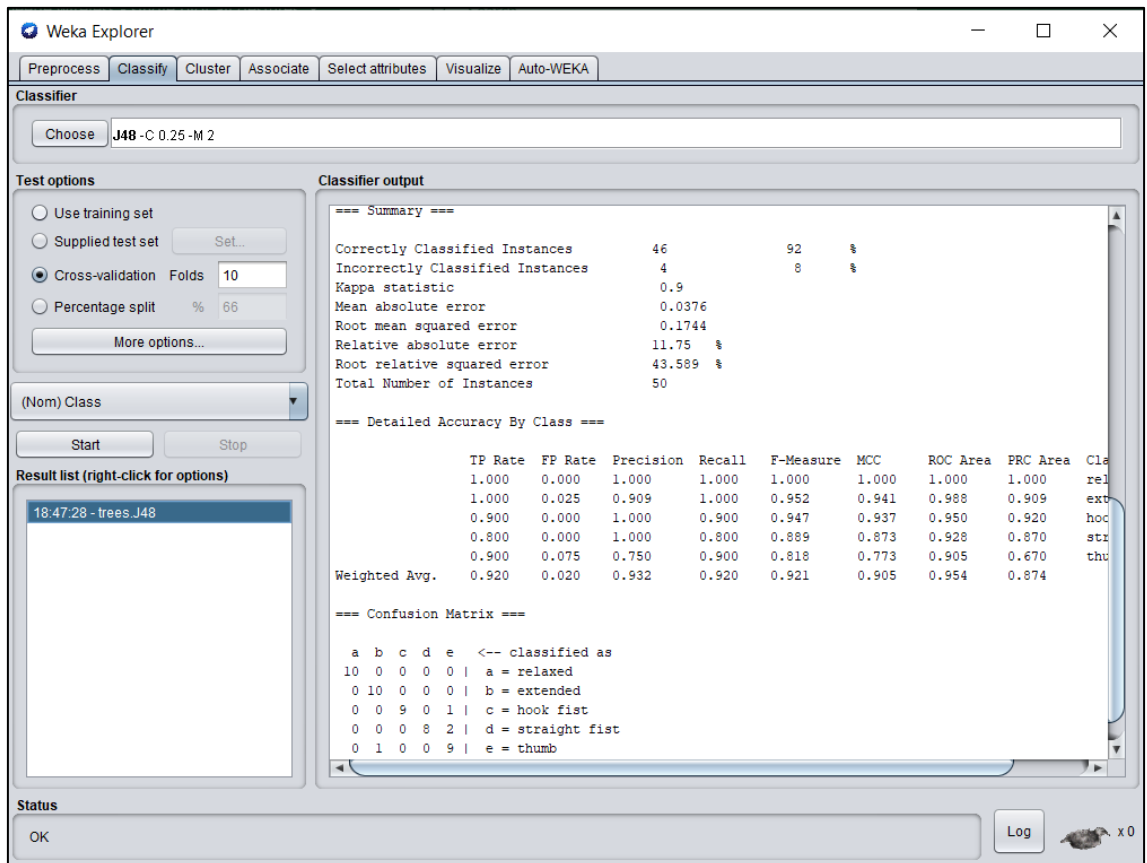


Figure 5.13: Screenshot of WEKA results for J48 algorithm

5.6.4 Demonstration of a Real-Time Multi-Class Classifier

The decision tree algorithm of subsection 5.6.3 was used to program a simple real-time classifier in LabVIEW (Appendix C). The decision tree algorithm taken from WEKA is shown by Figure 5.14. The algorithm makes the following predictions for hand position based on the training data discussed in subsection 5.6.2:

- *relaxed* predicted when FSR 2 voltage is equal to 0
- *hook fist* predicted when FSR 2 voltage is greater than 0 but less or equal to 2.16
- *flat fist* predicted when FSR 2 voltage is greater than 2.16 and FSR 1 voltage is less or equal to 3.54
- *thumb flexion* predicted when FSR 2 voltage is greater than 2.16 and FSR 1 voltage is greater than 3.54 but less or equal to 3.79
- *extended hand* predicted when FSR 2 voltage is greater than 2.16 and FSR 1 voltage is greater than 3.79

In this particular case, even though training data from all three FSRs was provided, the algorithm only used data from FSR 1 and 2 to make predictions for new data on the same brace fit with the same user.

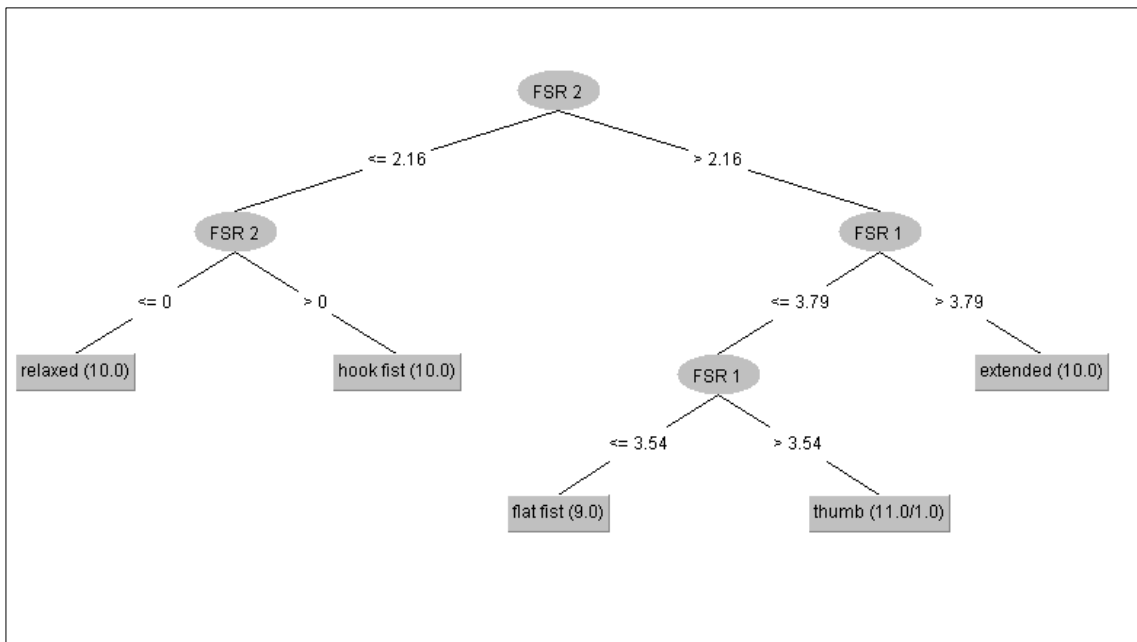


Figure 5.14: J48 decision tree algorithm used for five gesture classifier

For the demonstration, a simple graphical interface was also created in LabVIEW to show which gesture is currently being predicted and how many times it has already been predicted. This graphical interface is shown by Figure 5.15. An image of the real-time classifier demonstration is shown in Figure 5.16.

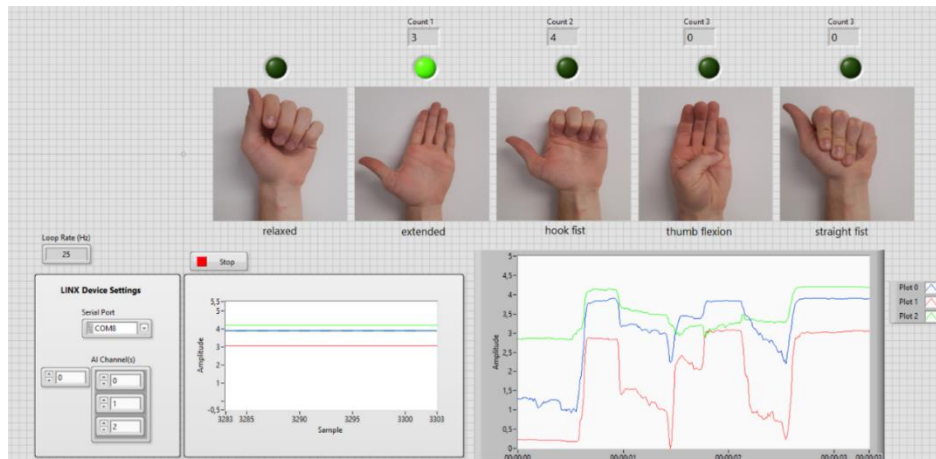


Figure 5.15: Graphical interface designed for real-time gesture classifier

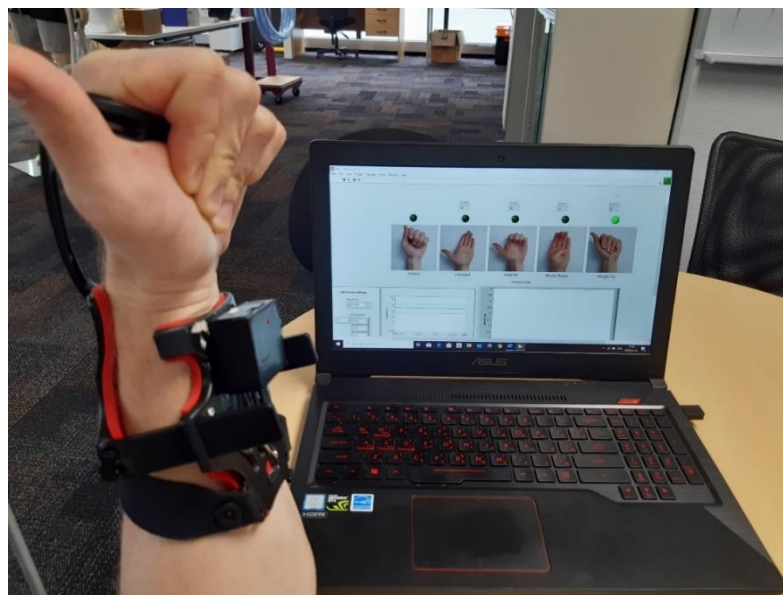


Figure 5.16: Image of the wireless classifier demonstration

5.7 Closure

In this chapter the fundamental concepts and terminology of machine learning were discussed in more detail. The WEKA software for applied machine learning was described and some popular classification algorithms available in the application were briefly explained. Finally, a real-time hand gesture classifier was demonstrated using the POC embedded sensor system integrated with Zero-Cast Wx. The following chapter discusses an in-house pilot study undertaken for the purpose of assessing the viability of classifying hand rehabilitation exercises and functional hand tests using data from multiple users.

Chapter 6: Pilot Study Investigating Multi-User Force Myography Training Data for Algorithms that Classify Fitting Force and Hand Motion Artefacts

6.1 Introduction

This chapter discusses an in-house pilot study undertaken to evaluate the POC Zero-Cast Wx embedded sensor system using training data from multiple users. It addresses the objective of evaluating the feasibility of classifying fitting force, rehabilitation exercises and functional hand tests using data from multiple users in a small pilot study of 21 participants. The results of the study are also used to achieve the final objective of this project which is to determine a configuration of an improved sensor array that can be used in future design and study iterations.

6.2 Study Design and Methodology

6.2.1 Justification for a Pilot Study

The intention of this study was to validate the POC Zero-Cast WX embedded sensor system and provide the data required to determine if an algorithm for fitting force could be generalized across patients and subsequently give clinicians a more objective method for fitting the brace.

The results of the previous chapter showed how embedded FSRs in Zero-Cast Wx could apply FMG and machine learning to accurately classify five hand rehabilitation gestures using training data from a single user. Although this was a positive outcome, it was also required to investigate the possibility of using training data from multiple users to produce a generalized classification algorithm that would recognize a hand gesture or hand function with a high degree of accuracy on any user. The justification for this was based on the premise that some patients who have suffered a DRF would have difficulty in training a hand gesture recognition algorithm in the early stages of recovery.

Previous research on hand gesture recognition has shown that highly accurate cross-session classification can be difficult to accomplish due to anatomical differences among participants and the difficulty in achieving identical fits when applying the device to the hand or arm [61, 66]. It was hypothesized, however, that given sufficient data and by limiting the number of classes in each algorithm, it may be possible to produce universal algorithms for brace fits, rehabilitation exercises, and specific functional hand

tests. The following subsections outline the four high-level outcomes which if met, would achieve the objectives of this pilot study.

After consulting with the Surgisplint medical team, it was agreed that the research objectives would be achieved via four high-level outcomes. These outcomes are described in the following subsections.

6.2.2 Outcome 1: Classifying Fitting Force in the Two Stage Fit of Zero-Cast Wx

This outcome would be met by developing two separate classification algorithms, one for the ratchet arm fit and one for the dorsal tilt fit. For both fitting stages it was decided that three classes of fit would be used as the classifier outputs. These classes were labelled as a tight fit, loose fit, and good fit. The fit types were quantified based on FSR voltage readings. A tight fit was declared when at least one FSR voltage read 3V and above; a loose fit declared when all FSR voltages read below 1.5V; and a good fit declared when at least two FSR voltages read between 1.5V and 3V. The voltage boundaries defined were used for both ratchet arm and dorsal tilt fits. The fitting values were determined from initial self-performed fitting tests with the aid of the official Zero-Cast Wx fitting guidelines. Fitting data would be acquired from multiple participants to train the algorithms. An acceptable classification accuracy was defined as 75% and above.

6.2.3 Outcome 2: Classifying Passive Finger and Thumb Motion

Subsection 2.3.5 discussed the potential utility of passive finger and thumb motion as an early stage rehabilitation intervention that would not risk injury to callus bone tissue. For practical purposes, a physician may want to know if a patient has engaged in active hand motion when they should only be practicing passive motion. Passive digit extension, passive thumb extension and active hand extension were therefore selected as the first motion artefacts to be investigated in a multi-class classifier using training data from multiple users. Motion data would be acquired from multiple participants to train the algorithm. An acceptable classification accuracy was defined as 75% and above.

6.2.4 Outcome 3: Classifying Tendon Gliding Exercises

The use of tendon gliding exercises as a mitigation measure for multiple DRF complications has been strongly motivated in this thesis. Classifying selected tendon gliding exercises using embedded sensor technology in Zero-Cast Wx and single-user training data has been validated and demonstrated in previous chapters. Given the potential significance of these exercises during immobilization it was necessary to test the viability of a multi-user classification algorithm. The same sequence described in

subsections 3.2.7 and 5.6.1 was used in data gathering from participants: relaxed, extended hand, hook fist, flat fist and thumb flexion. An acceptable classification accuracy was defined as 75% and above.

6.2.5 Outcome 4: Classifying Functional Hand Tests

The importance of patient-rated functional outcomes with regard to overall rehabilitation success was outlined in subsection 2.3.5 of the literature review. Several in-house tests were therefore selected that simulated to some degree the functional tasks represented by the DASH and PRWE scale questionnaires. These exercises place a larger focus on the functional ability of the hand such as wrist rotation and grip strength as opposed to ROM alone. Their inclusion in this study was therefore imperative in the validation of a multi-user classifier using the POC smart brace system. The tests included the use of three tools:

- A hand exercise ball
- A 3D printed torque resisting device shown by Figure 6.1
- A bottle filled with water

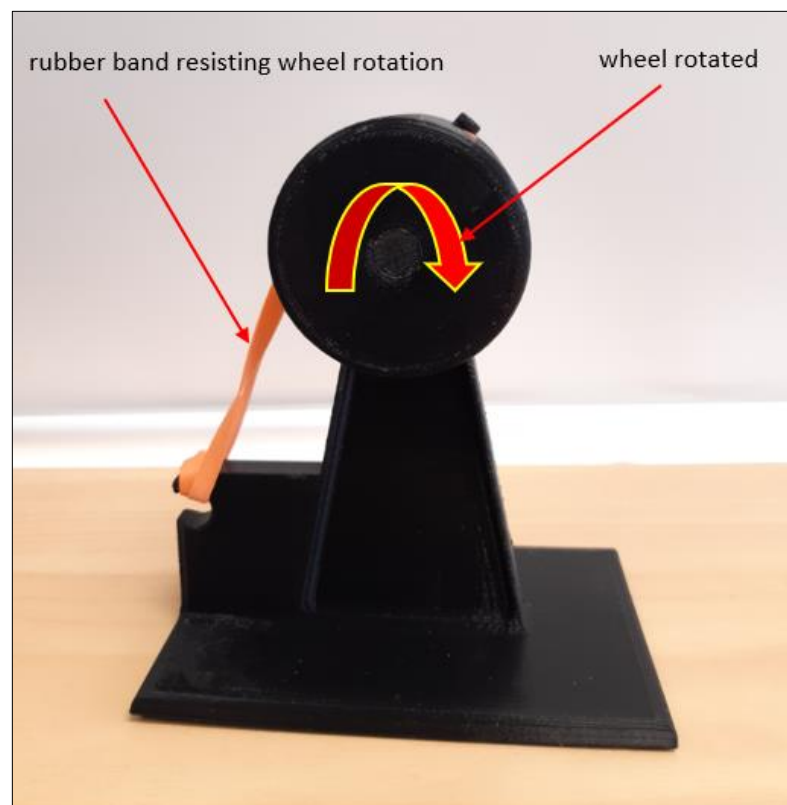


Figure 6.1 : Image of 3D printed hand torque device used to simulate wrist rotation tasks

With recommendations from the Surgisplint medical team, the functional tests selected were:

1. Squeezing the hand exercise ball using the fingertips and thumb only
2. Squeezing the hand exercise ball in the palm using the entire hand
3. Rotating the hand torque device away from the body (supinating)
4. Rotating the hand torque device toward the body (pronating)
5. Lifting and holding the water-filled bottle

These exercises are shown in more detail in the data gathering protocol described in subsection 6.2.9. For the classifier generated, an acceptable classification accuracy was defined again as 75% and above.

6.2.6 Summary of Classification Algorithms Produced from Pilot Study

Table 6-1 summarizes the classification algorithms and their respective classes that would be generated from the data obtained in the pilot study.

Table 6-1: Classification Algorithms Generated from Pilot Study

Algorithm number	Algorithm Application	Defined Classes
1	Ratchet arm fit	tight
		loose
		good
2	Dorsal tilt fit	tight
		loose
		good
3	Passive motion	passive finger extension
		passive thumb extension
		full hand active extension
4	Tendon gliding exercises	hand extended
		hook fist
		flat fist
		thumb flexion
5	Functional tests	ball fingertip squeeze
		palm fingertip squeeze
		supination
		pronation
		bottle lift

6.2.7 Pilot Study Ethics Approval

This pilot study was approved by the Auckland University of Technology Ethics Committee on 28 November 2019. The AUTEK reference number is 19/347. See Appendix D for details.

6.2.8 Hardware Preparation and Data Acquisition Tools

FSR Preparation

All FSRs used in the study were tested with a standardized mass to ensure that they conform to the manufacturer's specifications given in Table 3-1.



Figure 6.2: 3D-printed mass holder (left) and FSR tested with standardized mass (right)

Preparation of Zero-Cast Wx Braces

Left and right volar plates of sizes ranging from 2 (small) to 4 (large), were modified to mount FSR sensors. To determine which areas of the volar plate was most receptive to exerted tendon force, it was decided that the entire available area of the volar plate be equipped with FSR sensors. As there were three different sized braces, it was expected that different sensor arrays would be required for each size. After experimenting with various sensor configurations, two array types were selected for the experiment. Size four plates were able to contain six FSR 402, while sizes three and two could only accommodate four. Two FSR 400 was therefore added to the smaller brace sizes to cover the remaining volar plate area. The images shown by Figure 6.3 show the sensor arrays for all three brace sizes. The overlapping sensor strips did not impede the performance of the bottom sensors (this was verified with testing). It was noted that while there was still some uncovered sensing area, a maximum of six FSRs could only be used as there are only six analogue channels on the Arduino Uno.



Figure 6.3: FSR configuration for brace size 4 (left) and brace sizes 2 & 3 (right)

The FSR's were labelled in relation to wrist anatomy in the supinated position, thereby avoiding error between left and right-handed individuals. Figure 6.4 shows how the FSR sensors were tagged based on the forearm anatomy. The abbreviations and descriptions are shown in Table 6-2.

Table 6-2: FSR position tags and descriptions

Tag	Description
DR	distal radius
DM	distal medial
DU	distal ulna
PR	proximal radius
PM	proximal medial
PU	proximal ulna



Figure 6.4: Anatomy-based FSR tagging scheme

Data Acquisition Tools

The same electronic hardware described in subsection 3.2.6 was used for this study, with the exception of the three additional FSRs added to the circuit. The Arduino code was modified accordingly to read a further three analogue channels. Each FSR voltage value was sampled from an analogue channel on the Arduino Uno microcontroller. The output voltage range was from 0 to 5V, where a 0V reading corresponded to no force being applied to an FSR and 5V to a maximum force applied (~20N).

All FSR voltage values sampled throughout this study was recorded with the same LabVIEW program as described in subsection 3.2.6 of Chapter 3. FSR voltage readings were sampled at approximately 125 Hz.

Before the start of every participant test, each FSR was mapped to its corresponding analogue channel and recorded in the participant's file. This ensured that data was

recorded correctly when participants of different brace sizes were tested (part of the circuit had to be removed each time the brace had to be changed).

The results for each stage of the experiment was exported to an Excel file corresponding to the participant's reference number. The data for each participant was processed separately before combining data of all participants into a single excel document.

6.2.9 Testing and Data Gathering Protocol

A total of 21 healthy participants were recruited for the study, 12 male and 9 female, all between the ages of 18 and 65. The only exclusion criterion applied was previous wrist fracture in the dominant arm or a history of any musculoskeletal or neurological disorders. All participants were right hand dominant except for one. Out of the 12 male participants, 9 were fitted with a size 3 brace and 3 fitted with size 2. All female participants were fitted with a size two brace. Each participant was tested in a single session consisting of four stages which took approximately 30 minutes to complete. A reference code was assigned to each participant which indicated gender, brace size, hand dominance and serial number. For example, F2R01 indicates female, size 2, right arm, test 1. The testing protocol was approved by the Surgisplint head surgeon and CEO and both individuals were present to supervise the first test.

Table 6-3: Participant breakdown

	Size 2R	Size 3R	Size 3L	Total
Male	3	8	1	12
Female	9	0	0	9
Total	12	8	1	21

Stage 1: Data capture for brace fitting algorithms

1. The participant was asked to be seated with the elbow of their dominant arm placed on the desk and their forearm hanging in a relaxed position over the desk edge in a pronated position. A correctly sized modified volar plate was fitted to the participant's forearm as shown by Figure 6.5. This entailed the brace being placed at a two-finger width distance from the wrist crease as demonstrated by Figure 6.6.



Figure 6.5: Image of volar plate strapped to the right forearm of a participant



Figure 6.6: Image of volar plate fitted to right forearm at two-finger width distance from wrist crease

2. The dorsal plate was then fitted to the volar plate by guiding the ratchet arms through the volar slots and pressing the plates together evenly until the desired initial fitting force was reached. This step is illustrated by Figure 6.7.



Figure 6.7: Image of dorsal plate fitted volar plate via ratchet arms

3. The plates were then locked together by adjusting the locking screws on the volar plate to the 'locked' position.
4. FSR force data was recorded for the three fit types - tight, loose, and good and exported to an excel file
5. The ratchet arm screws were then tightened to the desired fit. Tightening the ratchet arm screws changes the dorsal plate angle relative to the forearm which increases pressure near the wrist.
6. FSR force data was recorded for the three fit types - tight, loose, and good and exported to an excel file
7. The hand bridge and C-arm was adjusted to position the wrist at an angle such that the thumb was aligned with the forearm. The hand-bridge screws were tightened to fully lock the hand bridge in position.
8. The participant was asked if they could make a full-fist and extended hand (fingers fanned out) with minimal discomfort



Figure 6.8: Image of hand-bridge and c-arm fitted on participant

Stage 2: Data capture for passive motion exercises

1. Continuing from stage one with a correctly sized and fitted Zero-Cast Wx brace
2. The participant was asked to place elbow on desk with forearm perpendicular to desktop surface
3. With the participant's hand completely relaxed, the researcher extended the fingers of the participant without the participant initiating any muscular contractions in the forearm
4. FSR force data was recorded for passive finger extension and exported to an excel file
5. With hand completely relaxed, the researcher extended the thumb of the participant
6. FSR force data was recorded for passive thumb extension and exported to an excel file



Figure 6.9: Image of participant's elbow perpendicular to desktop surface

Stage 3: Data capture of tendon gliding exercises

1. The participant was asked to place their elbow on desk with the forearm perpendicular to the desk surface
2. Starting in the relaxed position, participants were asked to perform the sequence of tendon gliding exercises, holding each one for about 3-5 seconds until FSR readings for each were stable:
 - extended,
 - hook fist,
 - flat fist and
 - thumb flexion
3. FSR force data was recorded continuously throughout the successive gestures and exported to an excel file
4. The participant was asked to repeat the exercise sequence for a second recording

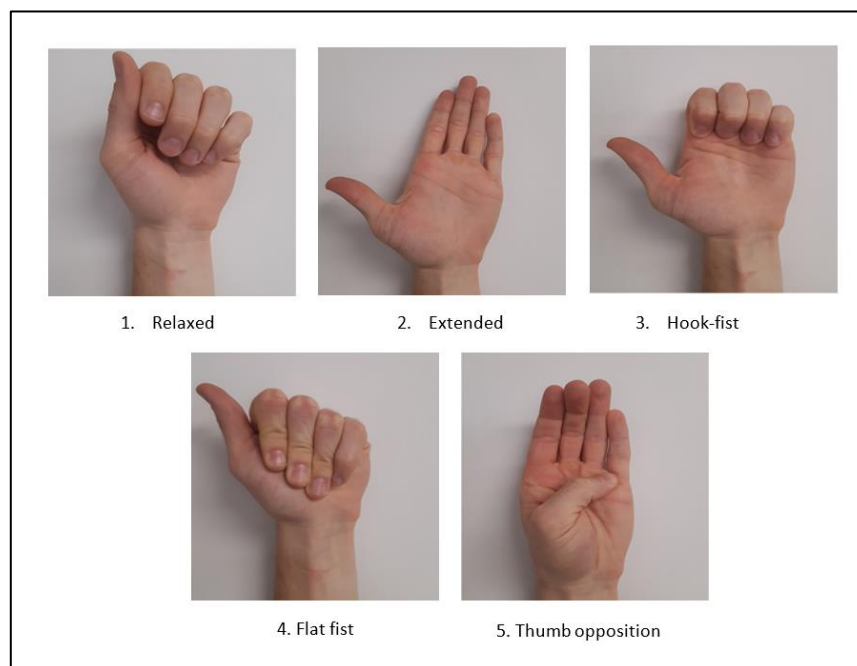


Figure 6.10: Sequence of tendon gliding exercises performed

Stage 4: Data capture for functional hand tests

1. The participant was asked to perform the following series of functional hand tests:

- Squeezing the hand exercise ball in fingertips

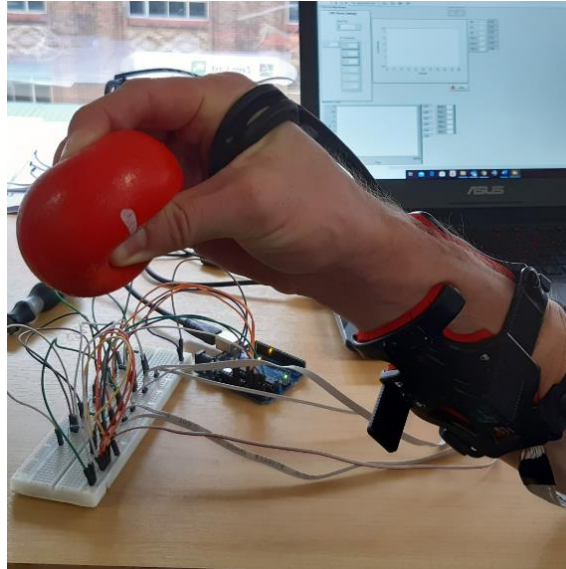


Figure 6.11: Image of participant performing ball finger-tip squeeze

- Squeezing the hand exercise ball with the full hand

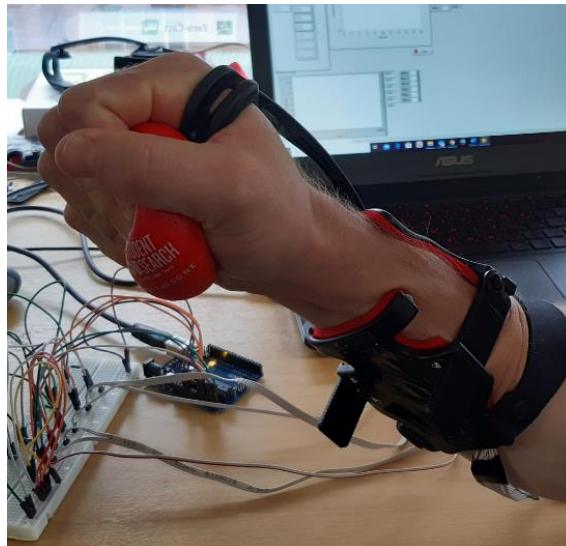


Figure 6.12: Image of participant performing ball palm squeeze

- Rotating the hand torque device to a fixed angular displacement in the supinated direction (away from body)



Figure 6.13: Photograph of participant rotating torque instrument by supinating the forearm

- Rotating the hand torque device to a fixed angular displacement in the pronated direction (toward body – torque device flipped around with rubber band on opposite side to that shown by Figure 6.13)
- Lifting and holding a filled water bottle for three seconds



Figure 6.14: Photograph of participant performing bottle lift

2. FSR force data was recorded separately for each functional hand test and exported to an excel file

6.3 Closure

This chapter reported the design and methodology of a multi-user ML pilot study using a POC embedded sensor system in Zero-Cast Wx. The next chapter discusses the data processing, ML analysis and results of the pilot study described in this chapter.

Chapter 7: Machine Learning Analysis and Pilot Study

Results

7.1 Introduction

This chapter discusses the process of a ML analysis using the data acquired from the pilot study. The results are reported, discussed interpreted and used to define an improved sensor array that can be used for future work.

7.2 Feature Engineering using Excel and Waikato Environment for Knowledge Analysis

This section reports the feature extraction, feature scaling and feature selection steps performed on the data acquired from the pilot study.

7.2.1 Feature Extraction

In this study, the most suitable features which could be extracted from the data were averages taken for stable FSR voltage amplitudes. A maximum of six features could therefore be used to predict a class output. At this stage of the analysis it was not known which features or combinations of features would generate the most accurate learning model. For each stage of the data gathering protocol as described in subsection 6.2.9 the appropriate features to generate a usable dataset for ML were extracted from data stored in the Excel files. The same feature extracting method was used as the one described in 5.6.2 of the single-user ML demonstration. Examples of the feature extraction process for a tight ratchet arm fit and the sequence of tendon gliding exercises are shown by Figure 7.1 and Figure 7.2 respectively.

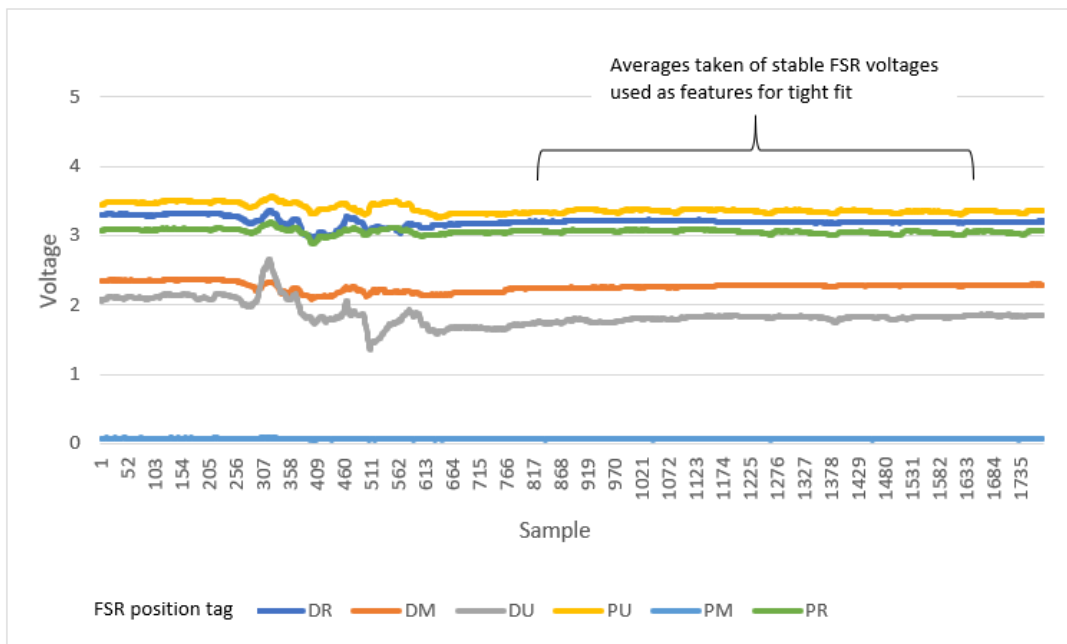


Figure 7.1: Participant M3R09 - Sampled FSR voltage data for a 'tight' fit in the ratchet arm fitting stage of Zero-Cast Wx

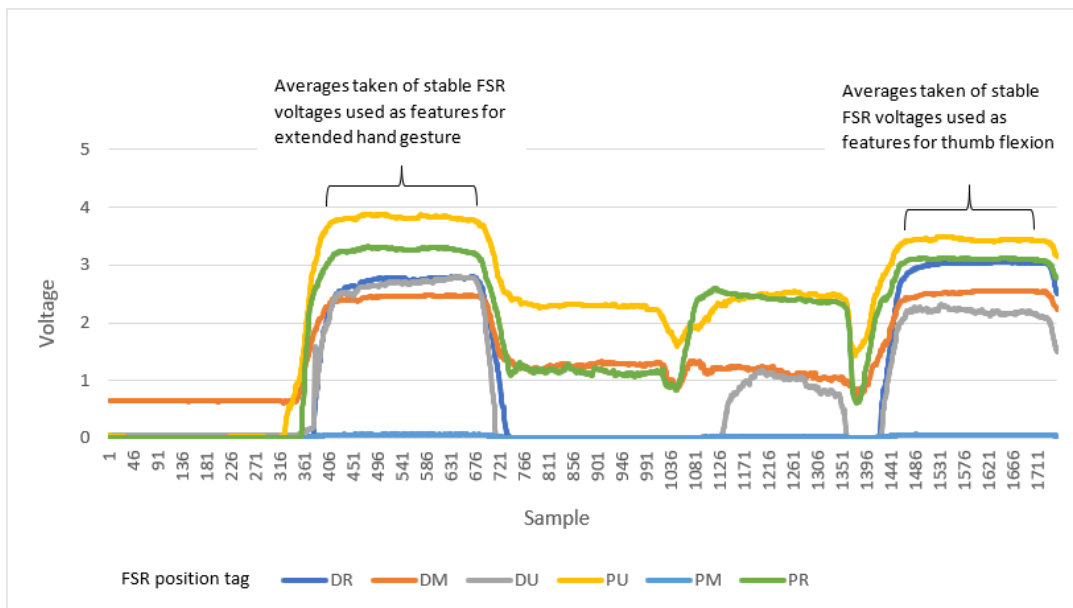


Figure 7.2: Participant M3R09 – Sampled FSR voltage data for Tendon Gliding Exercises

7.2.2 Feature scaling/normalization

As described in subsection 5.2.2, different features often need to be normalized so that they have the same scale. Typically, normalization is applied per feature, that is to say that each feature uses its own separate dataset to find maximum and minimum values. In our study, however, it was more appropriate to normalize by participant since each person had varying voltage ranges for the same hand gesture or functional test. For example, some participants saw a maximum FSR voltage of more than 4 while others

were as low as 2.5. The relative voltage differences in each participant when a change of hand position occurs is what was needed to be normalized, i.e. mapping each participant's max and min range to 0 and 1, respectively. Equation 5-1 was applied to individual participant data collected in the passive motion, tendon gliding and functional hand test stages of the study. Normalization was not applied to fitting data because the non-scaled values are indicative of actual forces applied to the wrist during brace fitting. To test the effect of this normalization method both sets of data, non-scaled and scaled datasets were used to train the classification algorithms.

7.2.3 Feature Selection Using Waikato Environment for Knowledge Analysis

Subsection 5.2.3 briefly discussed three common statistical feature selection methods. WEKA's feature selection tool, as outlined in subsection 5.4.2 was used to implement these selection methods for all the datasets extracted from the study. The most relevant features were ranked according to the feature selection method used. For each selection method, only the top three features were selected (i.e. three sensors out of a possible six), and using these top three features, a dataset was compiled that could be used for algorithm training.

7.2.4 Algorithm Training and Evaluation Using WEKA

Subsection 5.4.2 highlighted the WEKA Experiment Environment which allows the user to create a controlled experiment. With this tool, the user is able to train and test multiple algorithms on different datasets at the same time.

A total of 24 experiments were run, testing all selected algorithms on three to four datasets for each experiment (depending on overlapping feature selections). The flowchart diagram shown by Figure 7.3 illustrates the ML analysis carried out in the WEKA Experiment Environment.

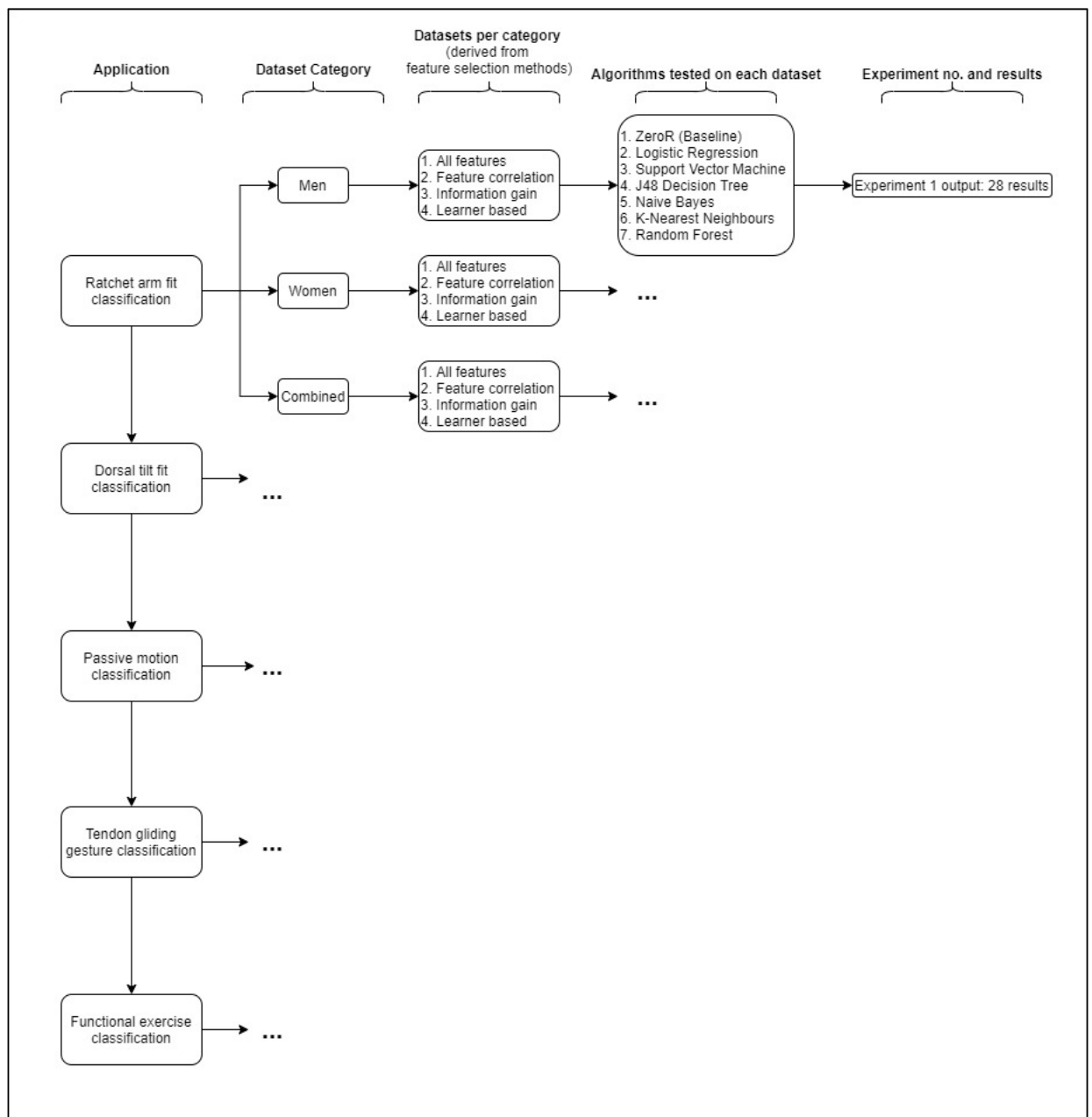


Figure 7.3: Flowchart showing experiment breakdown in WEKA

The flowchart (Figure 7.3) shows that three experiments for each application was performed, each one comprising the men, women and combined (men and women) dataset categories. The purpose of this method was to determine if combined men and women algorithms would be better or worse than individually learned algorithms. For passive motion, tendon gliding and functional hand test algorithms, an extra dataset was derived for each category through the feature normalization process. The 24 experiments can therefore be broken down as follows:

- Ratchet arm fit – 3 experiments
- Dorsal tilt fit – 3 experiments
- Passive motion – 6 experiments (2 x 3: regular data and normalized)

- Tendon gliding gestures – 6 experiments (2 x 3: regular data and normalized)
- Functional tests – 6 experiments (2 x 3: regular data and normalized)

For each dataset category (men/women/combined), seven algorithms (one baseline and six selected) were trained and evaluated using all four datasets containing the selected feature combinations (including all features).

Figure 7.4 shows the resultant output of one experiment in the WEKA Experiment Environment. The ratchet arm fit application using the combined men and women dataset. Each row corresponds to the classification accuracies (Equation 5-2) of the six selected algorithms using a single dataset. For example, considering the result of the second row and second column, it shows a classification accuracy of 87.83%. The algorithm used here is the Logistic Regression and the dataset used to train it is titled 'Feature correlation'. This dataset therefore only contains the top three features pertaining to the selection method 'Feature correlation'. WEKA calculates the average performance by using 100 iterations of the stratified 10-fold cross-validation (CV) technique (indicated to left of first column) – i.e. the process involves splitting the dataset randomly into 10 equal subsets with 9 for training and one for testing, performed 100 times.

Ratchet arm fit - combined								
Dataset	(1) rules.ZeroR	(2) funct	(3) funct	(4) trees	(5) bayes	(6) lazy.	(7) trees	
'All features'	(100) 33.33	82.67 v	93.33 v	87.33 v	87.17 v	89.33 v	91.83 v	
'Feature correlation'	(100) 33.33	87.83 v	93.33 v	87.33 v	93.50 v	93.33 v	91.67 v	
'Information gain'	(100) 33.33	87.83 v	93.33 v	87.33 v	93.50 v	93.33 v	91.67 v	
'Learner based'	(100) 33.33	91.00 v	89.83 v	88.67 v	91.67 v	89.83 v	89.67 v	
		(v/ /*)	(4/0/0)	(4/0/0)	(4/0/0)	(4/0/0)	(4/0/0)	(4/0/0)
Key:								
(1) rules.ZeroR '' 48055541465867954								
(2) functions.Logistic '-R 1.0E-8 -M -1 -num-decimal-places 4' 3932117032546553727								
(3) functions.SMO '-C 1.0 -L 0.001 -P 1.0E-12 -N 2 -V -1 -W 1 -K \"functions.supportVector.PolyKernel								
(4) trees.J48 '-C 0.25 -M 2' -217733168393644444								
(5) bayes.NaiveBayes '' 5995231201785697655								
(6) lazy.IBk '-K 3 -W 0 -A \"weka.core.neighboursearch.LinearNNSearch -A \\\\\"weka.core.EuclideanDistan								
(7) trees.RandomForest '-P 100 -I 100 -num-slots 1 -K 0 -M 1.0 -V 0.001 -S 1' 1116839470751428698								

Figure 7.4: Results table from a single experiment in the WEKA Experiment Environment

In each iteration, the training sets and testing sets were randomized, producing a slightly different result each time. The overall result was taken as the average across all 100 iterations. The first column shows the results of the baseline algorithm performance, Zero-Rule – which is an algorithm that selects the most frequently appearing class. Since there are only three class values in these datasets (tight, loose, good) and there are an equal number of instances for each class, the expected result

of 33.33% is obtained i.e all classes appear an equal number of times since the dataset is balanced.

All of the algorithms trained and tested were therefore compared to this statistical baseline performance. WEKA performs a pairwise t-test (95% confidence) with each algorithm and the baseline, showing if the difference is statistically significant. A statistically positive difference (algorithm performs much better than Zero-Rule) is indicated by the small 'v' next to the result. A statistically negative difference is indicated by an asterisk. The advantage of this test is that it provides confidence in the fact that the performance difference between the selected algorithm and Zero-Rule is not pure chance. After each completed experiment, the best results were extracted along with their corresponding algorithm and feature set. The dataset was then imported in the *WEKA Explorer* application and trained on the algorithm which scored highest from the experiment. This was the final step in the machine learning analysis which provided the algorithm's confusion matrix along with it's classification accuracy.

7.3 Machine Learning Results

The results shown in the following subsections are presented by application. For example, all results for the ratchet arm fit output are shown followed by dorsal tilt fit and so-forth. Each confusion matrix shows the 10-fold CV results of the top performing algorithm for each respective dataset category. The diagonals indicate the number of correctly classified instances for each class. The sum of each row represents the total number of instances for each class. The overall classification accuracy along with the algorithm name is indicated in brackets in the title of each matrix table. Within each confusion matrix, a green entry indicates the highest performing class, a red entry indicates the lowest performing class, and yellow or orange entries indicate the middle performing classes. The classification accuracy by class is shown in the last column on the right. The average of the class accuracies is equal to the overall accuracy shown in brackets in the matrix title. After the results for each algorithm have been presented, key observations and interpretations are reported.

7.3.1 Application 1: Ratchet Arm Fit

Table 7-1: Confusion matrix for ratchet arm fit – males (92% / KNN)

Predicted			Actual	Accuracy by class %
tight	loose	good		
12	0	0	tight	100
0	12	0	loose	100
0	3	9	good	75

Table 7-2: Confusion matrix for ratchet arm fit – females (96% / NBY)

Predicted			Actual	Accuracy by class %
tight	loose	good		
9	0	0	tight	100
0	9	0	loose	100
1	0	8	good	89

Table 7-3: Confusion matrix for ratchet arm fit – combined (95% / NBY)

Predicted			Actual	Accuracy by class %
tight	loose	good		
21	0	0	tight	100
0	20	1	loose	95
1	1	19	good	90

Observations & discussion

Overall, the top performing algorithms for the ratchet arm fits exceeded the target classification accuracy of 75%. In both male and female datasets, the misclassified instances were exclusively from the 'good fit' class. The global results from the combined dataset indicate an average performance of the separate global male and female datasets. The individual class performance of the combined dataset, however, does not suggest a combined average from the male and female datasets. This is verified by the fact that 'loose fit' class had one misclassified instance in the combined dataset, whereas in male and female sets there were none. Finally, it is worth noting that the top performing algorithm was not the same for each dataset category – K-nearest neighbours was the top performing algorithm in the male dataset.

7.3.2 Application 2: Dorsal Tilt Fit

Table 7-4: Confusion matrix for dorsal tilt fit – males (53% / J48)

Predicted			Actual	Accuracy by class %
tight	loose	good		
8	4	0	tight	67
0	11	1	loose	92
3	9	0	good	0

Table 7-5: Confusion matrix for dorsal tilt fit – females (89% / RF)

Predicted			Actual	Accuracy by class %
tight	loose	good		
9	0	0	tight	100
0	8	1	loose	89
0	2	7	good	78

Table 7-6: Confusion matrix for dorsal tilt fit – combined (68% / SVM)

Predicted			Actual	Accuracy by class %
tight	loose	good		
17	1	3	tight	81
0	15	6	loose	71
3	7	11	good	52

Observations & discussion

Classification accuracies for the dorsal tilt fit application were mixed. The male dataset performed considerably worse than the female dataset. There was not a single correctly classified instance in the 'good fit' class of the male dataset. The reason for the large performance discrepancy between the gender groups possible lie in the morphological differences of the wrists. The male participants typically had a larger wrist circumference, along with firmer soft tissue. Female participants had smaller wrists overall compared to males and their wrist taper was generally more pronounced as well. What this could mean is that a small change in the dorsal tilt angle results in a proportionate change in the FSR response, thereby producing distinct force patterns for each fit type which allows for better classification accuracy. In contrast, having a larger wrist already places some pressure on the dorsal plate, even in a completely loosened position. FSRs experience a decrease in sensitivity with increasing force. If the FSRs are therefore slightly compressed in the loose dorsal position, then any further pressure applied during tightening may not have produced a proportionate force response. The outcome is thus a three-class dataset with considerable overlap, making machine learning significantly more challenging. The box and whisker plot shown by Figure 7.5 supports this claim. It shows the force range of sensor PR (Proximal Radius side) in male participants for each class - the only sensor used in the highest performing algorithm. The force distribution of the 'loose' class falls entirely within the interquartile range of the 'good' class. Furthermore, both classes share an almost identical average voltage value making it highly improbable for an algorithm to distinguish between these two classes.

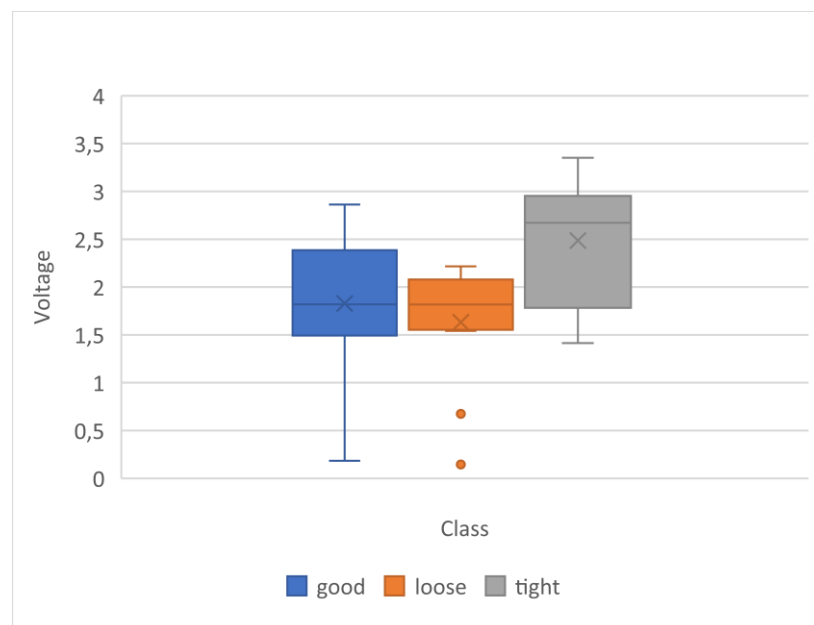


Figure 7.5: FSR Force range across all three classes for sensor PR - Dorsal Tilt Fit Males

7.3.3 Application 3: Passive Motion Detection

Table 7-7: Confusion matrix for passive motion detection – males (78% / LR)

Predicted			Actual	Accuracy by class %
pf ext	pt ext	act		
9	1	2	pf ext	75
2	10	0	pt ext	83
3	0	9	act	75

Table 7-8: Confusion matrix for passive motion detection – females (85% / RF)

Predicted			Actual	Accuracy by class %
pf ext	pt ext	act		
7	1	1	pf ext	78
1	8	0	pt ext	89
1	0	8	act	89

Table 7-9: Confusion matrix for passive motion detection – combined (84% / KNN)

Predicted			Actual	Accuracy by class %
pf ext	pt ext	act		
16	2	3	pf ext	76
3	18	0	pt ext	86
2	0	19	act	90

Observations & discussion

All classification accuracies achieved were 75% and above with three different algorithms yielding the top results for each dataset category. Examining the FSR data of these three classes verify the performance shown in these confusion matrices. Across all participants the passive motion classes had significantly lower FSR values compared to the active hand extension motion; thereby providing the algorithm with distinct classes to be trained on. These results suggest that a multi-user trained algorithm in the Zero-Cast brace could potentially detect the difference between muscle-activated finger extension and externally based passive finger extension in patients with fractured wrists. Further training data and algorithm tuning may further improve the accuracy of this classification algorithm.

7.3.4 Application 4: Tendon Gliding Exercises

Table 7-10: Confusion matrix for tendon gliding exercises – males (80% / RF)

Predicted				Actual	Accuracy by class %
extended	hook fist	flat fist	thumb		
17	0	0	4	extended	81
0	19	1	1	hook fist	90
0	4	15	2	flat fist	71
1	3	1	16	thumb	76

Table 7-11: Confusion matrix for tendon gliding exercises – females (75% / RF)

Predicted				Actual	Accuracy by class %
extended	hook fist	flat fist	thumb		
10	0	0	6	extended	63
0	12	2	2	hook-fist	75
0	0	16	0	flat fist	100
4	2	0	10	thumb	63

Table 7-12: Confusion matrix for tendon gliding exercises – combined (75% / RF)

Predicted				Actual	Accuracy by class %
extended	hook fist	flat fist	thumb		
28	0	0	9	extended	76
0	31	2	4	Hook fist	84
0	6	30	1	flat fist	81
11	3	1	22	thumb	59

Observations & discussion

The classification accuracy for tendon gliding exercises were very good in the context of a multi-user trained algorithm. All dataset categories (men/women/combined) scored an overall accuracy of 75% and above. For the both male and female categories, the majority of misclassifications occurred between gestures that produced a similar FSR response. For example, in the female category, most of the misclassifications occurred between the 'thumb' and 'extended' gesture classes.

7.3.5 Application 5: Functional Hand Tests

Table 7-13: Confusion matrix for functional tests – male (38% / J48)

Predicted					Actual	Accuracy by class %
fingertip	palm	supinate	pronate	bottle		
9	0	0	1	2	fingertip	75
1	4	2	2	3	palm	33
4	2	0	1	5	supinate	0
4	4	1	0	3	pronate	0
0	1	1	0	10	bottle	83

Table 7-14: Confusion matrix for functional tests – female (53% / RF)

Predicted					Actual	Accuracy by class %
fingertip	palm	supinate	pronate	bottle		
4	3	2	0	0	fingertip	44
1	5	2	1	0	palm	56
3	2	2	2	0	supinate	22
0	0	2	5	2	pronate	56
0	0	0	1	8	bottle	89

Table 7-15: Confusion matrix for functional tests – combined (42% / J48)

Predicted					Actual	Accuracy by class %
fingertip	palm	supinate	pronate	bottle		
11	3	3	2	2	fingertip	52
4	13	0	2	2	palm	62
7	6	1	0	7	supinate	5
4	9	0	1	7	pronate	5
2	1	0	0	18	bottle	86

Observations & discussion

The overall classification accuracies for functional hand exercises across all dataset categories (men/women/combined) were poor. The confusion matrices show that most of the misclassifications occurred in the 'supinate' and 'pronate' classes. In contrast, the 'ball fingertip squeeze' and 'bottle grip' classes were accurately predicted in the male category. Similarly, a good level of accuracy can be seen in the 'bottle-grip' class of the female category. An overall average effect is again seen in the combined data category for this application. The wide distribution of misclassifications in the 'supinate' and 'pronate' classes of the male data category suggest FSR force patterns were highly inconsistent across participants. This also appears to be the case in the 'supinate' class

of the female data category. Recommendations for improving the accuracies of these classes are made in Chapter 7.

7.3.6 FSR Contribution to Algorithm Training

In Subsection 6.2.8 it was explained that the entire available area of the volar plate be mounted with FSRs because it was not known which areas of the wrist would be most active in terms of fitting force and forces exerted due to tendon and muscle activity. The data acquired from this pilot study along with the ML analysis provided some insight into which areas of the wrist are better locations for FSR placement when it comes to classifying fitting force and various hand motion artefacts. This was achieved by analysing the frequency of features (FSRs) selected in the best performing algorithms. Together, the feature selection methods and top performing algorithms indicate which FSRs are more likely to contribute to the training of an algorithm.

Table 7-16 summarizes which FSRs were selected across all three dataset categories (men/women/combined) for each algorithm application. For reference, FSR positions are again shown by Figure 7.7. As an example, the ratchet-arm fit application in column one shows that sensor DU was selected in two out of three (67%) dataset categories i.e. it was selected for the male and female dataset but not for both datasets combined. From the results in the table it is evident that sensors DU, PR and PU contributed to the best performing algorithms most frequently.

Table 7-16: FSR Selection Frequency by Application

FSR	Ratchet arm fit (%)	Dorsal tilt fit (%)	Passive motion (%)	Tendon gliding (%)	Functional tests (%)	Overall selection frequency %
DU	67	67	67	100	33	67
DR	67	0	0	67	33	33
DM	33	33	0	67	0	27
PM	33	0	33	67	0	27
PR	100	67	67	100	67	80
PU	67	0	67	100	33	53



Figure 7.7: FSR Position Reference

7.4 Summary of Results

The results presented in this chapter have shown which machine learning applications are feasible solutions using embedded FSR sensors in the Zero-Cast Wx brace. The best performing classes for each application were identified and explanations for poor performing classes were provided where possible. Results have shown which machine learning algorithms are best suited to these particular classification problems and which FSRs are most likely to provide the greatest contribution in algorithm performance. Finally, they have revealed which applications require further investigation and what research questions are to be addressed in future work.

In summary, the Ratchet Arm Fit, Passive Motion and Tendon Gliding exercise applications achieved the objective of attaining overall classification accuracy of 75% and above using multi-user training data. With the individual exception of the 'bottle lift' class, The Dorsal Tilt Fit and Functional Test applications did not achieve the overall objective in all dataset categories and require further investigation, possibly including minor alterations in experimental procedure and hardware. The results also indicate that combining data from male and female categories does not produce superior performance compared to individual category performance – in almost all applications the combined data category reflects an approximate combined average of individual category performance. With regard to algorithms, Random Forest made up 40% of all top performing ML algorithms and the J48 decision tree algorithm made up a further 20%. Therefore 60% of all the top algorithms were decision tree type models. Finally,

the results of the ML analysis highlighted which FSRs had a larger contribution to algorithm training and performance. These FSRs were identified by the position tags, DU, PR and PU.

7.5 Closure

This chapter reported and interpreted the results of a multi-user machine learning pilot study using a POC embedded FSR sensor system in the Zero-Cast Wx brace. The final chapter of this thesis draws conclusions from this project and provides recommendations for future work.

Chapter 8: Conclusions, Recommendations, and Future Work

8.1 Introduction

This chapter draws conclusions and makes recommendations for future work based on the results of the pilot study and observations made in earlier chapters of this thesis.

8.2 Conclusions

The findings of this project support the conclusion that embedded smart technology can be used to classify fitting force and various hand motion artefacts in the Zero-Cast Wx brace system. The following subsections summarize the achieved objectives that contributed to satisfactorily answering the research question. The shortcomings are also discussed which serve to justify the recommendations for future work that follow in section 8.3.

8.2.1 The Design and Development of a Proof-of-Concept Embedded Technology System in Zero-Cast Wx was Successfully Achieved

Chapter 3 and 4 discussed the successful design and development of a POC embedded technology system in the Zero-Cast Wx brace for the purpose of detecting fitting force and various hand motion artefacts. It was shown that the FMG technique using FSR sensors was the most appropriate method to achieve this. Furthermore, it was shown that wireless data acquisition was possible with the combined use of simple off-the-shelf electronic components and readily available signal sampling software.

8.2.2 Applied Machine Learning with Force Myography Data from a Single User is Feasible using the Zero-Cast Wx Brace

Chapter 5 showed that it is possible to accurately classify several hand motion artefacts in a single user (tendon gliding exercises and relaxed hand position) with a simple classification algorithm generated with training data obtained from the same user (accuracy above 90%). Achieving this objective provided initial validation for the claim that hand motion artefacts could be classified using embedded smart technology in the Zero-Cast Wx brace system.

8.2.3 Applied Machine Learning with Multi-User Force Myography Data is Feasible using the Zero-Cast Wx Brace

The pilot study reported in Chapter 6 showed the feasibility of implementing the FMG technique with Zero-Cast Wx for the applications of classifying the ratchet arm fit, passive hand motion and tendon gliding exercises using cross-user training data. These applications all met or exceeded the specified benchmark accuracy of 75%. The

classification accuracies obtained for the functional hand tests were inadequate for this application to be declared feasible using FMG exclusively. The number of misclassifications that occurred between classes as shown in Table 7-13 to Table 7-15 of the results, suggest that FSR data alone is likely insufficient for classifying functional hand tests. Subsection 8.3.1 proposes a solution that could improve the results of this application and possibly improve the classification accuracy of the other applications in this project.

8.2.4 The Identification of Improved Force Sensing Resistor Positions was Achieved

The ML analysis performed in the pilot study included the statistical techniques of feature selection. As applied to this project, the features directly correspond to FSR position and their contribution to algorithm training and performance. Hence the results of the analysis informed which sensors were more relevant to the top performing algorithms for brace fitting and motion artefact detection. Specifically, FSR positions tagged by DU, PR and DU provided the largest contribution to the successful results.

8.3 Recommendations

8.3.1 Integrate Inertial Measurement Unit with Current Embedded Technology

An inertial measurement unit (IMU) is an electronic device typically combining an accelerometer and gyroscope to measure acceleration and spatial orientation of a body. They are manufactured in many sizes for a wide range of applications including everyday wearable devices like smartwatches and pedometers. Integrating an IMU with the POC brace in this project will provide an additional source of data for machine learning at a minimal financial, time and space cost. More importantly, having IMU data will significantly increase the classification performance of the Functional Testing application of the brace. The results of the pilot study suggest that FSR data alone may be insufficient for training algorithms to recognize the 'supinate' and 'pronate' classes of the functional hand exercises application. Since these two exercises differ physically by almost a 180° rotation about the forearm, an IMU would produce spatial orientation data unique to each gesture. Additionally, it is probable that the IMU data will further improve the classification performance of other classes in all gesture-based applications of the brace. Hongyi Wen et al. demonstrated the use of an IMU for finger gesture recognition by using a smartwatch alone and achieved excellent results [72]. It is therefore strongly recommended that serve as the first step in any future developments of this research.

8.3.2 Increase Number of Participants in Future Studies

The investigative pilot study conducted in this project tested the brace on 21 participants. The predictive power and reliability of machine learning models typically improve with increasing training data. We therefore recommend that any further planned studies for the purpose of multi-user training data be conducted with at least 50 participants comprising approximately equal number of male and females across various age groups and brace sizes. Using a larger sample size in future studies may support the findings of this project and will also give researchers the opportunity to compare classification models by brace size (an outcome not achieved in this project due to low sample size). This step will be necessary before taking the brace to a prototype phase of development.

8.3.3 Consult Data Scientists for Algorithm Tuning to Boost Classification Performance

The suite of machine learning algorithms in WEKA were used with default parameter settings which means they have not necessarily been optimized for the problem they are applied to. It is therefore recommended that Surgisplint consulting a data scientist specialist or statistician with expertise in algorithm tuning and performance boosting. Doing so may enhance the classification accuracy of some or all the applications tested in this project, enabling better decisions to be made on future algorithm work. A data scientist or statistician would also be able to provide more detailed insights on other statistical parameters for each algorithm that extended beyond the scope of this project.

8.3.4 Perform Finite Element Analysis to Simulate and Quantify Force Distribution on Healthy and Injured Wrist

Before undertaking any clinical trials on injured patients, it is suggested that a Finite Element Analysis (FEA) of the Zero-Cast Wx brace applied to a wrist be performed. This is a computer aided engineering analysis which will allow forces distributed throughout wrist tissue to be quantified and visualized. This analysis should be performed on both simulated healthy tissue and injured tissue where localized swelling would occur in a typical DRF case. The results will assist the Surgisplint team in properly quantifying the acceptable forces applied to an injured wrist during the application of Zero-Cast Wx. It may also help the understanding of the effects of swelling on FSR response. Furthermore, these results could be used to validate the results of physical testing and provide more evidence before moving on to clinical trials.

8.3.5 Perform Physical Tests on Simulated Swollen Tissue

In conjunction with an FEA analysis, it is recommended that physical testing of the brace on simulated swollen tissue be undertaken. This may include the use of ballistics gelatin or a similar silicon-based material that could be placed on the wrist of a healthy individual. The machine learning experiments of the pilot study could then be repeated, and the results compared to the results obtained from healthy individuals.

8.3.6 Design Volar and Dorsal Plates with Integrated Electronic Hardware

After the results of recommendations one and two have been obtained, it is suggested that a wireless prototype brace, integrated with all necessary hardware, be designed, tested, and used in clinical trials. The electronic hardware should be built into either the dorsal or volar plates, accommodating all parts essential to pressure and gesture classification without compromising the fracture-supporting functions of the original design. The embedded sensor POC discussed in chapter four of this project should be used as a foundational concept in any further developments of the Zero-Cast Wx smart brace.

8.3.7 Include Additional Classes in Cross-User Algorithms and Automate Machine Learning for User-Specific Algorithms

The rationale behind using multi-user trained recognition algorithms negates the need for injured patients to train an algorithm, a potentially uncomfortable and possibly damaging practice to the patient. A disadvantage of this method, however, as shown by the results of the pilot study, is that there will inevitably be a reduction in gesture recognition performance due to morphological differences between users. Additionally, DRF patients are unlikely to perform gestures in a full range of motion compared to the healthy participants that were used to train the algorithms in this project. This would almost certainly produce a further reduction in classification performance. There are two potential solutions to this problem. The first solution would require that the multi-user algorithms incorporate partial gestures as additional classes to be recognized; a solution that would accommodate a variety of physical range limitations in DRF patients. This would naturally mean that more training data is needed for those classes to be accurately classified by the algorithm.

The second solution would require a further investigation using DRF patients to train their own unique gesture recognition algorithm using automated ML platforms such as Queexo [97]. Algorithm training is performed near real time and could potentially be done at the patient's first physiotherapy consultation. A drawback of this solution is that the algorithm may require re-training as the patient regains full range of motion in their

hand and wrist, requiring frequent visits to therapy. This solution, however, should not be dismissed until a thorough scientific investigation has been conducted.

8.3.8 Integrate App with Wireless Prototype Design

An app connected to the brace via the Bluetooth Low Energy (BLE) protocol is recommended for remote data acquisition. Under the author's direct supervision, two undergraduate electrical and electronics engineering students developed a POC, IOS mobile App that integrates with the FMG system developed by this project. It is recommended that the FMG system be integrated with the APP as a next step in the development of Zero-Cast Wx smart brace system.

8.3.9 Perform Clinical Trials on DRF Patients with Manufacturable Prototype

After all recommendations have been implemented, the next stage of development should include clinical trials on patients with DRF. Although there may be considerable efforts required to obtain ethical approvals from regulating bodies, it will be imperative to test a manufacturable prototype on real injured patients before the final phase of producing a production item ready for consumer use.

List of References

1. Zero-Cast. Available from: <https://www.zero-cast.com/page/product/> [Accessed: 12 August 2019].
2. Kuo, L.C., et al., *Is progressive early digit mobilization intervention beneficial for patients with external fixation of distal radius fracture? A pilot randomized controlled trial.* Clin Rehabil, 2013. **27**(11): p. 983-93.
3. Slutsky, D.J. and M. Herman, *Rehabilitation of distal radius fractures: a biomechanical guide.* Hand Clin, 2005. **21**(3): p. 455-68.
4. Gutiérrez-Espinoza, H., et al., *Supervised physical therapy vs home exercise program for patients with distal radius fracture: A single-blind randomized clinical study.* Journal of Hand Therapy, 2017. **30**(3): p. 242-252.
5. Lyngcoln, A., et al., *The relationship between adherence to hand therapy and short-term outcome after distal radius fracture.* J Hand Ther, 2005. **18**(1): p. 2-8; quiz 9.
6. McIntyre, M., L.R. Robinson, and A. Mayo, *Practical Considerations for Implementing Virtual Care in Physical Medicine and Rehabilitation: For the Pandemic and Beyond.* American Journal of Physical Medicine & Rehabilitation, 2020. **99**(6): p. 464.
7. Hong, Z., et al., *Telemedicine During the COVID-19 Pandemic: Experiences From Western China.* 2020.
8. Gosling, J.A.M.D.M.B.C.F.F.A.S., et al., *Upper Limb*, in *Human Anatomy, Color Atlas and Textbook*, J.A.M.D.M.B.C.F.F.A.S. Gosling, et al., Editors. 2017. p. 71-133.
9. McKinley, M.P., V.D. O'Loughlin, and E.E. Pennefather-O'Brien, *Human Anatomy.* 5 ed. 2017, NY, UNITED STATES: McGraw-Hill Higher Education.
10. Barclay, T. *Muscles of the Arm and Hand.* 3 July 2018; Available from: <https://www.innerbody.com/anatomy/muscular/arm-hand#continued> [Accessed: 3 September 2019].
11. Stirling, E.R.B., N.A. Johnson, and J.J. Dias, *Epidemiology of distal radius fractures in a geographically defined adult population.* J Hand Surg Eur Vol, 2018. **43**(9): p. 974-982.
12. Shehovych, A., et al., *Adult distal radius fractures classification systems: essential clinical knowledge or abstract memory testing?* Annals of the Royal College of Surgeons of England, 2016. **98**(8): p. 525-531.
13. *What is a Distal Radius Fracture?* 1 May 2019; Available from: <http://www.smitmedimed.com/what-is-a-distal-radius-fracture/> [Accessed: 3 September 2019].
14. *Distal Radius Fractures (Broken Wrist).* March 2013; Available from: <https://orthoinfo.aaos.org/en/diseases--conditions/distal-radius-fractures-broken-wrist> [Accessed: 17 September 2019].
15. Jerrhag, D., et al., *Epidemiology and time trends of distal forearm fractures in adults - a study of 11.2 million person-years in Sweden.* BMC Musculoskelet Disord, 2017. **18**(1): p. 240.
16. MacIntyre, N.J. and N. Dewan, *Epidemiology of distal radius fractures and factors predicting risk and prognosis.* J Hand Ther, 2016. **29**(2): p. 136-45.
17. Wilcke, M.K.T., H. Hammarberg, and P.Y. Adolphson, *Epidemiology and changed surgical treatment methods for fractures of the distal radius.* Acta Orthopaedica, 2013. **84**(3): p. 292-296.
18. Hove, L.M., et al., *Distal radius fractures : current concepts.* 2014: Springer.
19. Szostakowski, B., P. Smitham, and W.S. Khan, *Plaster of Paris-Short History of Casting and Injured Limb Immobilization.* Open Orthop J, 2017. **11**: p. 291-296.

20. *Care of Casts and Splints*. 2019 August 2015; Available from: <https://orthoinfo.aaos.org/en/recovery/care-of-casts-and-splints/> [Accessed: 19 September 2019].
21. *Changqing Medical Products Co.* Available from: <http://www.surgmedical.com/sale-7310650-medical-orthopedic-casting-tape-and-splint-strong-for-gobal-fiberglass-casting-supporting.html> [Accesses: 12 October 2019].
22. *BSN Medical Specialist® Quick Setting Plaster Bandages*. Available from: <https://www.quickmedical.com/bsn-medical-specialist-quick-setting-plaster-bandages.html> [Accessed: 12 October 2019].
23. Bayne, G. and R.G. Turner, *Closed fracture manipulation--improving Charnley's three point fixation technique*. *Annals of the Royal College of Surgeons of England*, 2006. **88**(5): p. 504-504.
24. *Distal radius and or ulna metaphyseal fractures - Emergency Department*. Available from: https://www.rch.org.au/clinicalguide/guideline_index/fractures/Distal_radius_and_or_ulna_metaphyseal_fractures_Emergency_Department_setting/ [Accessed: 20 October 2019].
25. Nemeth, B., et al., *High risk of recurrent venous thrombosis in patients with lower-leg cast immobilization*. *J Thromb Haemost*, 2018. **16**(11): p. 2218-2222.
26. Ovidiou, A., *MANAGEMENT OF COMPLICATION OF DISTAL RADIUS AND ULNA FRACTURES*. *Orthopaedic Proceedings*, 2002. **84-B**(SUPP_III): p. 358-359.
27. Bobos, P., et al., *Recovery of grip strength and hand dexterity after distal radius fracture: A two-year prospective cohort study*. *Hand Therapy*, 2017. **23**(1): p. 28-37.
28. Ikpeze, T.C., et al., *Distal Radius Fracture Outcomes and Rehabilitation*. *Geriatr Orthop Surg Rehabil*, 2016. **7**(4): p. 202-205.
29. Bruder, A.M., et al., *Validity and reliability of an activity monitor to quantify arm movements and activity in adults following distal radius fracture*. *Disability and Rehabilitation*, 2018. **40**(11): p. 1318-1325.
30. Kumar, D.P., *Use of Passive Finger Motion in Early Stage Distal Radius Fracture Rehabilitation*, M.v. Wyk, Editor. 2020.
31. *5 Exercises To Improve Hand Mobility And Reduce Pain*. Available from: <https://www.health.harvard.edu/pain/5-exercises-to-improve-hand-mobility-and-reduce-pain> [Accessed: 5 November 2019].
32. Quadlbauer, S., et al., *Rehabilitation after distal radius fractures: is there a need for immobilization and physiotherapy?* *Archives of Orthopaedic and Trauma Surgery*, 2020. **140**(5): p. 651-663.
33. *The DASH Outcome Measure*. Available from: <https://www.iwh.on.ca/tools-and-guides/dash-outcome-measure> [Accessed: 12 December 2019].
34. *Zero-Cast Wx Application Instructions*. Available from: https://www.zero-cast.com/site_files/17451/upload_files/100227-5.Application.Poster.pdf?dl=1 [Accesses: 12 August 2019].
35. Rodriguez-Villegas, E., S. Iranmanesh, and S.A. Imtiaz, *Wearable Medical Devices: High-Level System Design Considerations and Tradeoffs*. *IEEE Solid-State Circuits Magazine*, 2018. **10**(4): p. 43-52.
36. Aliverti, A., *Wearable technology: role in respiratory health and disease*. *Breathe* (Sheffield, England), 2017. **13**(2): p. e27-e36.
37. Lee, J., et al., *Sustainable Wearables: Wearable Technology for Enhancing the Quality of Human Life*. *Sustainability*, 2016. **8**: p. 466.
38. *Medical Device Illustrations*. Available from: <https://conceptdraw.com/a1865c4/preview> [Accessed: 9 January 2020].
39. Kalantar-zadeh, K., *Sensors: An Introductory Course*. 2013: Springer US. 196.
40. Grami, A., *Introduction to Digital Communications*. 2015, Saint Louis, UNITED STATES: Elsevier Science & Technology.

41. Hussain, Z.M., A.Z. Sadik, and P. O'Shea, *Digital signal processing : an introduction with MATLAB and applications*. 2011: Springer.
42. Knox, S.W., *Machine Learning : A Concise Introduction*. 2018, Newark, UNITED STATES: John Wiley & Sons, Incorporated.
43. Rebal, G., A. Ravi, and S. Churiwala, *An introduction to machine learning*. 2019: Springer.
44. Mohammed, M., M.B. Khan, and E.B.M. Bashier, *Machine learning : algorithms and applications*. 2017: CRC Press.
45. Alpaydin, E. and F. Bach, *Introduction to Machine Learning*. 2014, Cambridge, UNITED STATES: MIT Press.
46. Rouse, M. *Internet of Things (IoT)*. IoTAgenda 11 February 2020; Available from: <https://internetofthingsagenda.techtarget.com/definition/Internet-of-Things-IoT> [Accessed: 6 May 2020].
47. Xu, F., et al., *Recent Developments for Flexible Pressure Sensors: A Review*. Micromachines (Basel), 2018. **9**(11).
48. *TracPatch*. Available from: <https://www.tracpatch.com/> [Accessed: 5 December 2019].
49. *E-Vive*. Available from: <https://www.cymedicaortho.com/products/e-vive/> [Accessed: 5 December 2019].
50. *Carbonhand®*. Available from: <https://www.bioservo.com/healthcare/carbonhand> [Accessed: 6 December 2019].
51. *Device Advice: Comprehensive Regulatory Assistance*. Available from: <https://www.fda.gov/medical-devices/device-advice-comprehensive-regulatory-assistance> [Accessed: 20 February 2020].
52. *Medical Devices - Sector*. Available from: https://ec.europa.eu/health/md_sector/overview_en [Accessed: 28 May 2020].
53. Yeo, J.C. and C.T. Lim, *Wearable Sensors for Upper Limb Monitoring*, in *Wearable Technology in Medicine and Health Care*. 2018. p. 113-134.
54. Ambar, R., et al., *Multisensor arm rehabilitation monitoring device*. 2012.
55. Tenore*, F.V.G., et al., *Decoding of Individuated Finger Movements Using Surface Electromyography*. IEEE Transactions on Biomedical Engineering, 2009. **56**(5): p. 1427-1434.
56. You, K.-J., K.-W. Rhee, and H.-C. Shin, *Finger Motion Decoding Using EMG Signals Corresponding Various Arm Postures*. Experimental neurobiology, 2010. **19**(1): p. 54-61.
57. Zhang, Z., et al., *Real-Time Surface EMG Pattern Recognition for Hand Gestures Based on an Artificial Neural Network*. Sensors (Basel, Switzerland), 2019. **19**(14): p. 3170.
58. McIntosh, J., A. Marzo, and M. Fraser, *SensIR: Detecting Hand Gestures with a Wearable Bracelet using Infrared Transmission and Reflection*, in *Proceedings of the 30th Annual ACM Symposium on User Interface Software and Technology*. 2017, ACM: Quebec City, QC, Canada. p. 593-597.
59. McIntosh, J., et al., *EchoFlex: Hand Gesture Recognition using Ultrasound Imaging*, in *Proceedings of the 2017 CHI Conference on Human Factors in Computing Systems*. 2017, ACM: Denver, Colorado, USA. p. 1923-1934.
60. Eadicicco, L. *This Futuristic Armband Lets You Control Your Computer Like Magic*. 2016; Available from: <https://time.com/4173507/myo-armband-review/> [Accessed: 8 November 2019].
61. Li, N., et al., *Combined Use of FSR Sensor Array and SVM Classifier for Finger Motion Recognition Based on Pressure Distribution Map*. Journal of Bionic Engineering, 2012. **9**(1): p. 39-47.
62. Xiao, Z.G. and C. Menon, *A Review of Force Myography Research and Development*. Sensors (Basel, Switzerland), 2019. **19**(20): p. 4557.
63. Jiang, X., et al., *Exploration of Force Myography and surface Electromyography in hand gesture classification*. Medical Engineering & Physics, 2017. **41**: p. 63-73.

64. *Force Sensing Resistor Integration Guide and Evaluation Parts Catalog*, in *400 Series* Interlink Electronics.
65. Dementyev, A. and J.A. Paradiso, *WristFlex: low-power gesture input with wrist-worn pressure sensors*, in *Proceedings of the 27th annual ACM symposium on User interface software and technology*. 2014, ACM: Honolulu, Hawaii, USA. p. 161-166.
66. Zhang, Y. and C. Harrison, *Tomo: Wearable, Low-Cost Electrical Impedance Tomography for Hand Gesture Recognition*, in *Proceedings of the 28th Annual ACM Symposium on User Interface Software & Technology*. 2015, ACM: Charlotte, NC, USA. p. 167-173.
67. Kim, D., et al. *Digits: Freehand 3D interactions anywhere using a wrist-worn gloveless sensor*. in *UIST'12 - Proceedings of the 25th Annual ACM Symposium on User Interface Software and Technology*. 2012.
68. Zheng, Y.P., et al., *Sonomyography: Monitoring morphological changes of forearm muscles in actions with the feasibility for the control of powered prosthesis*. *Medical Engineering & Physics*, 2006. **28**(5): p. 405-415.
69. Hamid Muhammed, H. and J. Raghavendra, *Optomyography (OMG) : A Novel Technique for the Detection of Muscle Surface Displacement Using Photoelectric Sensors*, in *10th International Conference on Bioelectromagnetism, ISBEM 2015*. 2015: International Society for Bioelectromagnetism.
70. Muhammed, H.H. and R. Jammalamadaka. *A new approach for rehabilitation and upper-limb prosthesis control using optomyography (OMG)*. in *2016 1st International Conference on Biomedical Engineering (IBIOMED)*. 2016.
71. Ding, H., et al., *An Individual Finger Gesture Recognition System Based on Motion-Intent Analysis Using Mechanomyogram Signal*. *Frontiers in neurology*, 2017. **8**: p. 573-573.
72. Wen, H., J.R. Rojas, and A.K. Dey, *Serendipity: Finger Gesture Recognition using an Off-the-Shelf Smartwatch*, in *Proceedings of the 2016 CHI Conference on Human Factors in Computing Systems*. 2016, ACM: San Jose, California, USA. p. 3847-3851.
73. *Interlink Electronics - Technologies*. Available from: <https://www.interlinkelectronics.com/sensor-technologies> [Accessed: 18 November 2019].
74. *FSR 400 Series Data Sheet*. Interlink Electronics.
75. *BioDigital - Anatomy Software*.
76. *Arduino UNO R3, Pin Diagram, Specification and Applications*. Available from: <https://www.elprocus.com/what-is-arduino-uno-r3-pin-diagram-specification-and-applications/> [Accessed: 30 September 2019].
77. Xiao, Z.G. and C. Menon, *An Investigation on the Sampling Frequency of the Upper-Limb Force Myographic Signals*. *Sensors (Basel, Switzerland)*, 2019. **19**(11): p. 2432.
78. *Adafruit Feather NRF52840 Express*. Available from: <https://www.adafruit.com/product/4062> [Accessed: 14 November 2019].
79. *FLORA - Wearable electronic platform: Arduino-compatible - v3*. Available from: <https://www.adafruit.com/product/659> [Accessed: 14 November 2019].
80. *Particle Photon Data Sheet*. Available from: <https://docs.particle.io/datasheets/wi-fi/photon-datasheet/> [Accessed: 15 November 2019].
81. *Photon WiFi Development Board*. Available from: <https://www.buyapi.ca/product/particle-photon-headers/> [Accessed: 15 November 2019].
82. *Beetle BLE - The smallest Arduino bluetooth 4.0 (BLE)*. Available from: <https://www.dfrobot.com/product-1259.html> [Accessed: 15 November 2019].
83. *MicroBattery*. Available from: <https://www.microbattery.com/ex-l28px-bp-1-premium-l28px-2cr1-3n-photo-lithium-6v-170-mah-carded-1-p.html> [Accessed: 26 November 2019].

84. *Energizer A11 MN11 L1016 Battery | 2 Pack*. Available from: <https://www.batterystation.co.uk/energizer-a11-mn11-l1016-battery-2-pack/> [Accessed: 26 November 2019].
85. *6V Alkaline Battery*. Available from: <https://www.jaycar.co.nz/6v-alkaline-battery/p/SB2421> [Accessed: 27 November 2019].
86. *Maxell - CR2032 Data Sheet*. Available from: https://cdn-shop.adafruit.com/datasheets/maxell_cr2032_datasheet.pdf [Accessed: 27 November 2019].
87. *Micro Slide Switch*. Available from: <https://www.jaycar.co.nz/spdt-micro-slide-switch/p/SS0834> [Accessed: 29 November 2019].
88. *10Pcs DIP PCB Mini Latching Tactile Push Button Switch 12x12x9mm*. Available from: <https://www.aliexpress.com/i/32823253910.html> [Accessed: 28 November 2019].
89. Mechelli, A. and S. Viera, *Machine Learning in the Brain Sciences*. 2019, San Diego, UNITED STATES: Elsevier Science & Technology.
90. Brownlee, J., *Machine Learning Mastery With Weka*, in *Analyze Data, Develop Models and Work Through Projects*. 2018, Jason Brownlee. p. 240.
91. Mohammed, M., M.B. Khan, and E.B.M. Bashier, *Machine Learning : Algorithms and Applications*. 2016, Milton, UNITED KINGDOM: CRC Press LLC.
92. Brownlee, J. *How Much Training Data is Required for Machine Learning?* Machine Learning Process [Article] 2017 23 May 2019; Available from: <https://machinelearningmastery.com/much-training-data-required-machine-learning/> [Accessed: 20 November 2019].
93. Mitsa, T. *How Do You Know You Have Enough Training Data?* Towards Data Science [Article] 2019 23 April 2019; Available from: <https://towardsdatascience.com/how-do-you-know-you-have-enough-training-data-ad9b1fd679ee> [Accessed: 20 November 2019].
94. Figueroa, R.L., et al., *Predicting sample size required for classification performance*. BMC Med Inform Decis Mak, 2012. **12**: p. 8.
95. Junghwan Cho, K.L., Ellie Shin, Garry Choy, Synho Do, *How much data is needed to train a medical image deep learning system to achieve necessary high accuracy?* arXiv: Learning, 2015.
96. Haldar, M. *How much training data do you need?* [Article] 2015 20 November 2019; Available from: <https://medium.com/@malay.haldar/how-much-training-data-do-you-need-da8ec091e956> [Accessed: 21 November 2019].
97. *Queexo Automated Machine Learning*. Available from: <https://automl.queexo.com/> [Accessed: 15 December 2019].
98. James, G., et al., *An introduction to statistical learning : with applications in R*. [Corrected at 6th printing 2015]. ed. Springer texts in statistics: 103. 2015: Springer.

Appendix A-1: Arduino C code

```
// Define FSR pin:

#define fsrpin A0

#define fsrpin1 A1

#define fsrpin2 A2

//Define variable to store fsr readings:

int fsrreading; //Variable to store FSR value

int fsrreading1;

int fsrreading2;

int fsrreading3;

void setup() {

    // Begin serial communication at a baud rate of 9600:

    Serial.begin(9600);

}

void loop() {

    // Read the FSR pin and store the output as fsrreading:

    Fsrreading1 = analogRead(fsrpin);

    Fsrreading2 = analogRead(fsrpin1);

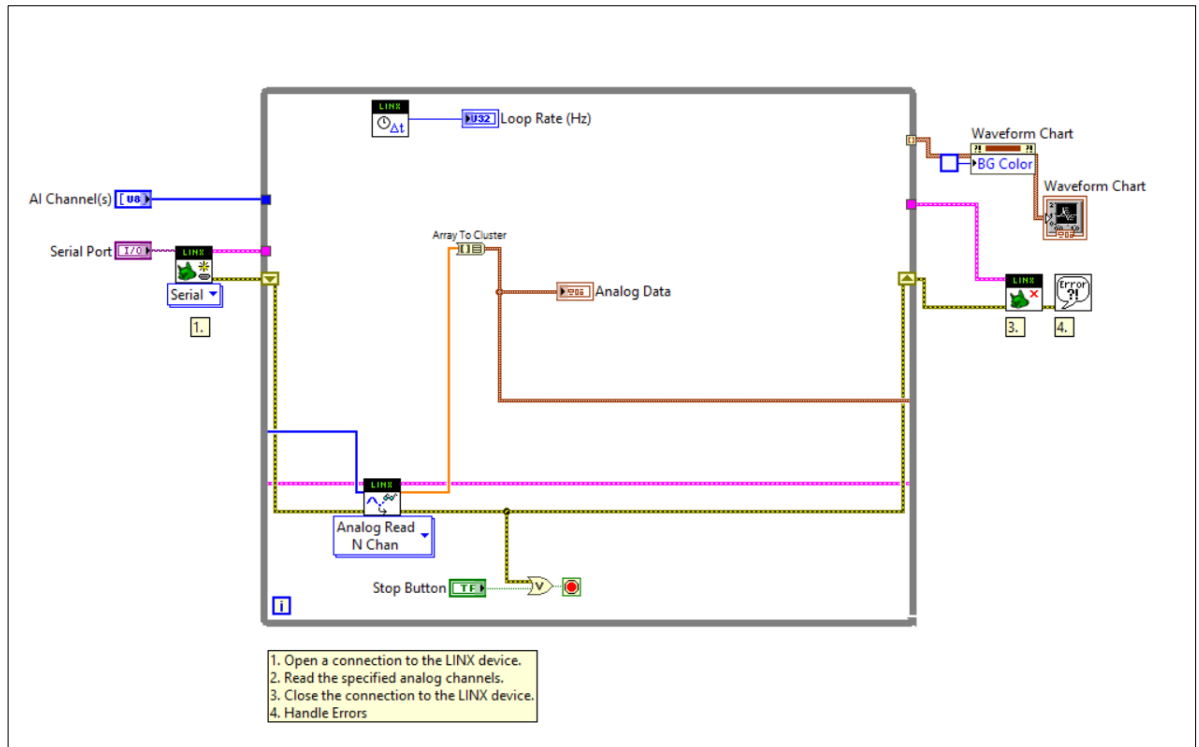
    Fsrreading3 = analogRead(fsrpin2);

    Serial.println(fsrreading);

    delay(10); //Delay 10 ms.

}
```

Appendix A-2: LabVIEW Code for Sampling Analogue Data from Arduino Device



Appendix B: Detailed Descriptions of Classification Algorithms Used

Logistic regression

Before considering how a logistic regression algorithm works, it is first necessary to briefly revise the main concept of the linear regression model. In statistics, a linear regression analysis is a quantitative method for understanding the relationship between two or more variables based on observational data. A linear regression can also be treated as a supervised learning model which can be used for predicting the value of a continuous variable. The mathematical representation of a simple linear regression can be expressed as:

$$y = \alpha_0 + \alpha_1 x$$

Where:

y = value to be predicted

α_0 = the intercept of the line

α_1 = the slope of the line

x = the predictor variable or feature

In developing a linear regression model, coefficients α_0 and α_1 have to be determined from a labelled dataset. If we consider for example, the labelled dataset of 200 observations for TV advertising budget (x) and number of units sold (y), we can establish the linear model shown by Figure B.1.

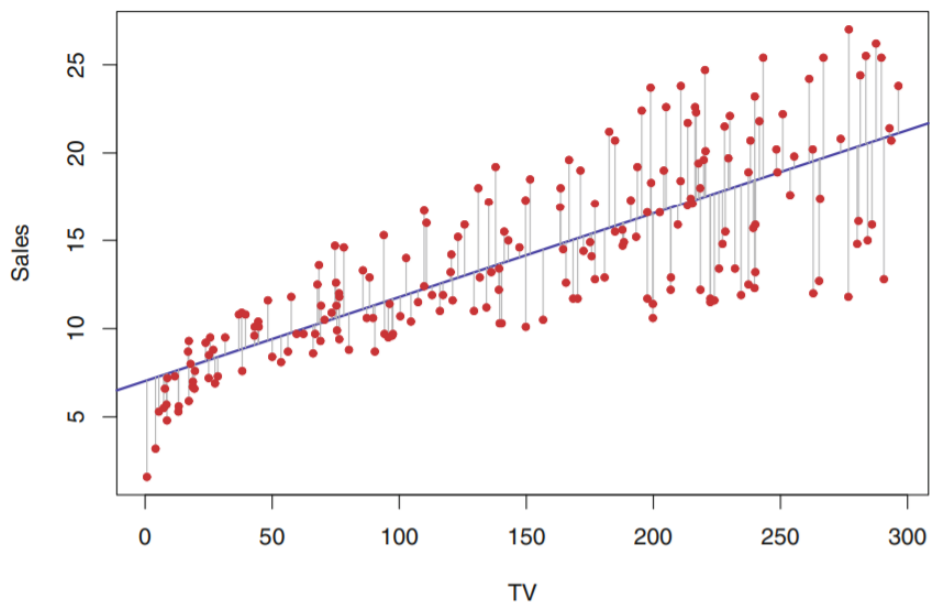


Figure B.1 [98]

The grey vertical lines represent the error of each data point with respect to the linear model. The best linear fit is found by minimizing the sum of the squared errors using the least squares method. The above example is the most simplified case of a linear regression.

A linear regression model makes a quantitative prediction for an output variable y using a linear combination of input variables. Classification models, however, predict a qualitative output, a variable that is categorical. A logistic regression model is therefore used to make a binary prediction ($Y = 1$ or $Y = 0$) as opposed to a value of a continuous variable. It does this by first developing a regression model and then implementing it in the logistic function (also called sigmoid function):

$$p(X) = \frac{e^{\alpha_0 + \alpha_1 X}}{1 + e^{\alpha_0 + \alpha_1 X}}$$

Where:

$p(X) = \Pr(Y = 1|X)$ (the probability that an input X falls into the class $Y = 1$, also called the default class)

X = the predictor variable or feature

$\alpha_1 \& \alpha_2$ = coefficients derived from training data

For a given input X , $p(X)$ will take on a continuous value between 0 and 1. For the output to be binary, we can define the constraints:

$\Pr(Y = 1|X) = 1$ if $p(X) \geq 0.5$ and

$\Pr(Y = 1|X) = 0$ if $p(X) < 0.5$

If we again consider the sales example, we could define the class $Y = 1$ as sales of 15 and above and $Y = 0$ as sales of below 15. If we trained a logistic model $p(X)$ based on this output parameter, we may want to know what the probability is of exceeding sales of 15 for a TV budget of 50. Looking at the linear regression graph we could reasonably estimate that this probability would fall below 0.5 and therefore fall into the class $Y = 0$, or sales not reaching or exceeding 15 [98].

Logistic regression is a simple and effective technique and mainly used for binary classification problems.

Naïve Bayes classifier

The Naïve Bayes classifier is a simple algorithm based on Bayes Theorem which is expressed mathematically as:

$$P(A|B) = \frac{P(B|A)P(A)}{P(B)}$$

Where

$P(A|B)$ denotes the probability of A , when B is observed

$P(B|A)$ denotes the probability of B , when A has occurred

$P(A)$ is the probability of A occurring

$P(B)$ is the probability of B occurring

Consider again the example of a classifier that distinguishes between images of a dog and cat. For simplicity, let it be assumed that this could be done with a single variable, say, the size of the animal in the image. A large animal (defined by a number of pixels representing the animal for example) is classified as a dog and a small animal classified as a cat. Therefore, given a new unseen image, it is found that the size of the animal in the image is large. Then the probability of it being a dog is given by:

$$P(dog|large) = \frac{P(large|dog)P(dog)}{P(dog) \times P(large|dog) + P(cat) \times P(large|cat)}$$

Using all the labelled training data (images of cats and dogs), the probability of a dog being classified is given by:

$$P(dog) = \frac{\text{number of dog images}}{\text{total number of images}}$$

And

$$P(large|dog) = \frac{\text{number of dogs classified as large}}{\text{total number of dog images}}$$

$$P(large|cat) = \frac{\text{number of cats classified as large}}{\text{total number of cat images}}$$

Most classification problems will use more than one feature or variable to make a prediction. The Naïve Bayes algorithm assumes that all the features used in the prediction are independent from one another and contribute equally to the outcome. These simplifying assumptions explain why the algorithm is referred to as *Naïve* [43].

Decision trees and random forests

A decision tree is a supervised ML algorithm produced with a series of decisions based on feature values. The tree is usually structured with binary questions about features represented as nodes and decision paths represented as branches. The predicted class value is represented by the leaf node or terminal node in the decision tree. For example, a simple decision tree algorithm that decides on good outdoor exercise conditions is shown by Figure B.2.

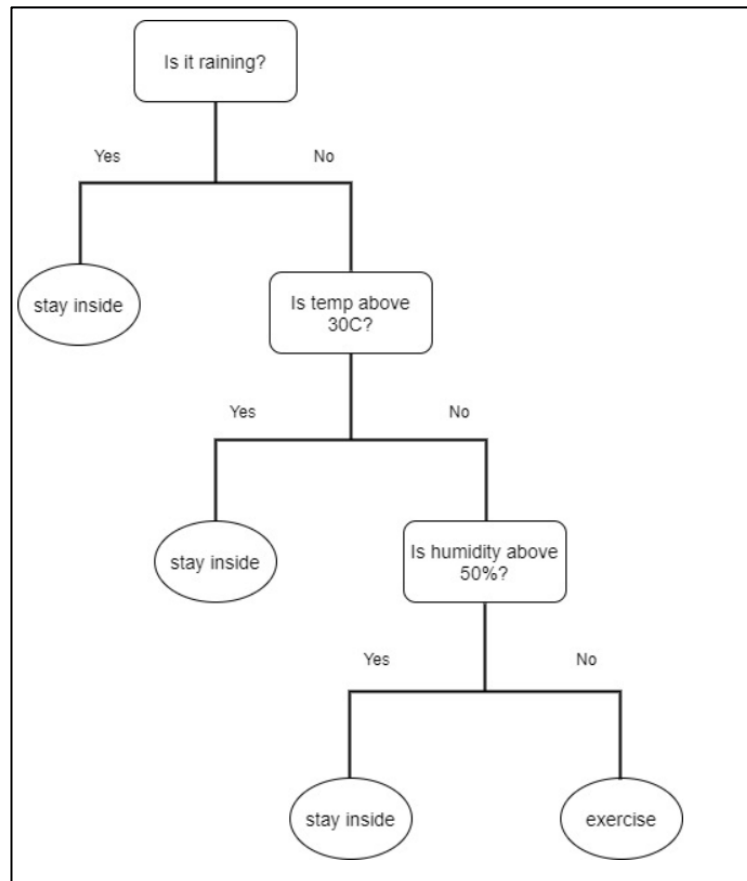


Figure B.2

A decision tree algorithm is created with training data according to the following general rules:

1. Select most important feature/s as the root node
2. Create a decision based on the highest information divide
3. Recursively repeat steps 1 and 2 until no further information can be divided at the edge nodes [43]

When there are a large number of features involved, it can be difficult to determine which ones are most important for building the tree. When this is the case, the top features or attributes are selected using statistical criteria known as information gain or Gini impurity. Information gain is determined by entropy calculations and is used

when the class value is categorical (as in the weather example shown above). The Gini impurity criterion is used to decide on variables which are continuous [43].

Random forest is an algorithm which takes the average of an array of decision trees which are built from various parts of the training data. This algorithm typically performs better than a single decision tree as it reduces overfitting i.e. when the model is too closely correlated with the training data and therefore cannot accurately classify new data [43].

K-nearest neighbour

The K-nearest neighbour (KNN) algorithm is a very simple algorithm where K data points that are nearest to a new data point are all similar. When the largest cluster of similar points have been identified, the new point is predicted to have the same class as the cluster. KNN is often called a *lazy* algorithm because no actual learning takes place, except for keeping a record of labelled data.

The KNN algorithm is illustrated by Figure B.3 shown below. The data points labelled with 'x' represent training data and 'o' represents a new data point with an unknown class label. The modal class of the three K nearest neighbours denoted by A, B and C is used to predict the class of the new data point 'o'. Various values for K can be chosen, with a special case being K=1. However, larger values for K is typical as it can nullify the effects of a single outlier. In cases where the K-nearest neighbours are represented by multiple classes, weightings are assigned to the nearest data points, so that distance is given priority over number of nearest points. The KNN algorithm is less accurate for datasets with unbalanced classes [43].

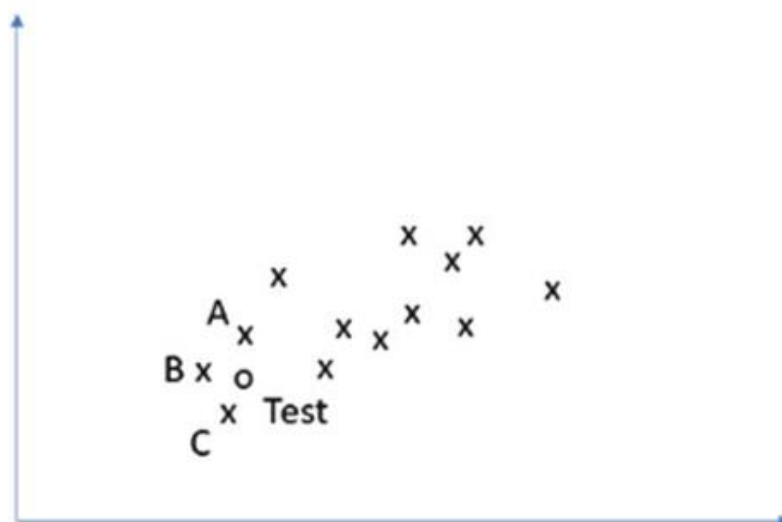


Figure B.3

Support vector machines

Support vector machines (SVM) are binary linear classifiers. They separate data into two classes with a decision boundary called a hyperplane. Data for which there exists a hyperplane boundary are said to be linearly separable and can therefore be classified with an SVM. In problems where the data are not linearly separable, the data can be transformed into a higher dimensional space using functions called kernels [43]. For a two-dimensional feature vector, an SVM uses a line as a hyperplane to divide the dataset. The equation for a line in a two-dimensional feature vector is defined as:

$$y = w \cdot f(x) + b$$

Where:

$f(x)$ is the feature vector

w is the weighting given to the feature vector

b is a bias term

In the example graph shown by Figure B.4, the data points (feature vectors) are separated by three possible decision boundaries a, b, and c. An SVM classifier will select a decision boundary that maximizes the distance between the boundary and the nearest data point (support vector) of each class. The boundary b is therefore the hyperplane chosen in the illustration. SVMs are effective classifiers where the training dataset is small, and the number of features are high.

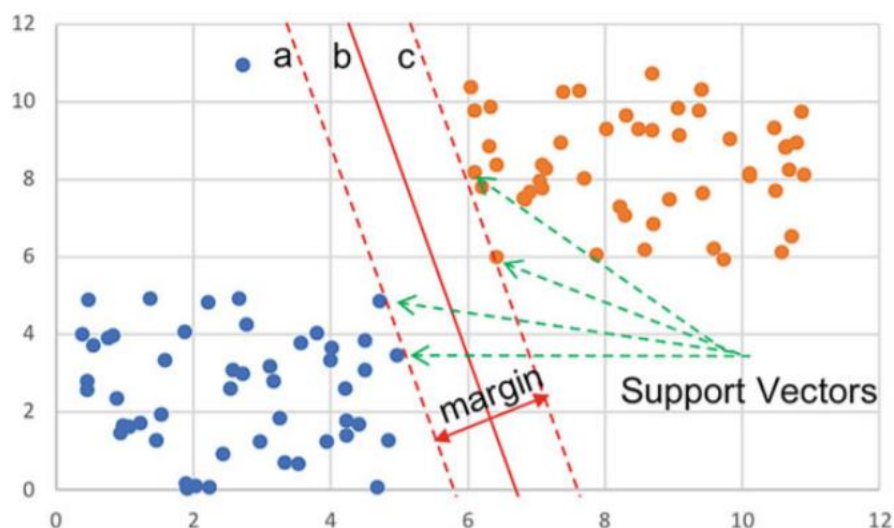
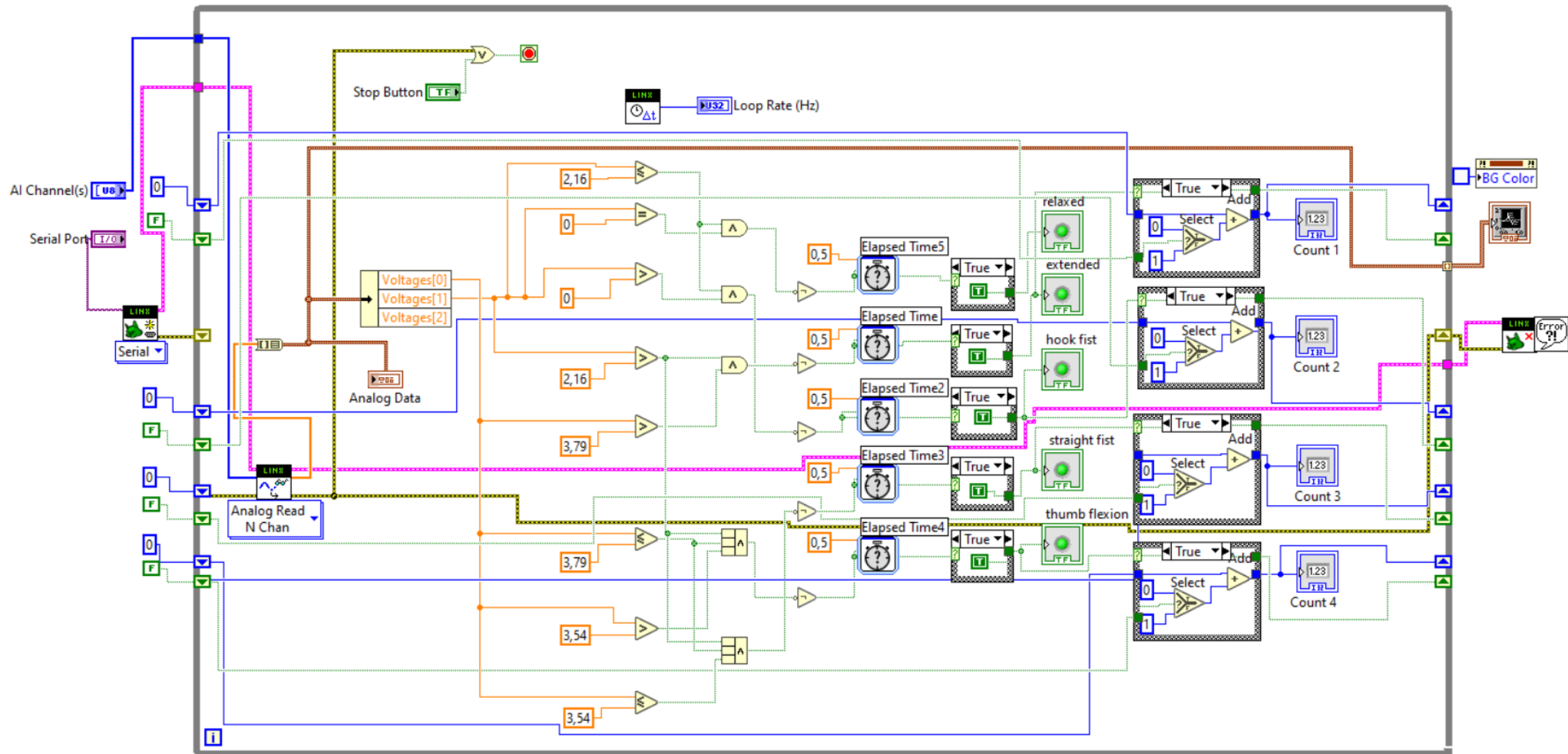


Figure B.4 [43]

Appendix C: LabVIEW Code Implementing J-48 Decision Tree Algorithm



Appendix D: Ethics Approval

Auckland University of Technology Ethics Committee (AUTEC)

Auckland University of Technology
D-88, Private Bag 92006, Auckland 1142, NZ
T: +64 9 921 9999 ext. 8316
E: ethics@aut.ac.nz
www.aut.ac.nz/researchethics

28 November 2019

David White
Faculty of Design and Creative Technologies

Dear David

Re Ethics Application: **19/347 Development of hand motion classification algorithm**

Thank you for providing evidence as requested, which satisfies the points raised by the Auckland University of Technology Ethics Committee (AUTEC).

Your ethics application has been approved for three years until 27 November 2022.

Standard Conditions of Approval

1. The research is to be undertaken in accordance with the [Auckland University of Technology Code of Conduct for Research](#) and as approved by AUTEC in this application.
2. A progress report is due annually on the anniversary of the approval date, using the EA2 form.
3. A final report is due at the expiration of the approval period, or, upon completion of project, using the EA3 form.
4. Any amendments to the project must be approved by AUTEC prior to being implemented. Amendments can be requested using the EA2 form.
5. Any serious or unexpected adverse events must be reported to AUTEC Secretariat as a matter of priority.
6. Any unforeseen events that might affect continued ethical acceptability of the project should also be reported to the AUTEC Secretariat as a matter of priority.
7. It is your responsibility to ensure that the spelling and grammar of documents being provided to participants or external organisations is of a high standard.

AUTEC grants ethical approval only. You are responsible for obtaining management approval for access for your research from any institution or organisation at which your research is being conducted. When the research is undertaken outside New Zealand, you need to meet all ethical, legal, and locality obligations or requirements for those jurisdictions.

Please quote the application number and title on all future correspondence related to this project.

For any enquiries please contact ethics@aut.ac.nz. The forms mentioned above are available online through <http://www.aut.ac.nz/research/researchethics>

Yours sincerely,



Kate O'Connor
Executive Manager
Auckland University of Technology Ethics Committee

Cc: scd3179@aut.ac.nz; jkilby@aut.ac.nz

Appendix E: Participant Information Sheet

Participant, Information Sheet



Date Information Sheet Produced:

30th August 2019

Project Title

The development of a classification algorithm using the Zero-Cast wrist-brace

An Invitation

Kia Ora,

Our names are Dr Pranesh Kumar, a Hand Surgeon and co-founder of Zero-Cast, Dr David White, Biomedical Engineer, and Michael van Wyk, Master of Engineering student, and we are researchers who are undertaking this task as an explorative study.

Zero-Cast, a start-up company based in Auckland have developed a novel wrist-brace for patients who have suffered a distal radius fracture. The wrist-brace is a dynamic and adjustable orthosis which has been designed to replace plaster and fibre-glass casts typically used to immobilize a fracture. A common problem seen in patients who have worn a plaster cast for up to 8 weeks is that they lose mobility and function of the joints and tissues near the fracture site. This is mainly because the entire hand or arm has been immobilized which does not allow the patient to maintain hand function and range of motion. The Zero-Cast system has been designed to solve this problem by immobilizing the fracture site securely while still providing the patient with significant hand function and range of motion.

During the immobilization period, it is vital that patients perform hand and finger exercises to ensure that they maintain function and dexterity throughout the healing process. Even with traditional plaster casts patients are infrequently referred to hand therapy during immobilization. Even if they are referred to physiotherapy, they often do not comply with the rehabilitation program as they might be weary or nervous of re-injuring the wrist and therefore unnecessarily limit their use. This study is the first stage for the development of a smart or digital wrist-orthosis that can detect and measure types of hand motion for the purpose of improving rehabilitation programs and healing outcomes. In order to proceed, we require hand motion data from a variety of healthy participants above the age of 18, with no previous injury to hand, wrist or arm and with no known neurological or musculoskeletal conditions.

Your participation is entirely voluntary, and you may withdraw at any time prior to the completion of data collection.



Image of Zero-Cast's adjustable wrist-orthosis

(Image credit Zero-Cast Ltd)**What is the purpose of this research?**

The main purpose of this research is to assist in developing a classification algorithm that can accurately identify a series of hand rehabilitation exercises and functional hand tests using embedded technology in the Zero-Cast wrist-brace. This classifier will be used in an electronic prototype of the Zero-Cast brace which will then be further tested. This research will also establish the limitations of the classifier – we do not know if it will work across different users, or if data unique to each user is required.

How was I chosen for this invitation?

You have responded to posters advertising this study, which invited healthy adults above the the age of 18, with no previous hand, wrist or arm injury to participate in this research. Also, if you are comfortable having a wrist-brace fitted on both hands, can perform simple repeated hand motions, and do not have any neurological or musculoskeletal disorders. You will unfortunately be excluded from participation if you are currently a student under Dr David White.

What will happen in this research?

1. After making initial contact with the Project Manager you will be asked to take part in a short telephonic interview to assess your suitability for the study. If you meet all the inclusion criteria and not disqualified by exclusion criteria, you will be added to a pool of suitable respondents for selection.
2. A selection process will then be undertaken to screen all respondents to provide a sample of participants who cover a range of age, gender and ethnicity representative of the population.
3. Respondents will be notified of the results of this screening process and will be asked to meet in the BioDesign Lab (WT307) at a convenient time to sign a confidentiality agreement and consent form. We will then proceed with the measurements and data collection.
4. During the session, a suitably sized experimental wrist-brace will be carefully fitted to the wrist of your dominant arm by the Project Manager, who will have been trained by Dr Pranesh Kumar.
5. The wrist-brace will be fitted to a standardized fitting force before any of the hand motion measurements are taken.
6. In a comfortable seated position, you will be asked to place the elbow of your dominant arm on the desk in front of you with the forearm at approximately 90 degrees to the upper arm. The hand will be in a neutral position facing toward your body.
7. With the aid of demonstrations by the Project Manager, you will be asked to perform the following series of hand gestures:
 - 7.1 Flexing and extending of the fingertips - bending occurring at the proximal and distal interphalangeal joints; also known as 'hook-fist'



7.2 Flexing and extending of the fingers with fingers flat against the palm- Bending occurring at the metacarpophalangeal and proximal interphalangeal joints; also known as 'flat-fist'



7.3 Thumb touching the base of the little finger; also known as 'thumb opposition'



8. All gestures will be performed successively with each gesture being held for approximately five seconds. This will be repeated two or three times.
9. You will also be asked to perform a series of simple functional hand tests. These include squeezing a hand exercise ball, rotating a knob, and lifting a water bottle.

What are the discomforts and risks?

There may be some slight discomfort during the application of the wrist-brace but no pain. Your hand may get a bit tired after repeatedly performing the exercises, however, you will be given rest between measurements to ensure your comfort. There are no risks associated with this procedure.

How will my privacy be protected?

Although your name will be recorded on the Consent Form this will only be accessed by the Project Manager for administrative purposes. Full confidentiality is guaranteed with only the researchers involved with this project having access to the unidentificated data.

The data will be securely stored on a separate hard drive locked within the researcher's office. Consent form and Participant Questionnaires will be securely stored at the AUT Design and Creative Technology Faculty Research Office, where access to it will be controlled.

Please note that the recorded data may be accessed for other research purposes and will be archived and securely stored for 6 years then destroyed.

What are the costs of participating in this research?

Your participation will require one session lasting approximately 30 minutes of your time.

How is this research being funded?

This study is being funded by a Callaghan Innovation R&D fellowship grant.

How is this research being managed?

A Master of Engineering Student, Michael van Wyk, is the **Project Manager and Primary Researcher** and will communicate with prospective participants and carry out the data collection.

Michael van Wyk email: scd3179@aut.ac.nz Phone: 027 616 6472

What are the benefits of this study?

This research forms part of a master's thesis as well as being essential to the development of a new Zero-Cast prototype. Ultimately it may serve to provide better treatment and rehabilitation options for people who have suffered distal radial fractures, thereby improving quality of life.

What compensation is available for injury or negligence?

In the unlikely event of a physical injury as a result of your participation in this study, rehabilitation and compensation for injury by accident may be available from a third-party insurance group equivalent to the Accident Compensation Corporation. This is subject to incident details that satisfy the requirements of the law and the third party's regulations.

What opportunity do I have to consider this invitation?

You are welcome to consider this invitation for as long as it takes you to make up your mind whether you would like to participate or not. We are happy to answer any questions that you may have.

Furthermore, since your participation is entirely voluntary, you may choose to withdraw at any time and for any reason prior to the completion of data collection.

How do I agree to participate in this research?

Contact the Project Manager who will then arrange for an appointment at a mutually agreeable time. The purpose of this meeting is to discuss your health state, confirm that you have had no previous injury

to the wrist, arm or upper limb and do not have any neurological or musculoskeletal conditions. We will also discuss any concerns and answer any questions you may have about this study.

You may also keep this participation information sheet if you wish to.

Will I receive feedback on the results of this research?

Yes. A summary of the research findings will be sent to you should you want this.

Whom do I contact for further information about this research?

Project Manager Contact Details:

Michael van Wyk email: scd3179@aut.ac.nz Phone: 027 616 6472

Research Supervisor Contact Details:

Dr David White email: david.white@aut.ac.nz Phone: 921-9999 extn. 8352

Researcher Contact Details:

Dr Pranesh Kumar email: pranesh@zero-cast.com Phone: 02102585294

Dr David White email: david.white@aut.ac.nz Phone: 921-9999 extn. 8352

What do I do if I have concerns about this research?

Any concerns regarding the nature of this project should be notified in the first instance to the Research Supervisor. His contact details are listed earlier.

Concerns regarding the conduct of the research should be notified to the Executive Secretary of AUTEK, Kate O'Connor, ethics@aut.ac.nz, 921 9999 ext 6038

**Approved by the Auckland University of Technology Ethics Committee on 28 November 2019
AUTEK Reference number 19/347**

Appendix F: Study Poster

AUT

Invitation to hand motion recognition study



Image of dynamic adjustable wrist orthosis
(Image credit Zero-Cast)

We are conducting research with the aim of developing a hand motion recognition system for people with distal radius fractures (a bone fracture near the wrist). To assist in this research, healthy adults above the age of 18 with no previous wrist/arm fractures or musculoskeletal conditions are invited to participate in the collection of data using an experimental wrist-brace.

If you are comfortable having a wrist-brace fitted on your dominant arm, can perform simple repeated hand motions, and interested in participating in this study, or require further information, please contact the Research Manager:

Contact Michael van Wyk
Ph 027 616 6470
Email: scd3179@aut.ac.nz

Note: If you are a student currently being supervised by Dr David White you are not encouraged to participate.

Approved by the Auckland University of Technology Ethics Committee on 28 November 2019
AUTEK Reference number 19/347

Appendix G: Participant Consent Form

Consent Form



Project title: *Development of hand motion classification algorithm*
Project Manager: *Michael van Wyk*
Researchers: *Dr David White, Dr Pranesh Kumar, Michael van Wyk*

- I have read and understood the information provided about this research project in the Information Sheet dated 30th August 2019
- I have had an opportunity to ask questions and to have them answered.
- I understand that I may withdraw myself or any information that I have provided for this project at any time prior to completion of data collection, without being disadvantaged in any way.
- I agree to discuss my health condition and answer all questions asked correctly to the best of my knowledge.
- I have no history of wrist, forearm or upper limb injury or any neurological and/or musculoskeletal conditions
- I agree to take part in this research and have researchers contact my dominant arm and have an experimental wrist brace fitted.
- I agree to have my hand motion data recorded as described in the Participant Information Sheet
- I am aware that this data will be maintained for a period of 6 years
- I am aware that the data collected from this project will be used for the thesis of master's student Michael van Wyk and may be used in journal and conference publications and may also be used for other similar research investigations.
- I wish to receive a copy of the report from the research (please tick one): Yes No

Participant's Signature:

Participant's Name:

.....

Participant 's Contact Details (if appropriate):

.....
.....
.....

Date:

Note: The Participant should retain a copy of this form.